AD NUMBER
AD483287
LIMITATION CHANGES
TO: **Approved for public release; distribution is unlimited.**
FROM: **Distribution authorized to U.S. Gov't. agencies and their contractors; Critical Technology; APR 1966. Other requests shall be referred to Air Force Materials Laboratory, Attn: MAMP, Wright-Patterson AFB, OH 45433. This document contains export-controlled technical data.**
AUTHORITY
AFML ltr, 29 Mar 1972

AFML-TR-66-89

INTERMEDIATE-TEMPERATURE DUCTILITY AND STRENGTH OF TUNGSTEN AND MOLYBDENUM TZM

B. A. Wilcox, A. Gilbert, and B. C. Allen

Battelle Memorial Institute

TECHNICAL REPORT AFML-TR-66-89

April, 1966

Air Force Materials Laboratory
Research and Technology Division
Air Force Systems Command
Wright-Patterson Air Force Base, Ohio

DISCLAIMER NOTICE

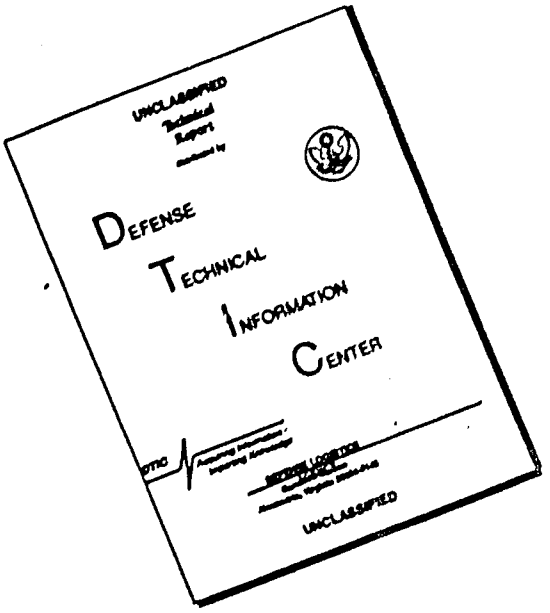

THIS DOCUMENT IS BEST QUALITY AVAILABLE. THE COPY FURNISHED TO DTIC CONTAINED A SIGNIFICANT NUMBER OF PAGES WHICH DO NOT REPRODUCE LEGIBLY.

NOTICES

When Government drawings, specifications, or other data are used for any purpose other than in connection with a definitely related Government procurement operation, the United States Government thereby incurs no responsibility nor any obligation whatsoever; and the fact that the Government may have formulated, furnished, or in any way supplied the said drawings, specifications, or other data, is not to be regarded by implication or otherwise as in any manner licensing the holder or any other person or corporation, or conveying any rights or permission to manufacture, use, or sell any patented invention that may in any way be related thereto.

Copies of this report should not be returned to the Research and Technology Division unless return is required by security considerations, contractual obligations, or notice on a specific document.

AF-WP-O-FEB 65 1500

INTERMEDIATE-TEMPERATURE DUCTILITY AND STRENGTH OF TUNGSTEN AND MOLYBDENUM TZM

B. A. Wilcox, A. Gilbert, and
B. C. Allen

FOREWORD

This report was prepared by Battelle Memorial Institute, under United States Air Force Contract Number AF33(615)-1727. This contract was initiated under Project Number 7351, "Metallic Materials," Task Number 735101, "Refractory Metals."

The project was administered under the direction of the Air Force Materials Laboratory, Research and Technology Division, with Captain J. R. Upp, and Mr. Larry D. Parsons as acting project engineers.

This report covers the period from 1 July 1964 to 30 August 1965.

The manuscript of this report was released by the authors February 1966 for publication as a RTD Technical Report.

This technical report has been reviewed and is approved.

I. PERLMUTTER
Chief, Physical Metallurgy Branch
Metals and Ceramics Division
AF Materials Laboratory

ABSTRACT

The ductility and strength of tungsten and molybdenum-TZM have been studied as a function of temperature with emphasis on investigating the effects of strain rate, structural condition, and carbon content on mechanical properties.

Both wrought-stress-relieved and recrystallized tungsten and Mo-TZM have been tested at strain rates of 0.01, 2, and 600 min^{-1} over the temperature range ~200 to 1850 C.

In recrystallized Mo-TZM alloys, an intermediate-temperature region (~1100-1500 C) of reduced ductility at the two lower strain rates was found to be caused by pronounced grain-boundary cracking. This phenomenon is associated with dynamic strengthening of the matrix as a result of precipitation during deformation.

TABLE OF CONTENTS

ILLUSTRATIONS

ILLUSTRATIONS
(Continued)

ILLUSTRATIONS
(Continued)

ILLUSTRATIONS
(Continued)

LIST OF TABLES

INTRODUCTION

Two refractory metals which show good promise as high-temperature structural materials are unalloyed tungsten and Mo-TZM alloy (nominally Mo-0.5Ti-0.1Zr-0.03C). However, results of previous investigations have indicated that there may be a region of reduced ductility at temperatures above the ductile-to-brittle transition temperature. If this phenomenon is sufficiently pronounced, it could be detrimental in intermediate-temperature fabrication processes and in certain practical applications, e.g., tungsten rocket nozzles, where thermal gradients exist and could create regions of material with high elastic-stress-concentration factors but poor crack-arresting properties.

Figure 1 summarizes mechanical-property data from the literature on unalloyed tungsten up to ~1200 C, and suggests that there might be a tendency for reduced ductility at about 500 C. The data in Figure 1, however, are not consistent, since materials of different structural conditions and compositions were tested by the various investigators. There is considerably less elevated-temperature mechanical-property data for Mo-TZM alloy than for unalloyed tungsten. Some unpublished results of Climax Molybdenum Company [reported in Reference (5)] as well as results from three other studies[6-8] show that the total elongation of wrought-stress-relieved Mo-TZM sheet decreases from ~20 percent at room temperature to ~3-10 percent over a wide temperature range of ~500-1200 C. Also, Dotson and Adams[6] have shown a reduction in area minimum at ~1200 C in recrystallized Mo-TZM sheet, tested at a strain rate of 0.05 min^{-1}. As will be shown later these results are consistent with the present findings on both wrought and recrystallized Mo-TZM bar.

The present program was conceived with the following objectives: (1) to evaluate the nature and extent of any intermediate-temperature ductility minima in unalloyed tungsten and Mo-TZM alloy; (2) to assess the effects of deformation rate, composition (particularly carbon content), and structural state on the ductility minima; and (3) to attempt to identify the responsible mechanism(s). The temperature range of interest is ~200-1850 C. Previous investigations[9-11] have shown that at temperatures ≥2000 C there is a drastic decrease in the ductility of tungsten, which is associated with intercrystalline void formation. A further investigation of this phenomenon was not included in the present program.

SUMMARY

The influence of strain rate, carbon content, and microstructure on the temperature dependence of mechanical properties has been studied for tungsten and molybdenum-TZM. Particular emphasis was placed on examining the effects of these variables on the intermediate-temperature ductility.

Intermediate-temperature regions of reduced total elongation were observed for wrought-stress-relieved tungsten and Mo-TZM. This was due to the lack of work hardening (i.e., necking occurred immediately after yielding), and cannot be considered a true ductility reduction, since the reductions in area remained relatively unaffected and very high (~90-100% RA).

*References are given on page 99.

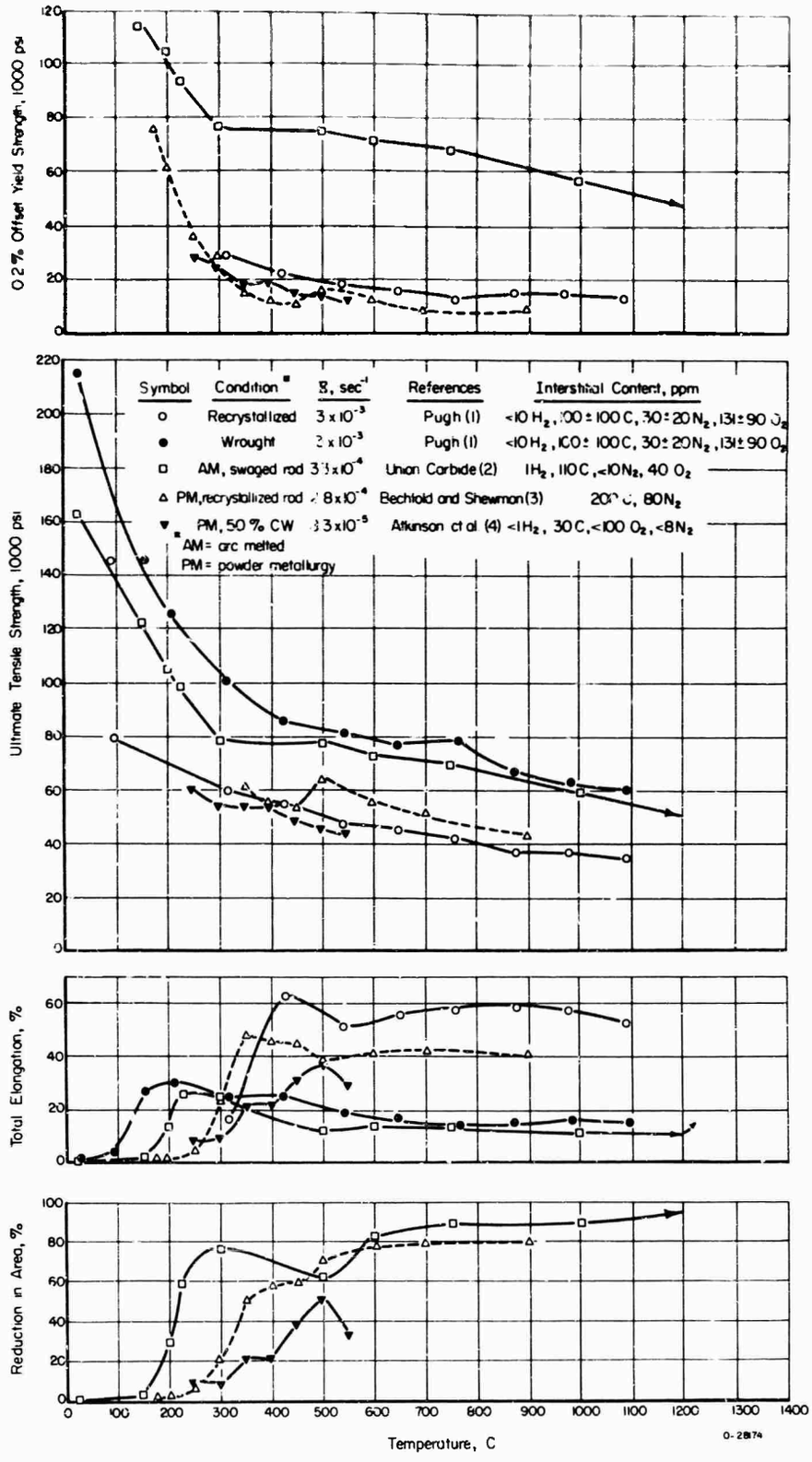

FIGURE 1. SUMMARY OF PREVIOUSLY REPORTED TENSILE PROPERTIES OF UNALLOYED TUNGSTEN AS A FUNCTION OF TEMPERATURE

Pronounced grain-boundary cracking was observed for recrystallized Mo-TZM at test temperatures of ~1100-1500 C, except for specimens tested at the highest strain rate, 600 min^{-1}. This phenomenon was associated with dynamic strengthening of the matrix due to precipitation during deformation and resulted in an intermediate-temperature region of reduced ductility.

Studies of the effect of heat treatment on Mo-TZM with the highest carbon content (190 ppm carbon) showed that quenching from 2100 C resulted in a fine carbide dispersion, which gave strengths much higher than those of the same material furnace cooled from 2100 C.

EXPERIMENTAL PROCEDURES

Materials

Five alloys were prepared in the form of 1/4-inch-diameter wrought-stress-relieved rod by the Universal Cyclops Steel Corporation, Bridgeville, Pennsylvania. Two tungsten heats (having nominal carbon contents of 10 and 35 ppm) and three Mo-TZM heats (with nominal carbon levels of 10, 100, and 190 ppm) were fabricated by vacuum arc casting, extrusion, and hot swaging. Chemical analyses of all materials are given in Tables I and II, and there is good agreement between Universal Cyclops and Battelle analyses on the final rod. Preparation of the alloys with intentional variations in carbon content resulted in only minor differences in the amounts of other interstitial elements present (i.e., nitrogen, oxygen, and hydrogen).

In addition to examining the effect of carbon content on mechanical behavior, the effect of structural state was studied by testing both wrought-stress-relieved and recrystallized specimens from three of the alloys (low-carbon tungsten, low- and high-carbon Mo-TZM). The influence of thermal treatment on the mechanical properties of the high-carbon Mo-TZM alloy was determined for three conditions: (1) recrystallized and furnace cooled, (2) recrystallized and quenched, and (3) recrystallized, quenched, and aged. Details of the materials and conditions tested are given in Table III, and results of annealing studies used to select the recrystallization treatments for the various alloys are presented in Table IV.

Structural Conditions of the Alloys

Photomicrographs in Figures 2-5 show the structures of the various alloys in the conditions tested (see also Table III). The recrystallization treatments were selected to produce nearly equivalent grain sizes (g. s.) in the two tungsten materials (g. s. $\simeq$ 0.12 mm) and three Mo-TZM alloys (g. s. $\simeq$ 0.20 mm). Increasing the nominal carbon content in tungsten from 10 to 35 ppm caused no noticeable structural changes at 100X (Figure 2). However optical examination at 1000X revealed occasional grain-boundary precipitates (presumably carbides) in the higher carbon tungsten, but none in the low-carbon material.

Increasing the carbon content of Mo-TZM resulted in a marked increase in the amount of carbide precipitate present both in the matrix and at grain boundaries of recrystallized alloys (Figure 4). No identification of the carbides was made in this study; however earlier work of Chang and Perlmutter[12] on a similar alloy (Mo-TZC) showed the precipitates in this class of alloys to be Mo_2C, TiC, and ZrC.

TABLE I. CHEMICAL ANALYSES OF Mo-TZM ALLOYS (PPM BY WEIGHT)

	C	N	O	H	Zr(a)	Ti(a)	Fe	W	V	Si
					Low Carbon					
Ingot Analyses (Universal Cyclops)	10	6	24	<1	0.16	0.64	15	<100	<10	38
Rod Analyses (Universal Cyclops)	13	8	20	<1	--	--	--	--	--	--
Rod Analyses (Battelle)	7	2	3	<0.1	0.11	0.46	--	--	--	--
					Intermediate Carbon					
Ingot Analyses (Universal Cyclops)	100	3	33	<1	0.18	0.60	19	<100	<10	75
Rod Analyses (Universal Cyclops)	90	5	31	<1	--	--	--	--	--	--
Rod Analyses (Battelle)	110	<0.5	3	0.3	0.13	0.50	--	--	--	--
					High Carbon					
Ingot Analyses (Universal Cyclops)	160	1	18	3	0.09	0.46	15	--	--	35
Rod Analyses (Universal Cyclops)	180	3	2	2	--	--	--	--	--	--
Rod Analyses (Battelle)	200	2	9	0.5	0.11	0.48	--	--	--	--

(a) Composition of titanium and zirconium are in weight percent.

TABLE II. CHEMICAL ANALYSES OF TUNGSTEN MATERIALS (PPM BY WEIGHT)

	C	N	O	H	Si	Fe	Ti	Ni	Mo
					Low Carbon				
Ingot Analyses (Universal Cyclops)	20	9	8	1.3	<20	4	<1	3	75
Rod Analyses (Universal Cyclops)	15	11	16	<1	--	--	--	--	--
Rod Analyses Battelle)	5	2	16	0.7	--	--	--	--	--
					High Carbon				
Ingot Analyses (Universal Cyclops)	75	8	10	1	<20	4	--	2	15
Rod Analyses (Universal Cyclops)	33	7	12	<1	--	--	--	--	--
Rod Analyses (Battelle)	34	0.7	8	0.5	--	--	--	--	--

TABLE III. MATERIALS AND CONDITIONS TESTED

Material	Condition	Strain Rate, min^{-1}	Nominal Test Temp Range, C
Low-carbon tungsten (10 ppm C)	Wrought stress relieved (as received)	0.01, 2, 600	350 - 1800
	Recrystallized, 2 hr, 2000 C, furnace cooled (g. s. = 0.14 mm)[a]	0.01, 2, 600	350 - 1800
High-carbon tungsten (35 ppm C)	Recrystallized, 1 hr, 2000 C, furnace cooled (g. s. = 0.11 mm)	2	350 -1800
Low-carbon Mo-TZM (10 ppm C)	Wrought stress relieved, (as received)	0.01, 2, 600	200 - 1550
	Recrystallized, 1 hr, 2000 C, furnace cooled (g. s. = 0.19 mm)	0.01, 2, 600	200 - 1850
Intermediate-carbon Mo-TZM (100 ppm C)	Recrystallized, 1 hr, 2000 C, furnace cooled (g. s. = 0.20 mm)	0.01, 2, 600	200 - 1850
High-carbon Mo-TZM (190 ppm C)	Wrought stress relieved, (as received)	0.01, 2, 600	200 - 1550
	Recrystallized, 1 hr, 2100 C, furnace cooled, (g. s. = 0.23 mm)	0.01, 2, 600	200 - 1850
	Recrystallized, 1 hr, 2100 C; quenched into molten tin at 250 C (g. s. = 0.23 mm)	2	200 - 1850
	Recrystallized, 1 hr, 2100 C; quenched into molten tin at 250 C; aged 100 hr, 1300 C, (g. s. = 0.23 mm)	2	200 - 1700

(a) g.s. = grain size, i.e., average grain diameter as measured by the lineal intercept method.

TABLE IV. EFFECT OF VACUUM-ANNEALING TEMPERATURE (1 HOUR, UNLESS OTHERWISE SPECIFIED) ON HARDNESS AND GRAIN SIZE OF Mo-TZM AND TUNGSTEN

Temperature, C	Mo-TZM					
	Low Carbon (10 PPM)		Intermediate Carbon (100 PPM)		High Carbon (190 PPM)	
	VHN	Grain Size, mm	VHN	Grain Size, mm	VHN	Grain Size, mm
As received	204	Wrought	271	Wrought	273	Wrought
1200	199	Wrought	263	Wrought	263	Wrought
1400	194	Wrought	244	Wrought	248	Wrought
1600	159	0.087	185	0.041	192	0.025
1800	158	0.13	169	0.052	179	0.033
2000	154	0.19	166	0.20	167	0.079
2100	--	--	--	--	153	0.23
2200	157	0.39	--	--	152	0.32

	Tungsten			
	Low Carbon (10 PPM)		High Carbon (35 PPM)	
	VHN	Grain Size mm	VHN	Grain Size, mm
As received	439	Wrought	444	Wrought
1200	430	Wrought	--	--
1600	359	0.040	351	0.063
1800	--	--	347	0.082
2000	352	0.078	345	0.11
2000 (2 hr)	354	0.14	--	--
2000 (8 hr)	303	0.17	--	--
2100	--	--	341	0.17
2200	--	--	332	0.27
2300	339	0.27	--	--

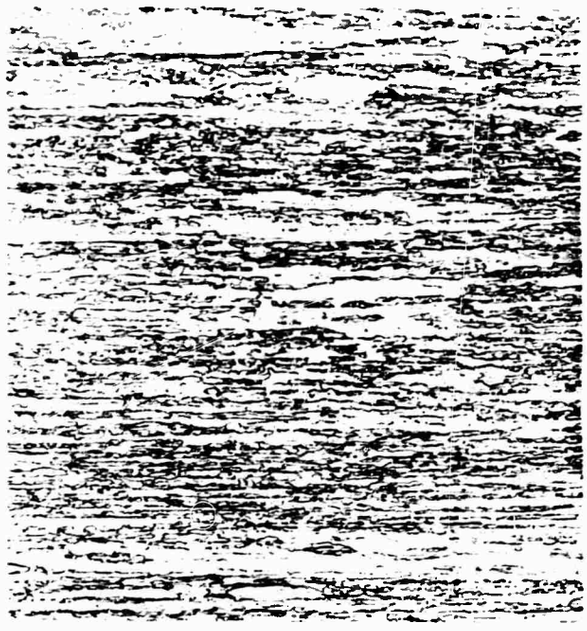

100X 17325

a. Wrought-Stress-Relieved Low Carbon (10 Ppm C, As Received)

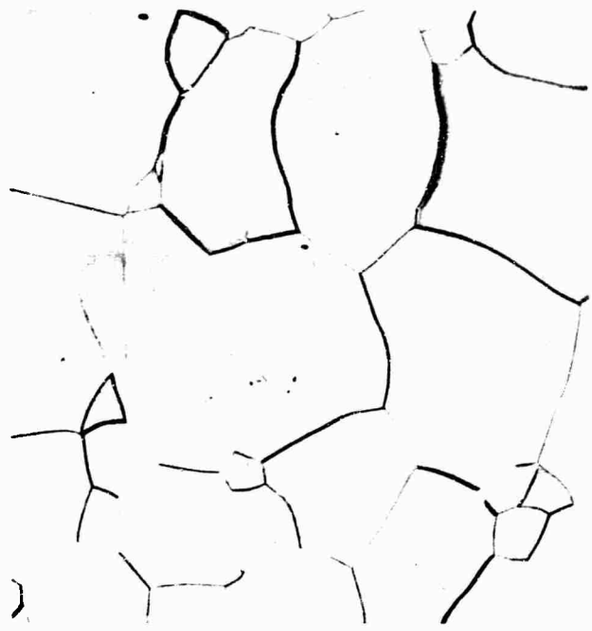

100X 17392

b. Recrystallized Low Carbon (10 Ppm C)

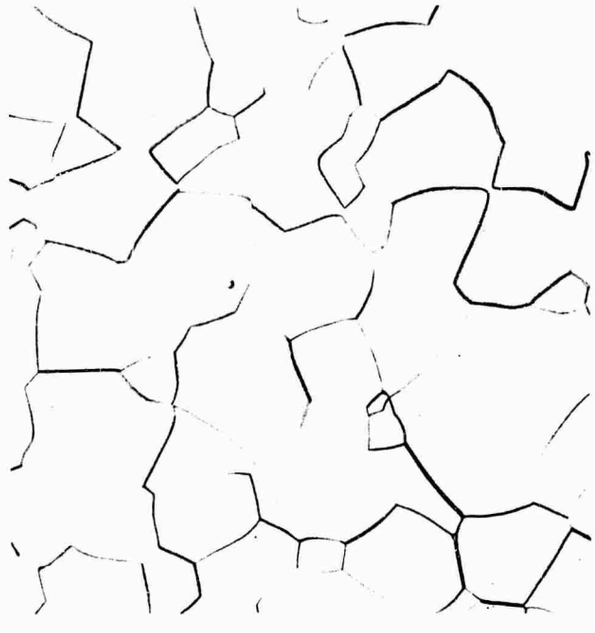

100X 29096

c. Recrystallized High Carbon (35 Ppm C)

FIGURE 2. MICROSTRUCTURES OF TUNGSTEN MATERIALS

See Table III for heat treatments.

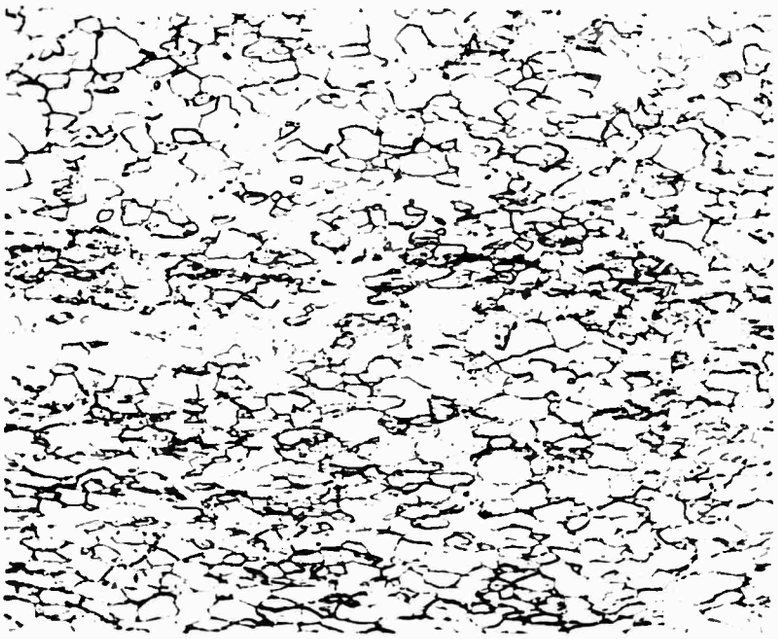

100X 23743

a. Low Carbon (10 Ppm C)

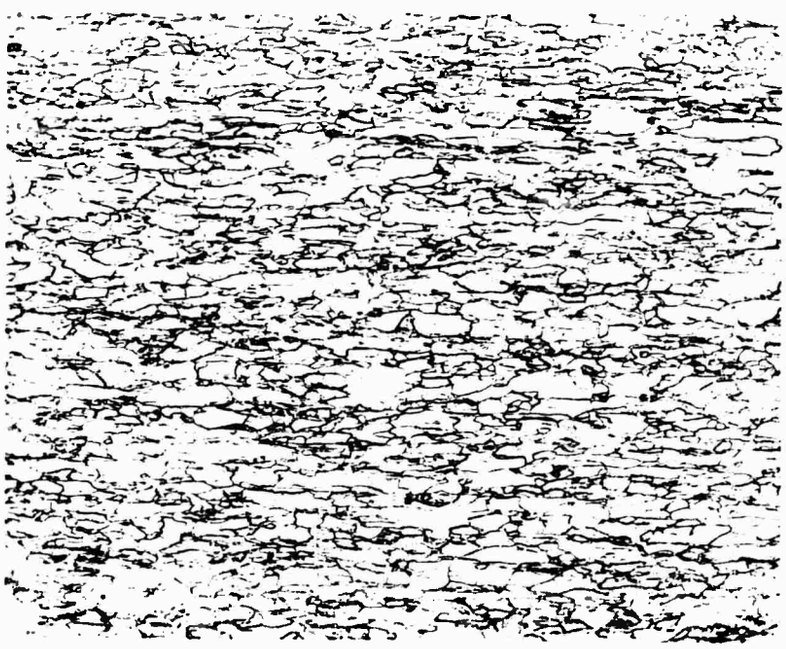

100X 23745

b. High Carbon (190 Ppm C)

FIGURE 3. MICROSTRUCTURES OF WROUGHT-STRESS-RELIEVED (AS RECEIVED) Mo-TZM ALLOYS

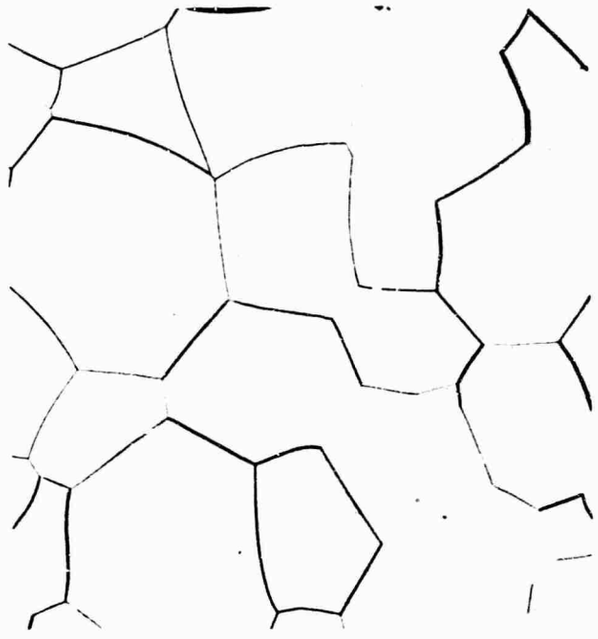

100X 23744

a. Low Carbon (10 Ppm C)

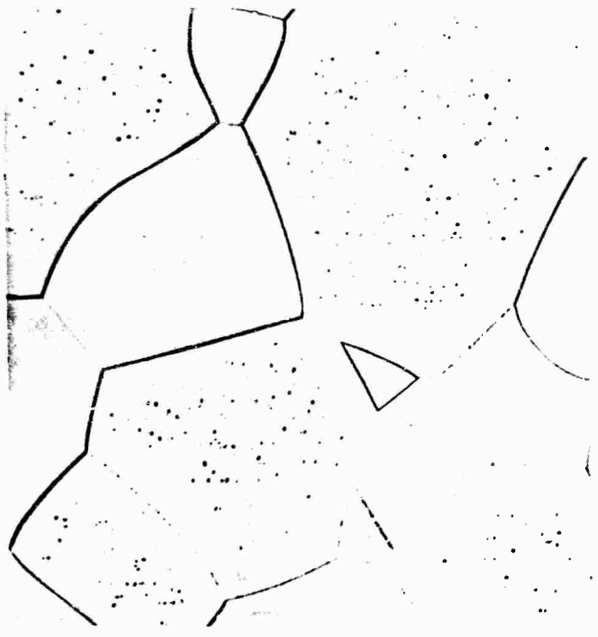

100X 23746

b. Intermediate Carbon (100 Ppm C)

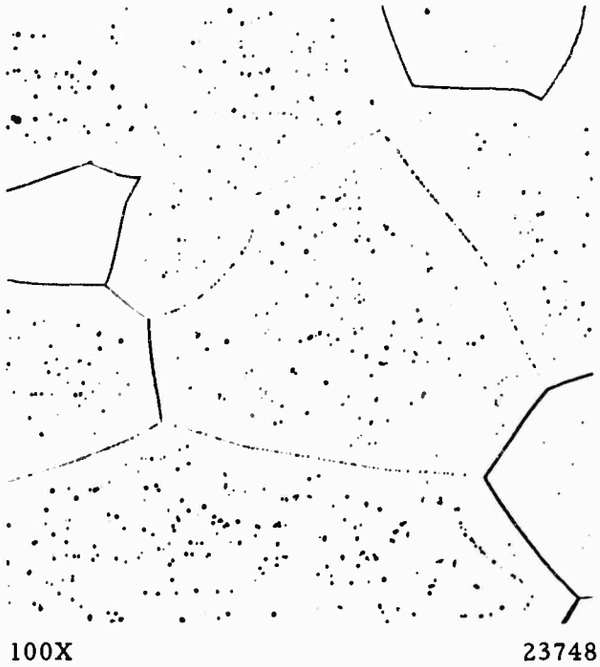

100X 23748

c. High Carbon (190 Ppm C)

FIGURE 4. MICROSTRUCTURES OF RECRYSTALLIZED Mo-TZM ALLOYS

See Table III for heat treatments.

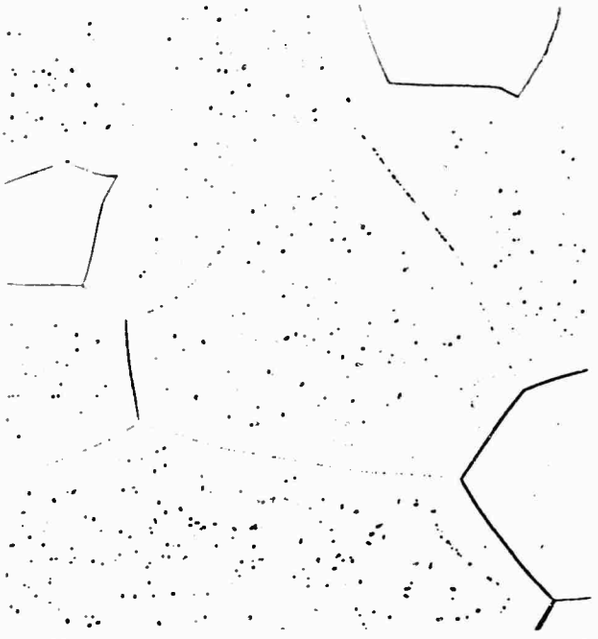

100X 23748

a. Recrystallized, Furnace Cooled

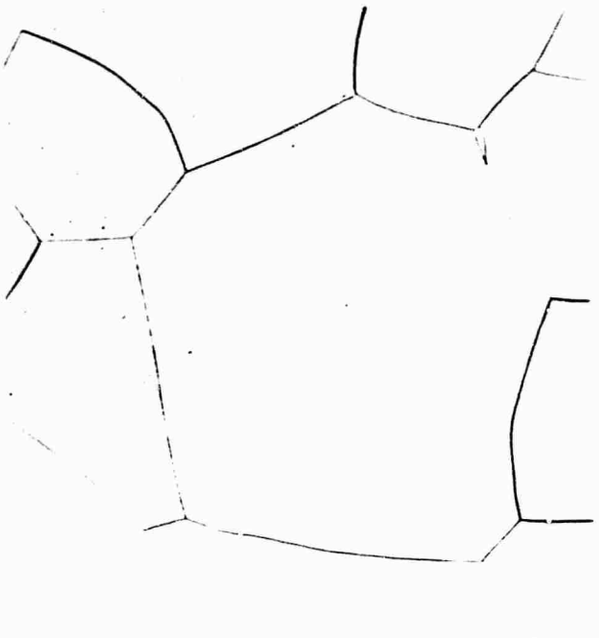

100X 23749

b. Recrystallized, Quenched

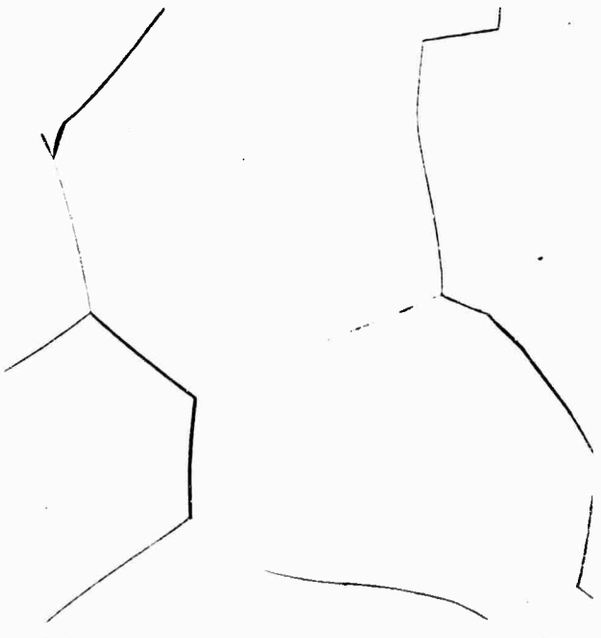

100X 24628

c. Recrystallized, Quenched, Aged

FIGURE 5. MICROSTRUCTURES OF HIGH CARBON (190 PPM C) Mo-TZM AFTER DIFFERENT HEAT TREATMENTS

See Table III for heat treatments.

In order to investigate the effect of heat treatment on the structure of the high-carbon Mo-TZM (190 ppm carbon), specimens were vacuum annealed 1 hour at 2100 C and quenched into molten tin (at 250 C). Various samples were then aged at 1300 and 1500 C for 1, 10, and 100 hr. The aging response, as measured by hardness, is shown in Table V. Aging for 100 hr at 1300 C produced the maximum hardness increase, and hence this treatment was used for the quenched-plus-aged tensile samples.

TABLE V. HARDNESS AS A FUNCTION OF AGING TIME AND TEMPERATURE FOR HIGH-CARBON Mo-TZM (190 PPM C) QUENCHED FROM 2100 C INTO MOLTEN TIN

Aging Temp, C	Aging Time, hours	VHN[a] (10-Kg Load)	VHN (Quenched Plus Aged) Minus VHN (As Quenched)
As quenched	--	198.3	--
1300	1	199.2	+ 0.9
1300	10	210.2	+ 11.9
1300	100	214.7	+ 16.4
1500	1	205.4	+ 7.1
1500	10	208.6	+ 10.3
1500	100	195.5	- 2.8

(a) The VHN of this material (recrystallized 1 hour, 2100 C, and furnace cooled) was 152.8. Aging as above caused no hardness change.

The effect of heat treatment on the microstructure of the high-carbon Mo-TZM is illustrated in Figure 5. The recrystallized-plus-furnace-cooled material had numerous "coarse" precipitates (shown at 100X, Figure 5a); whereas the quenched and quenched-plus-aged specimens showed a very fine distribution of precipitates barely resolvable at 1500X in the optical microscope. Transmission electron micrographs of the quenched and quenched-plus-aged materials, however, revealed the character and distribution of the very fine precipitates [see Figure 6(a, b), quenched, and Figure 6(c, d), quenched plus aged]. In the quenched specimens the precipitates ranged in size (diameter) from 270 to 1330 Å, and an average particle diameter of $2r_v = 560$ Å was measured from the electron micrographs. Using standard quantitative metallography[13, 14], the mean planar center-to-center particle separation, d, was determined from the formula

$$d^2 = \frac{8\, r_v^2}{3\, f} \quad , \tag{1}$$

where f is the volume fraction of precipitate, and r_v is the average precipitate radius. The volume fraction is related to the number of particles per unit volume, N_v, by

$$f = N_v \cdot \frac{4}{3} \pi\, r_v^3 \tag{2}$$

and N_v can be measured from electron micrographs by counting the total number of particles, N_T, in a given micrograph of Area A, and applying the relation

$$N_v = \frac{N_T\, (\text{mag.})^2}{tA} \quad , \tag{3}$$

where t is the foil thickness.

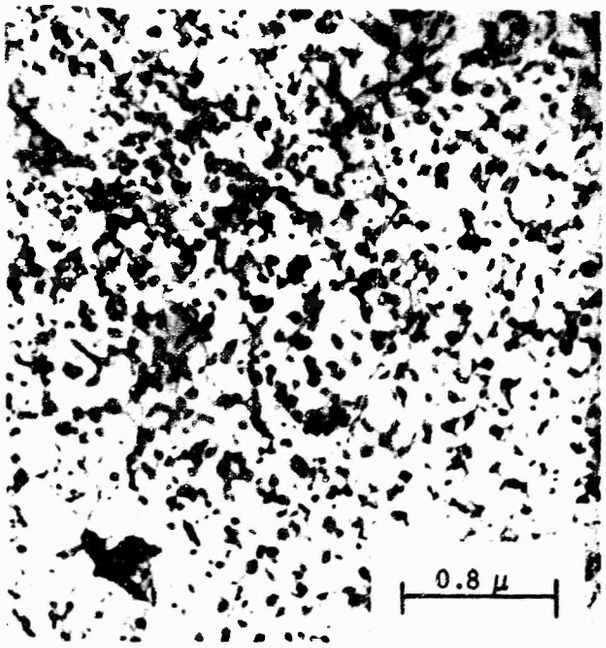

a. Annealed 1 Hr at 2100 C, Quenched Into Molten Tin

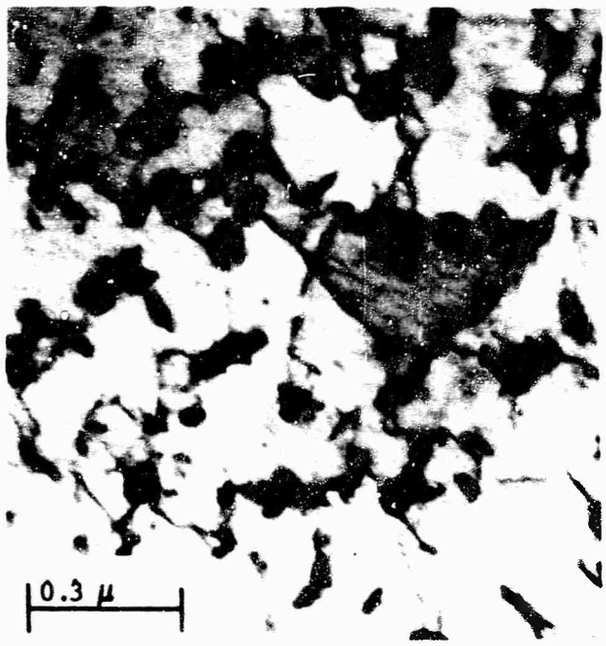

b. Annealed 1 Hr at 2100 C, Quenched Into Molten Tin

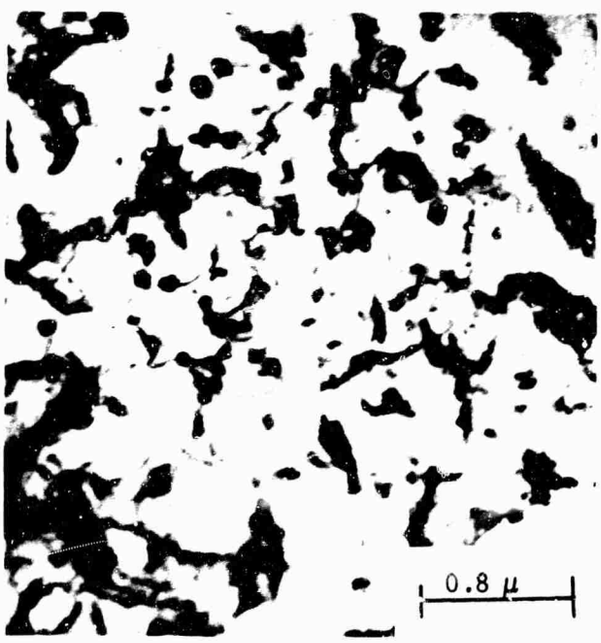

c. Annealed 1 Hr at 2100 C, Quenched Into Molten Tin, Aged 100 Hr at 1300 C

d. Annealed 1 Hr at 2100 C, Quenched Into Molten Tin; Aged 100 Hr at 1300 C

FIGURE 6. TRANSMISSION ELECTRON MICROGRAPHS OF HIGH CARBON Mo-TZM (190 PPM C)

Combining Equations (1), (2), and (3) gives d in terms of measurable parameters, t, A, N_T, and r_v.

$$d^2 = \frac{2\,t\,A}{\pi N_T\, r_v\, (\text{mag.})^2} \quad . \tag{4}$$

The above parameters were determined from a series of electron micrographs, and the mean planar center-to-center particle separation in the as-quenched condition was found to be d = 3130 Å, taking the foil thickness as 2000 Å.

Figure 6(a and b) show that the as-quenched material has a number of dislocations threading the particles. Presumably these were generated during the quench by macroscopic quenching strains, or possibly by the precipitates acting as dislocation sources during the rapid cooling. Aging at 1300 C for 100 hours caused the precipitates to coarsen from 560 Å to ~2000-3000 Å (Figure 6c and d), and those dislocations present in the as-quenched condition were strongly locked in place during aging, by precipitation along the dislocation lines.

Testing

Tensile specimens of all the alloys were machined (in the wrought condition) with a 1/2-inch gage length, a 1/8-inch gage diameter, and threaded ends (Figure 7). Three strain rates were used in testing: 0.01, 2, and 600 min^{-1}. Tests at the two lower rates were done in an Instron, and the high-strain-rate tests were made in a Krafft-Hahn Dynamic Loader[15]. A vacuum Brew resistance furnace (Figure 8) was used in conjunction with the Instron for tests over the temperature range 200-1300 C. It was necessary to use an electron beam furnace (Figure 9) with the Instron for higher temperatures. The electron beam heating is very rapid, and therefore particularly useful for high-temperature tests on wrought-stress-relieved material, where it is desirable to minimize recovery and recrystallization during testing.

Temperature was measured in the Brew furnace by attaching thermocouples to the specimen gage length (Chromel/Alumel for T < 900 C, and Pt-Pt/10Rh for T > 900 C). Details of the temperature measurement procedure for the electron beam furnace have been presented elsewhere[16], but are briefly reviewed in Appendix I. Vacuum induction heating was employed for the high-temperature tests in the Krafft-Hahn Dynamic Loader (for $\dot{\epsilon}$ = 600 min^{-1}). Figure 10 is a photograph of this apparatus, and experimental details are given in Appendix II.

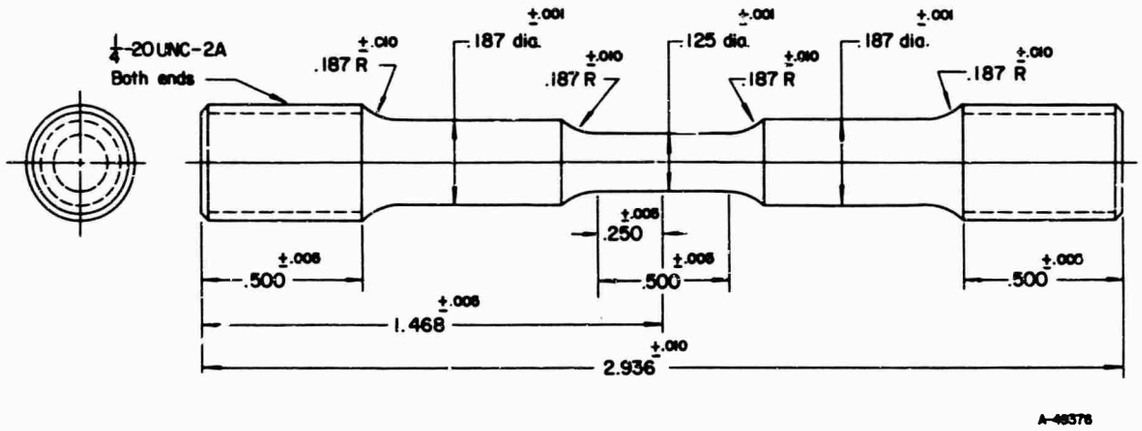

FIGURE 7. TENSILE SPECIMEN CONFIGURATION

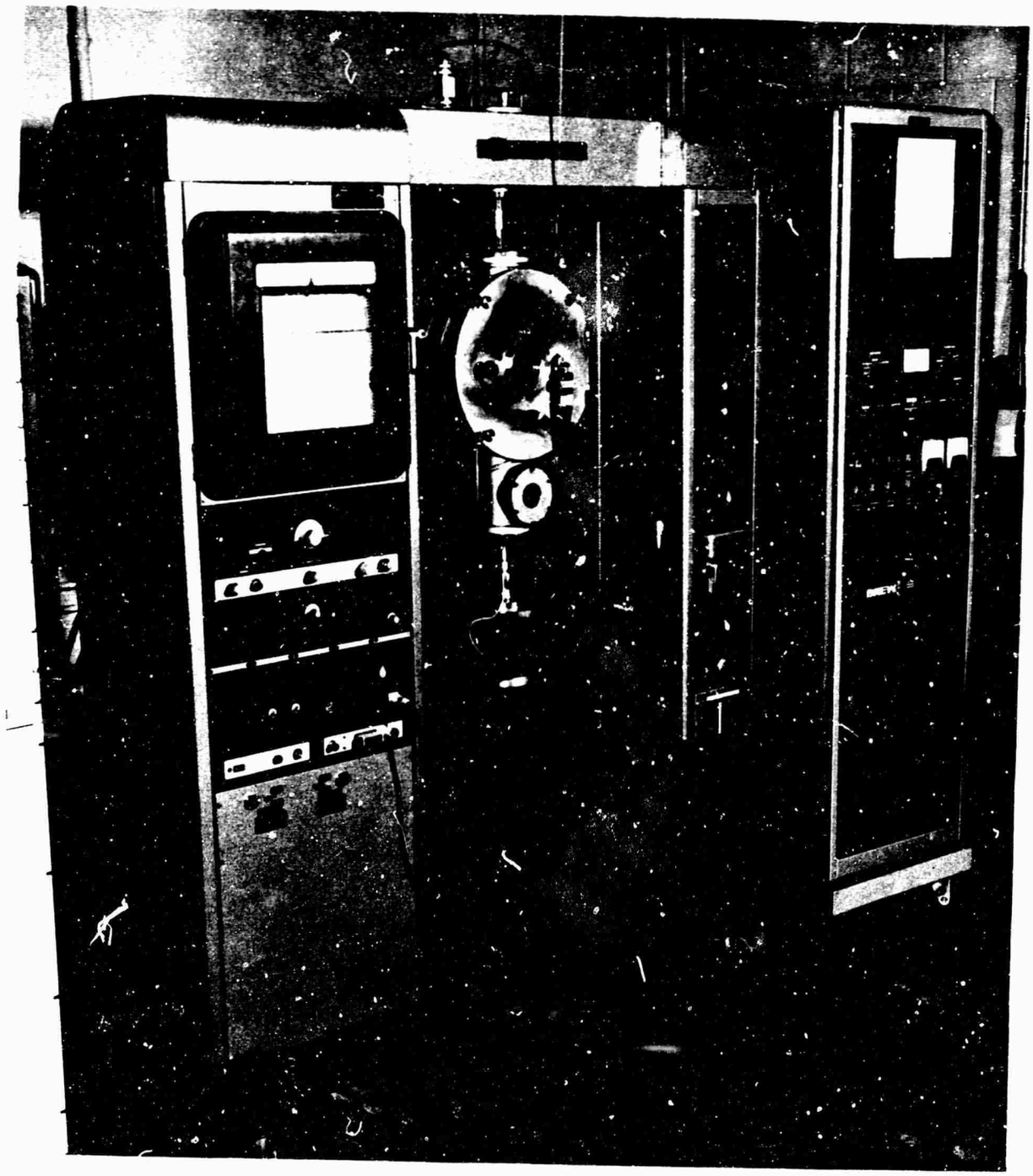

FIGURE 8. ELEVATED-TEMPERATURE BREW VACUUM FURNACE ATTACHED TO INSTRON TESTING MACHINE

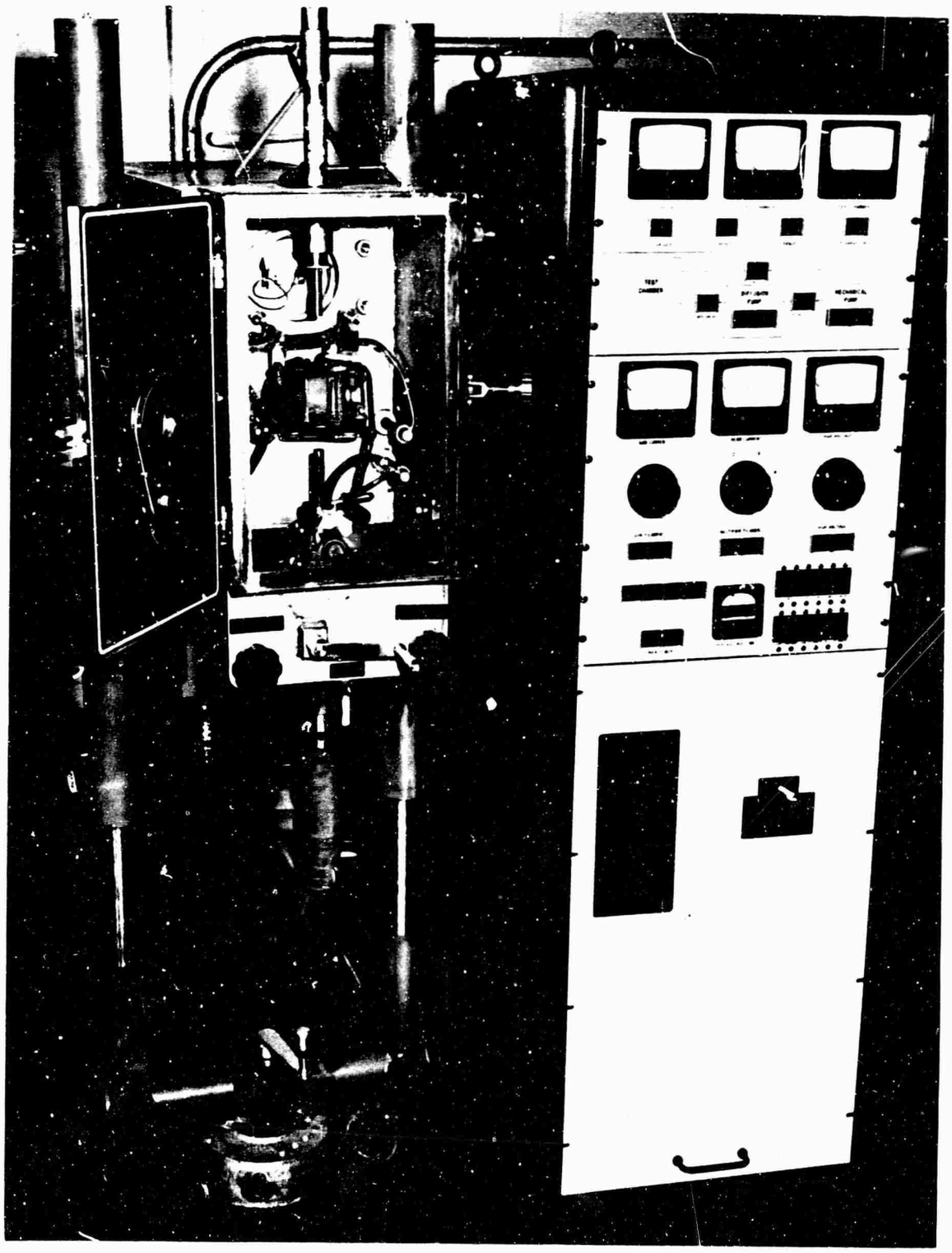

FIGURE 9. ELECTRON-BEAM VACUUM FURNACE WHICH WAS USED IN INSTRON FOR ELEVATED-TEMPERATURE TESTING

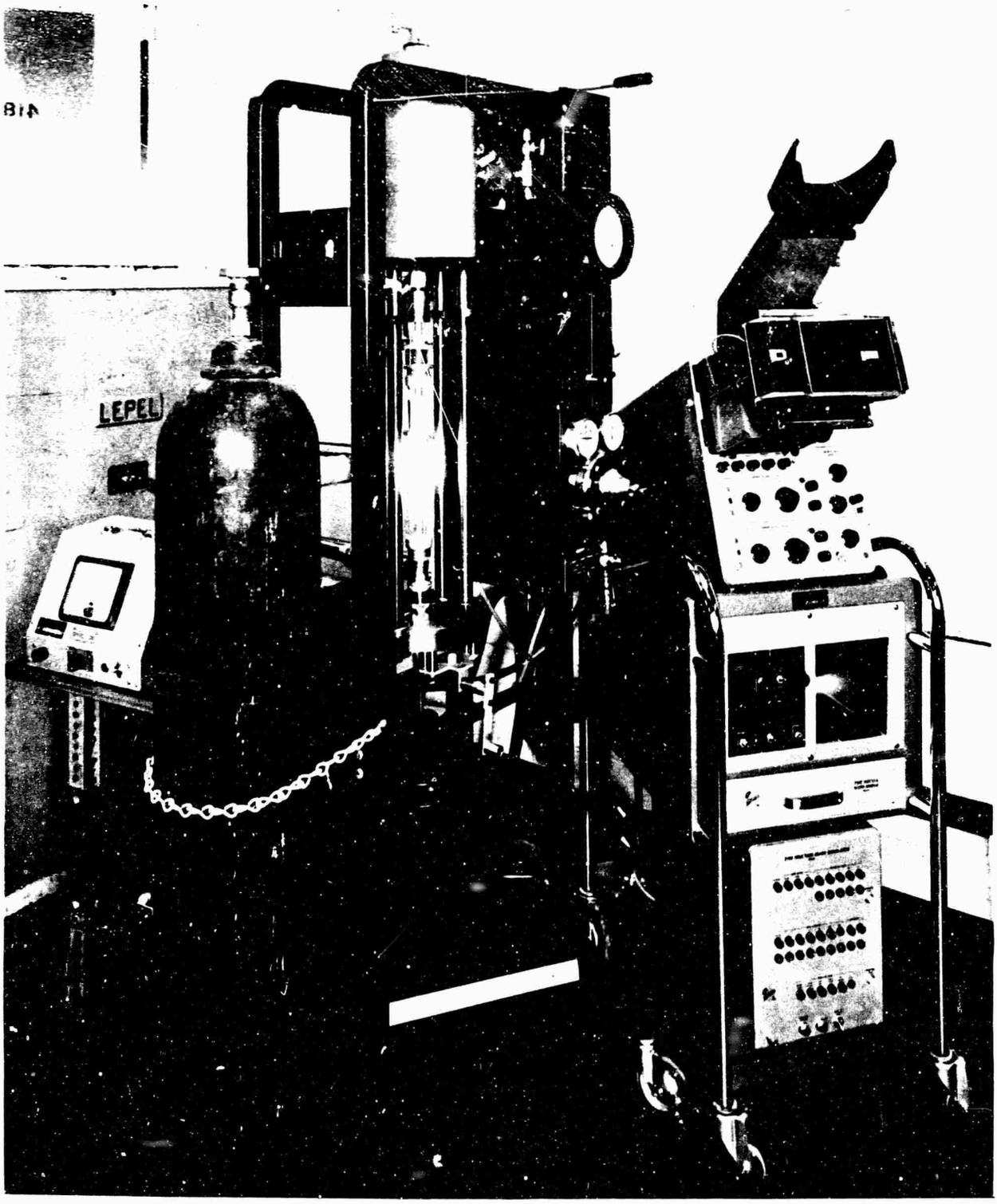

FIGURE 10. KRAFFT-HAHN DYNAMIC LOADER AND ACCESSORIES, WITH VACUUM INDUCTION HEATING ATTACHMENT

SUMMARY OF TENSILE STUDY RESULTS

For purposes of simplification all mechanical-property data are tabulated in Appendix III (Tables X through XVIII) together with individual property versus test-temperature plots for the various materials and test conditions (Figures 40 through 63). Tables X through XVIII also contain descriptions of the deformation characteristics of each specimen tested. In order to facilitate comparisons of the effects of strain rate, carbon content, and structure, summary comparative plots are shown in Figure 11-25, with data points omitted for clarity. In the case of wrought-stress-relieved materials, ultimate strength is not shown in these plots, since often the yield strength was identical with the ultimate strength. However the UTS data are reported in Tables X through XVIII.

Tungsten

Figures 11 and 12	Effect of strain rate
Figure 13	Effect of carbon content

Mo-TZM

Figures 14, 15, 19, 20, and 21	Effect of strain rate
Figures 16, 17, 18, 22, 23, and 24	Effect of carbon content
Figure 25	Effect of heat treatment (structure)

DISCUSSION

Tungsten

Previous work on tungsten by various investigators (see Figure 1) indicated a temperature region of slightly reduced ductility at ~500 C. Some indication of a strength peak in this general temperature range was also observed[3]. By comparison with other bcc metals, it appeared possible that some dynamic strengthening process (e.g., strain aging[17], Snoek ordering[18], or precipitation during deformation) was occurring. Since these processes are thermally activated, the effects should be strain rate dependent, and occur at higher temperatures with higher strain rates. Accordingly, wrought-stress-relieved and recrystallized specimens were tested at various temperatures (~350 - 1850 C) using three strain rates (0.01, 2, and 600 min^{-1}).

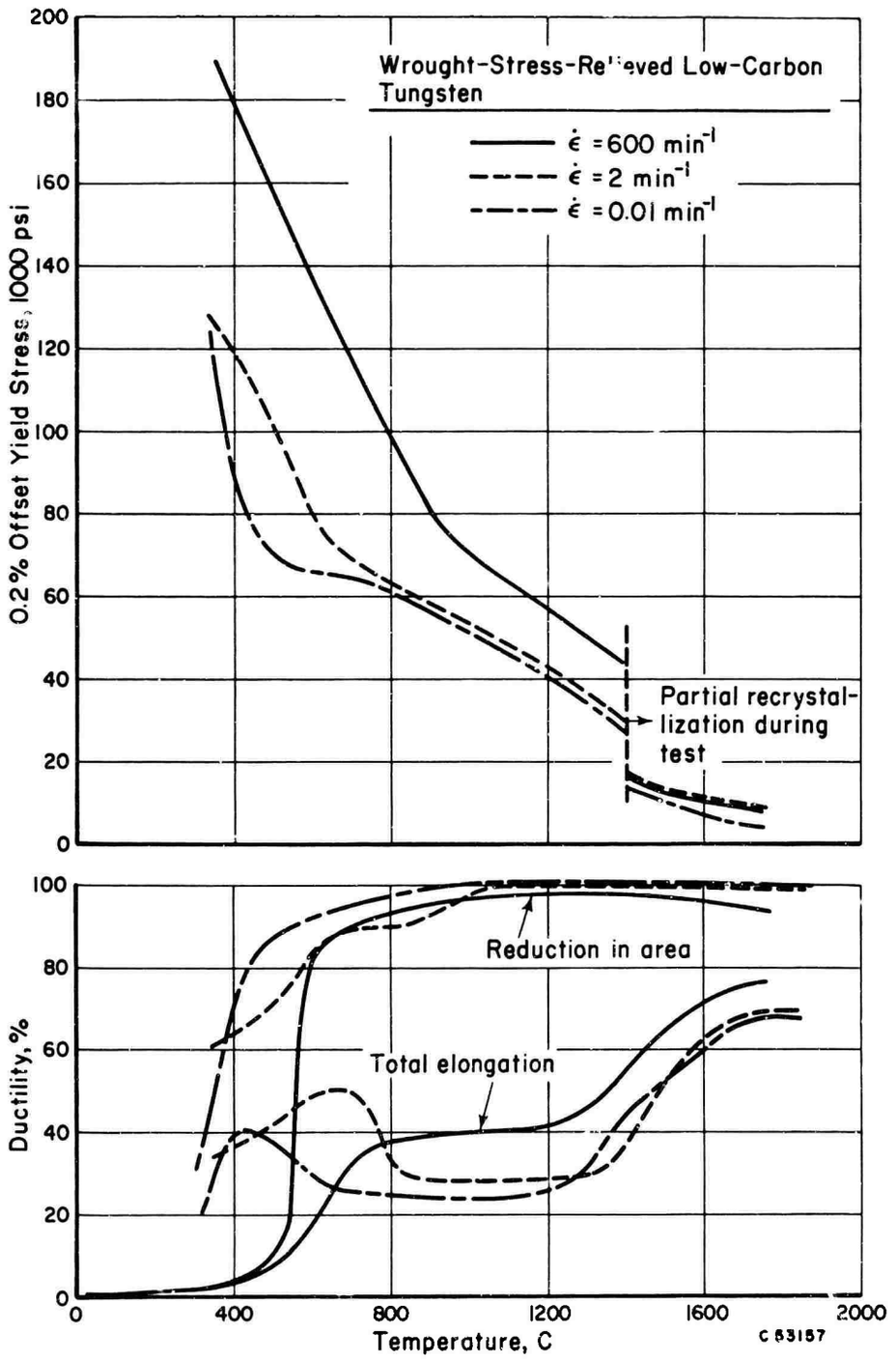

FIGURE 11. EFFECT OF STRAIN RATE ON MECHANICAL PROPERTIES OF WROUGHT-STRESS-RELIEVED LOW-CARBON (10 PPM CARBON) TUNGSTEN

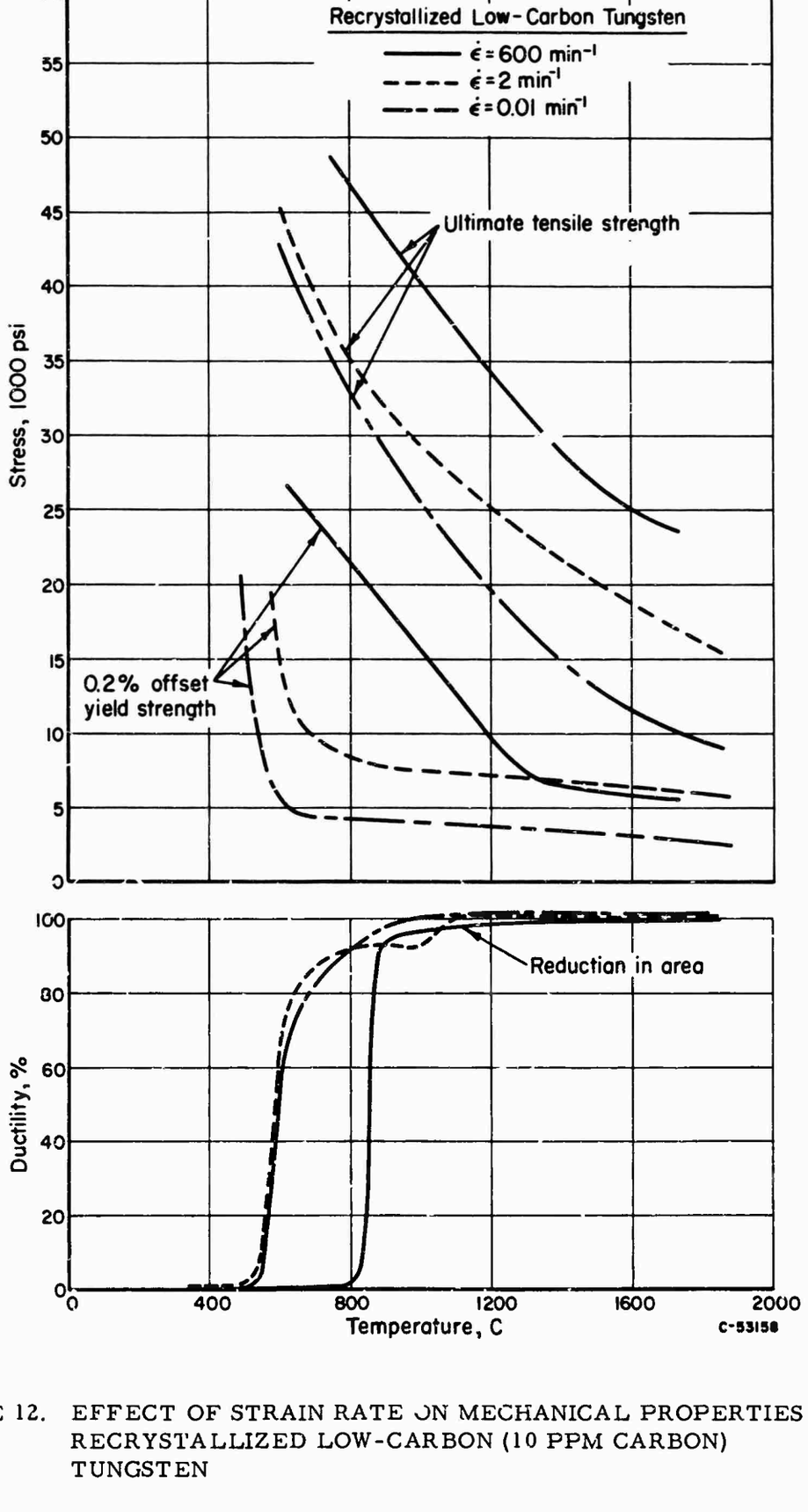

FIGURE 12. EFFECT OF STRAIN RATE ON MECHANICAL PROPERTIES OF RECRYSTALLIZED LOW-CARBON (10 PPM CARBON) TUNGSTEN

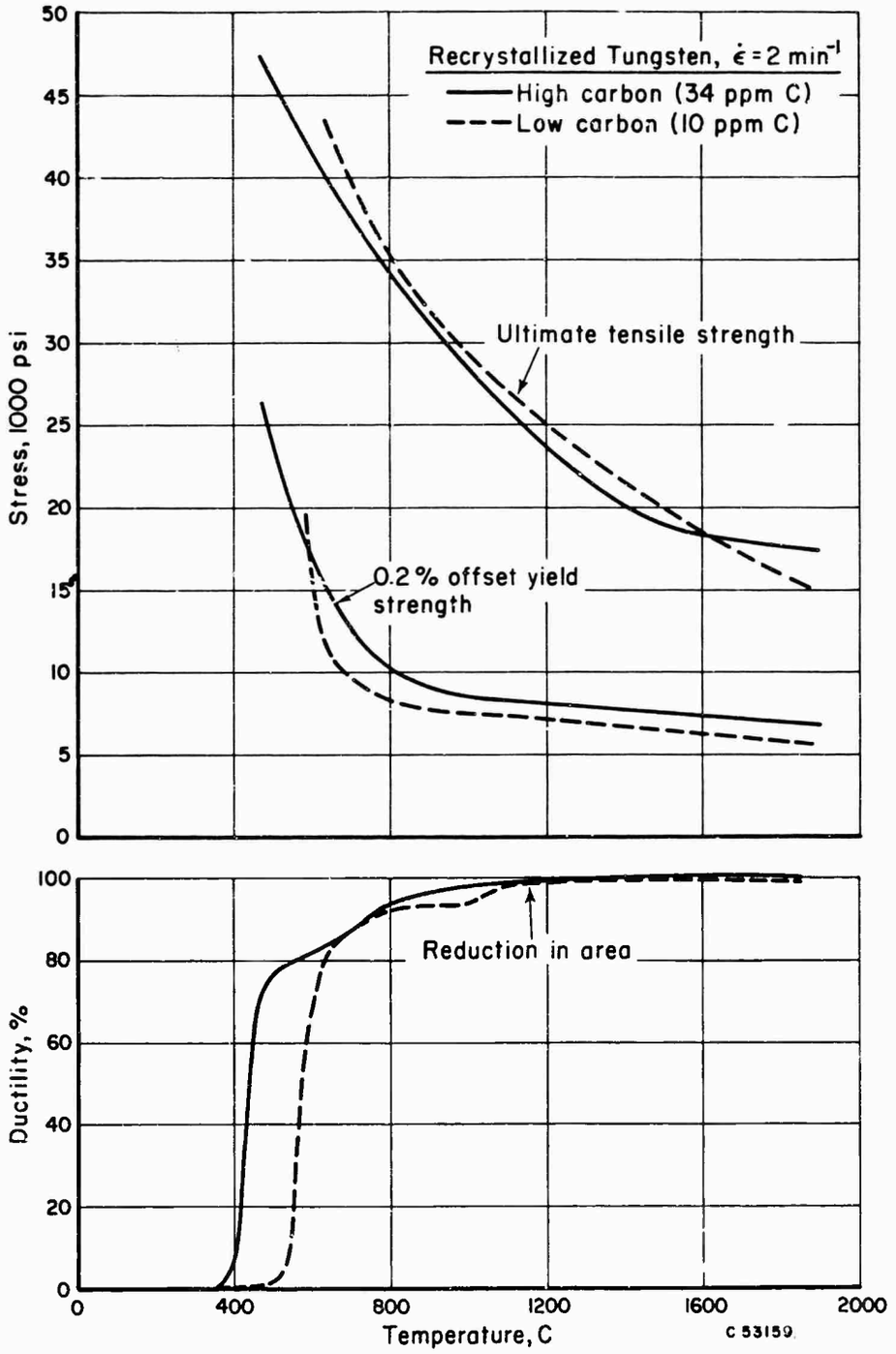

FIGURE 13. EFFECT OF CARBON CONTENT ON MECHANICAL PROPERTIES OF RECRYSTALLIZED TUNGSTEN, TESTED AT $\dot{\epsilon}$ = 2 MIN^{-1}

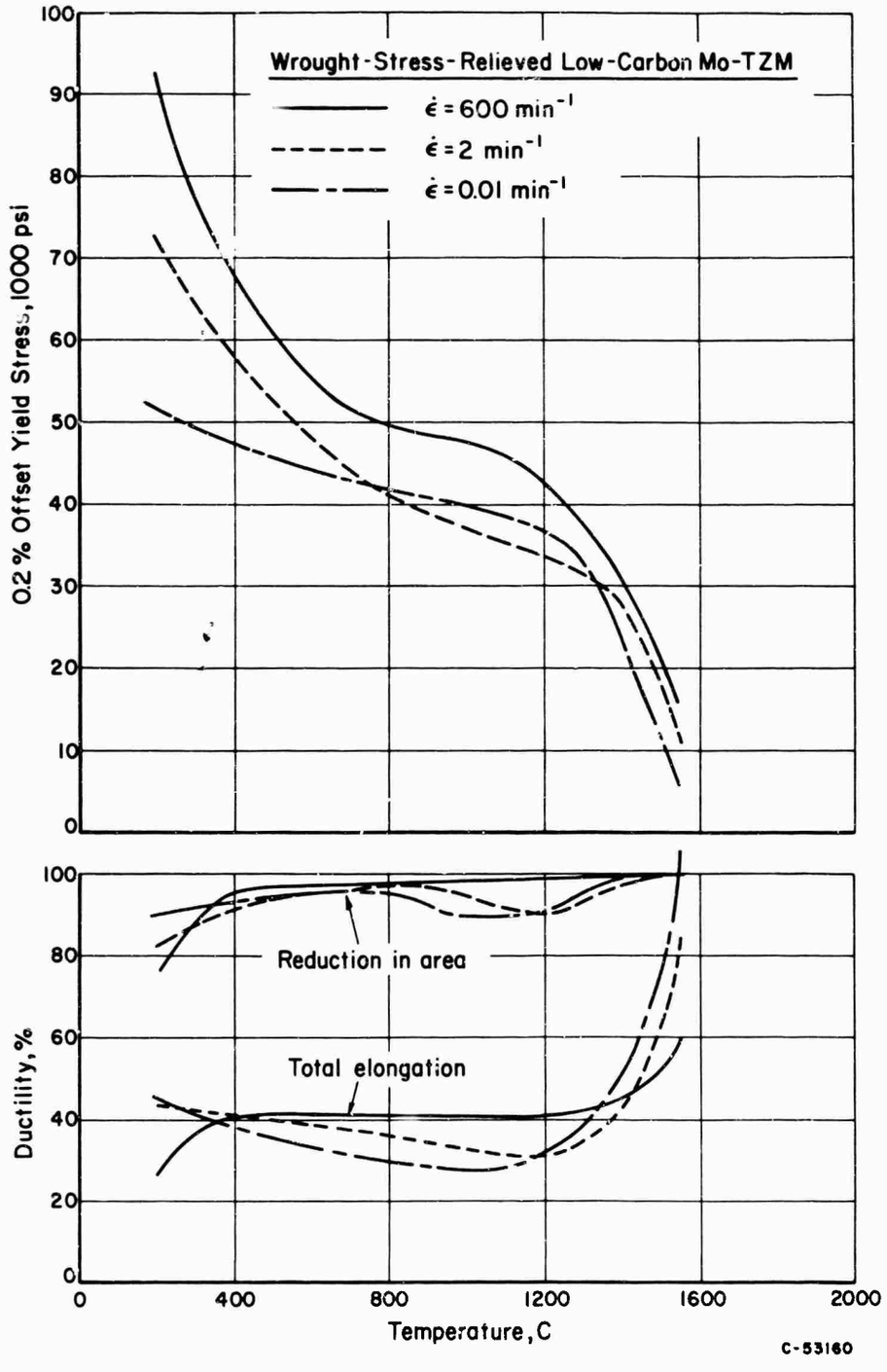

FIGURE 14. EFFECT OF STRAIN RATE ON MECHANICAL PROPERTIES OF WROUGHT-STRESS-RELIEVED LOW-CARBON (10 PPM CARBON) Mo-TZM

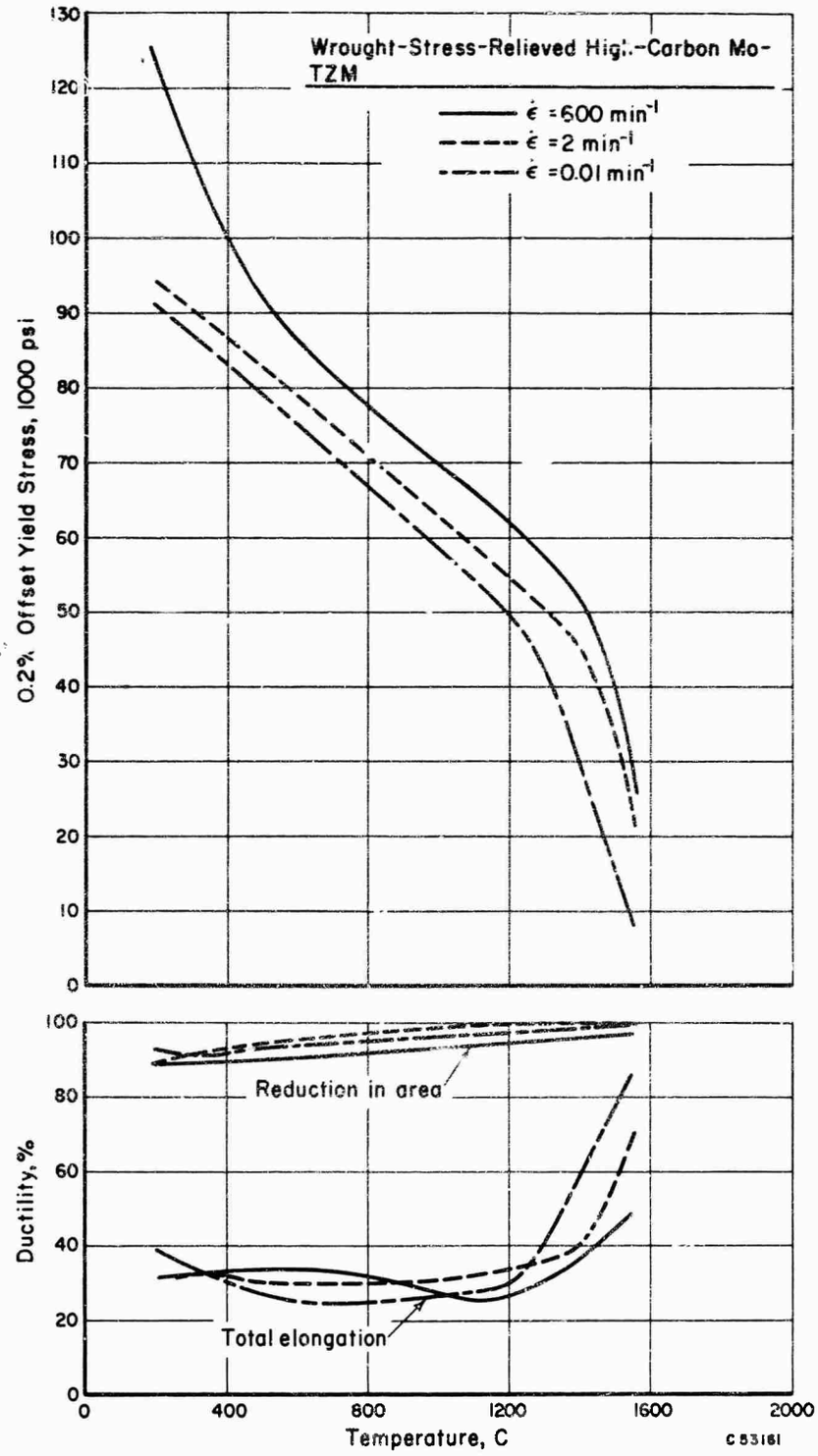

FIGURE 15. EFFECT OF STRAIN RATE ON MECHANICAL PROPERTIES OF WROUGHT-STRESS-RELIEVED HIGH-CARBON (190 PPM CARBON) Mo-TZM

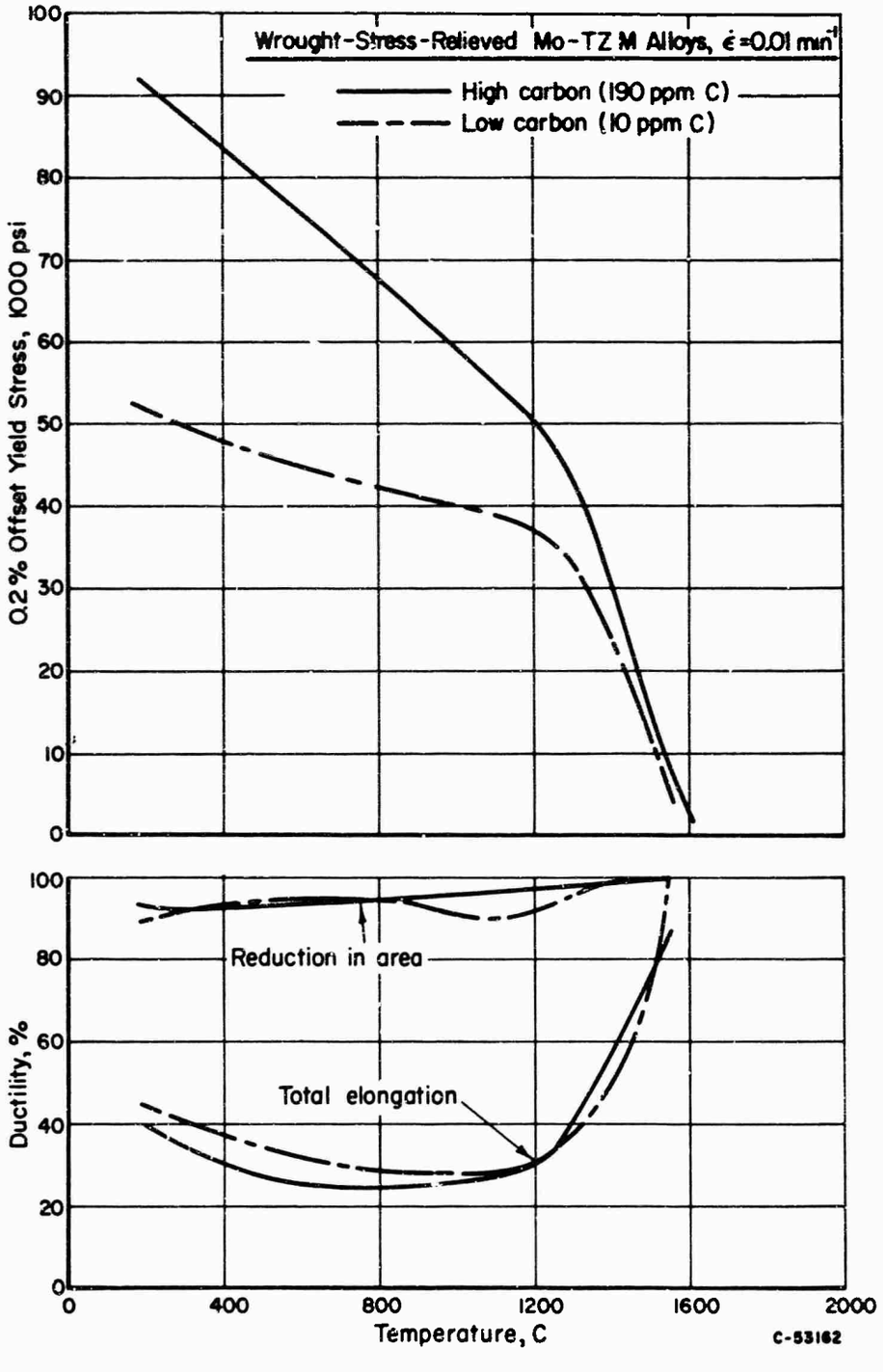

FIGURE 16. EFFECT OF CARBON CONTENT ON MECHANICAL PROPERTIES OF WROUGHT-STRESS RELIEVED Mo-TZM ALLOYS, TESTED AT $\dot{\epsilon}$ = 0.01 MIN^{-1}

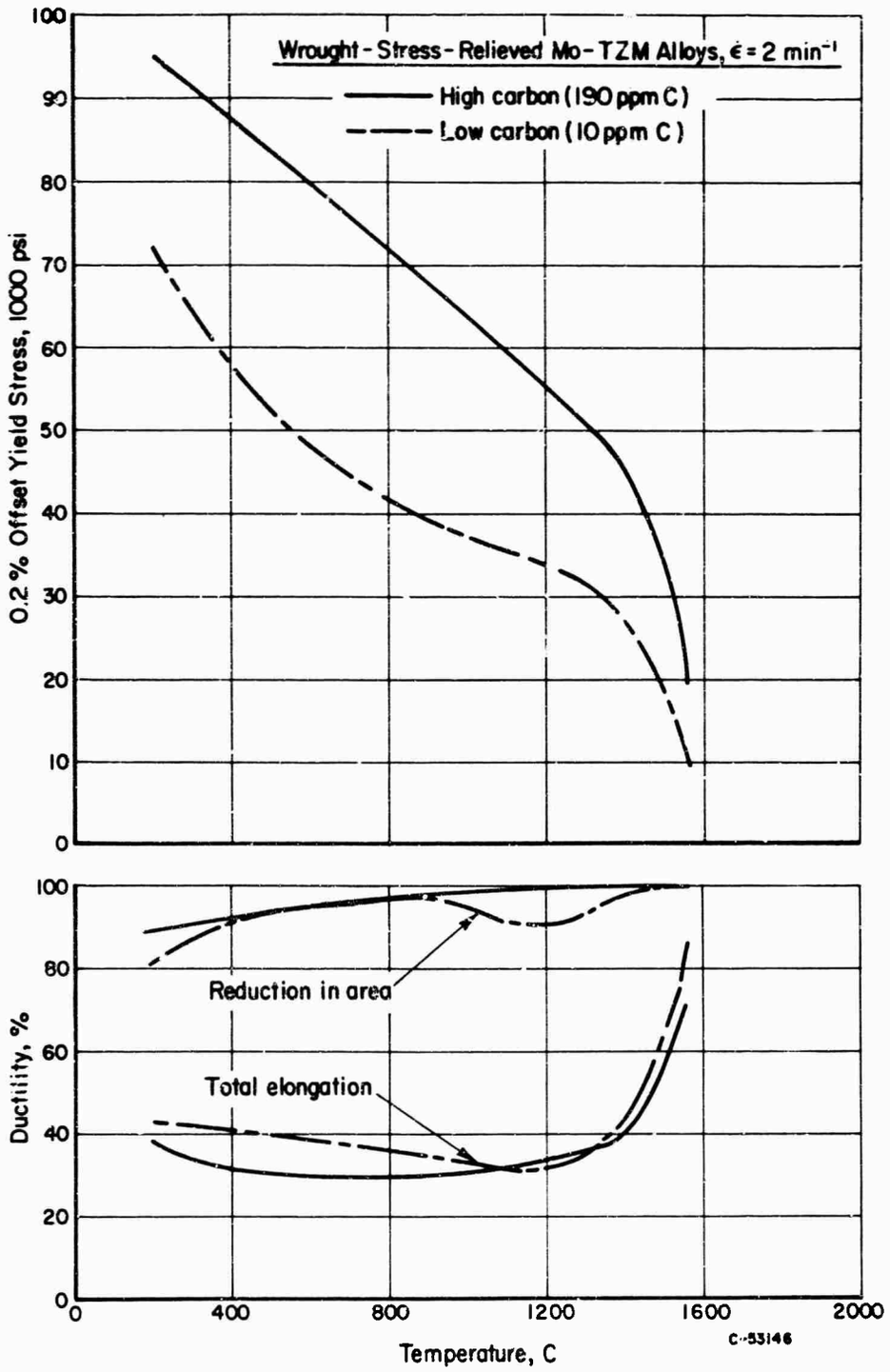

FIGURE 17. EFFECT OF CARBON CONTENT ON MECHANICAL PROPERTIES OF WROUGHT-STRESS-RELIEVED Mo-TZM ALLOYS, TESTED AT $\dot{\epsilon}$ = 2 MIN^{-1}

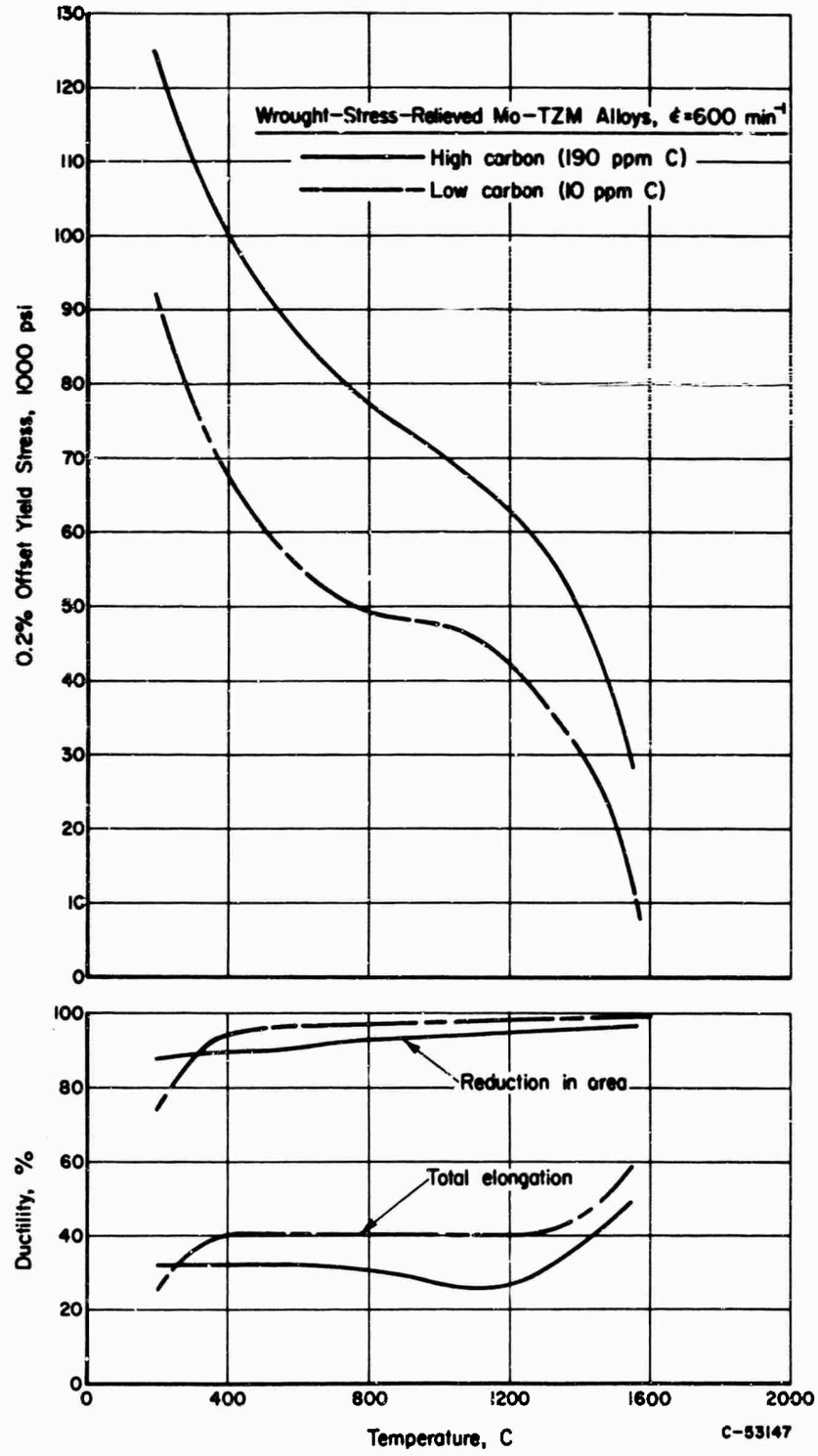

FIGURE 18. EFFECT OF CARBON CONTENT ON MECHANICAL PROPERTIES OF WROUGHT-STRESS-RELIEVED Mo-TZM ALLOYS TESTED AT $\dot{\epsilon}$ = 600 MIN^{-1}

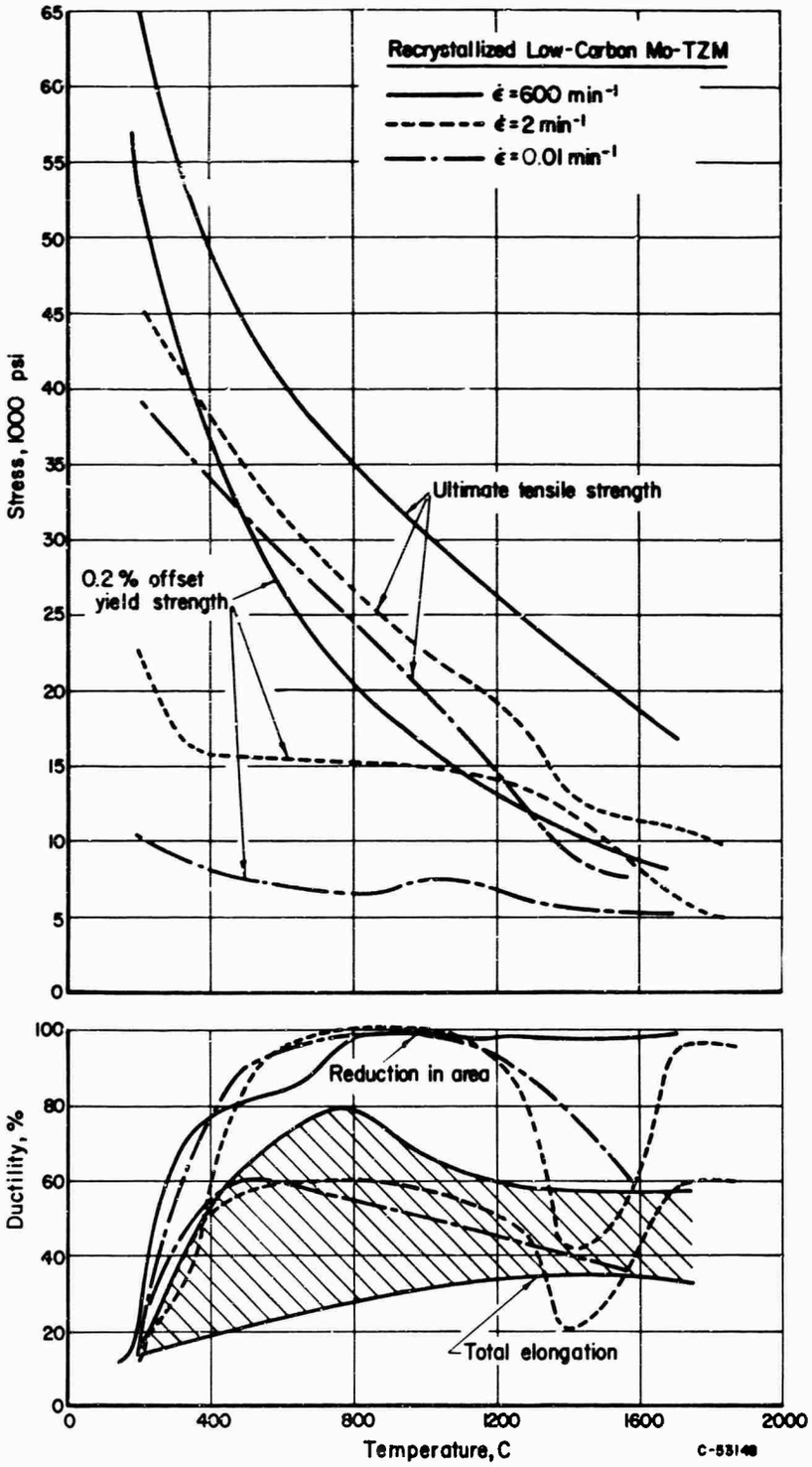

FIGURE 19. EFFECT OF STRAIN RATE ON MECHANICAL PROPERTIES OF RECRYSTALLIZED LOW-CARBON (10 PPM CARBON) Mo-TZM

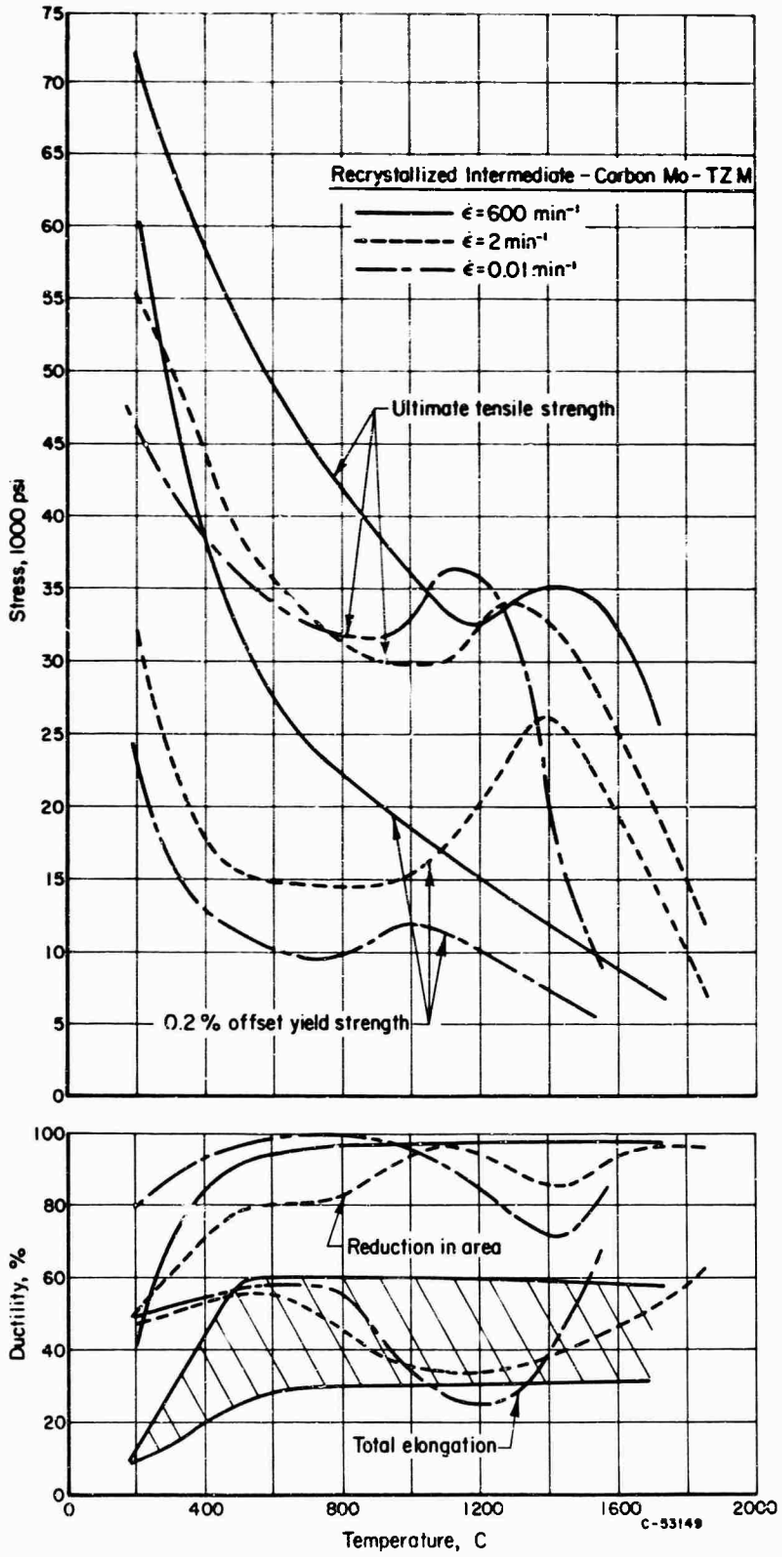

FIGURE 20. EFFECT OF STRAIN RATE ON MECHANICAL PROPERTIES OF RECRYSTALLIZED INTERMEDIATE-CARBON (100 PPM CARBON) Mo-TZM

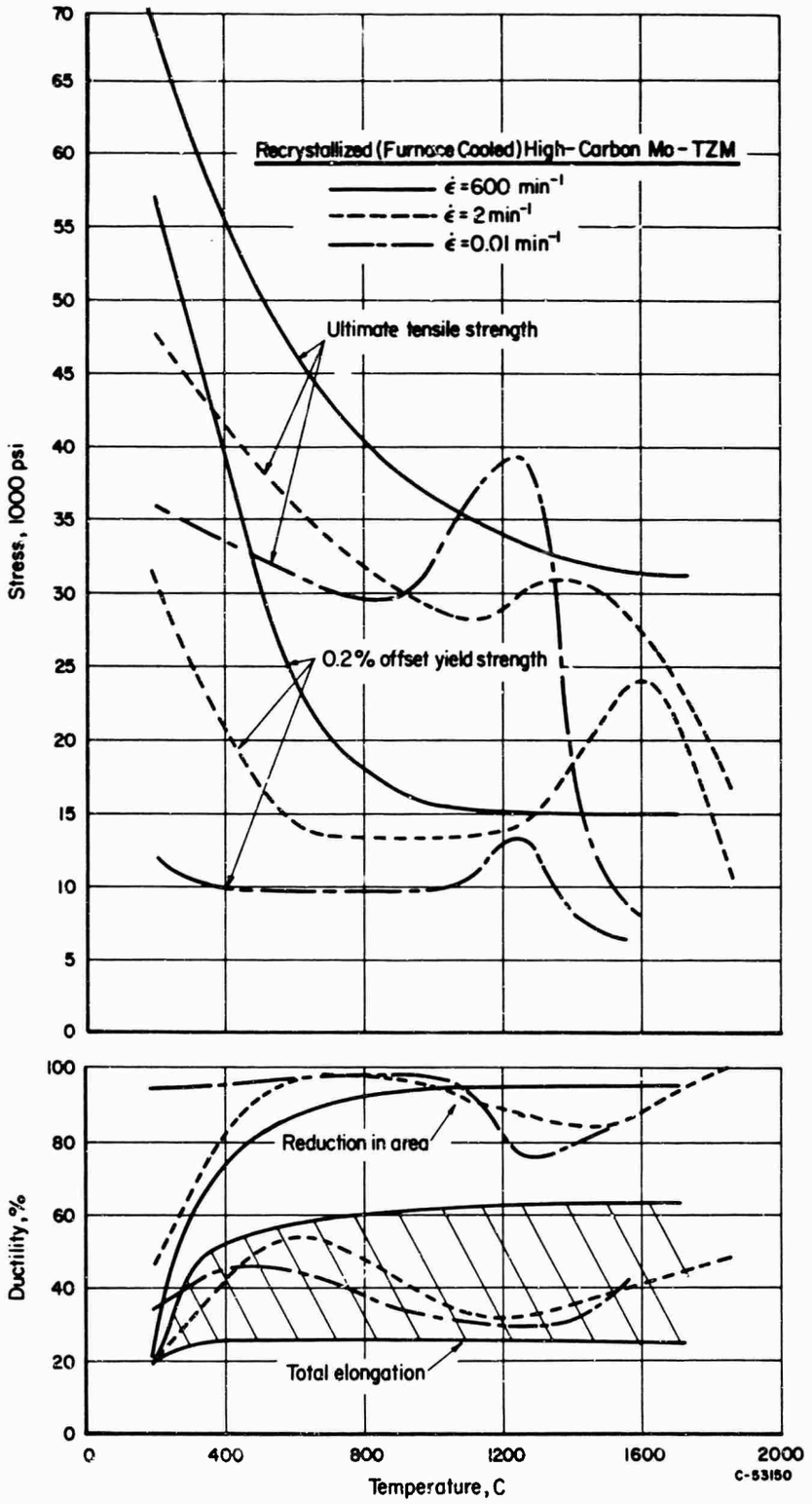

FIGURE 21. EFFECT OF STRAIN RATE ON MECHANICAL PROPERTIES OF RECRYSTALLIZED HIGH-CARBON (190 PPM CARBON) Mo-TZM

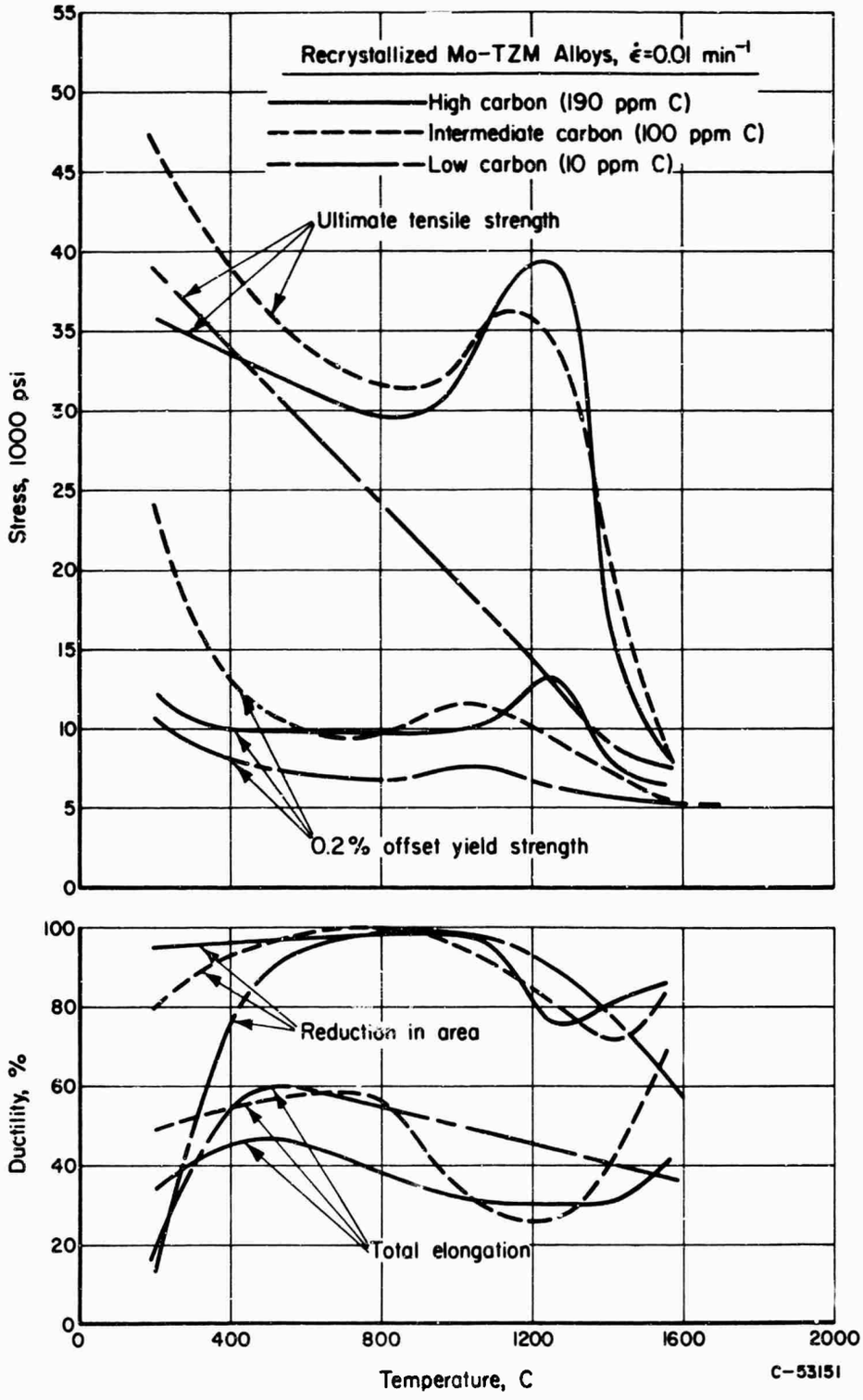

FIGURE 22. EFFECT OF CARBON CONTENT ON MECHANICAL PROPERTIES OF RECRYSTALLIZED Mo-TZM ALLOYS, TESTED AT $\dot{\epsilon}$ = 0.01 MIN^{-1}

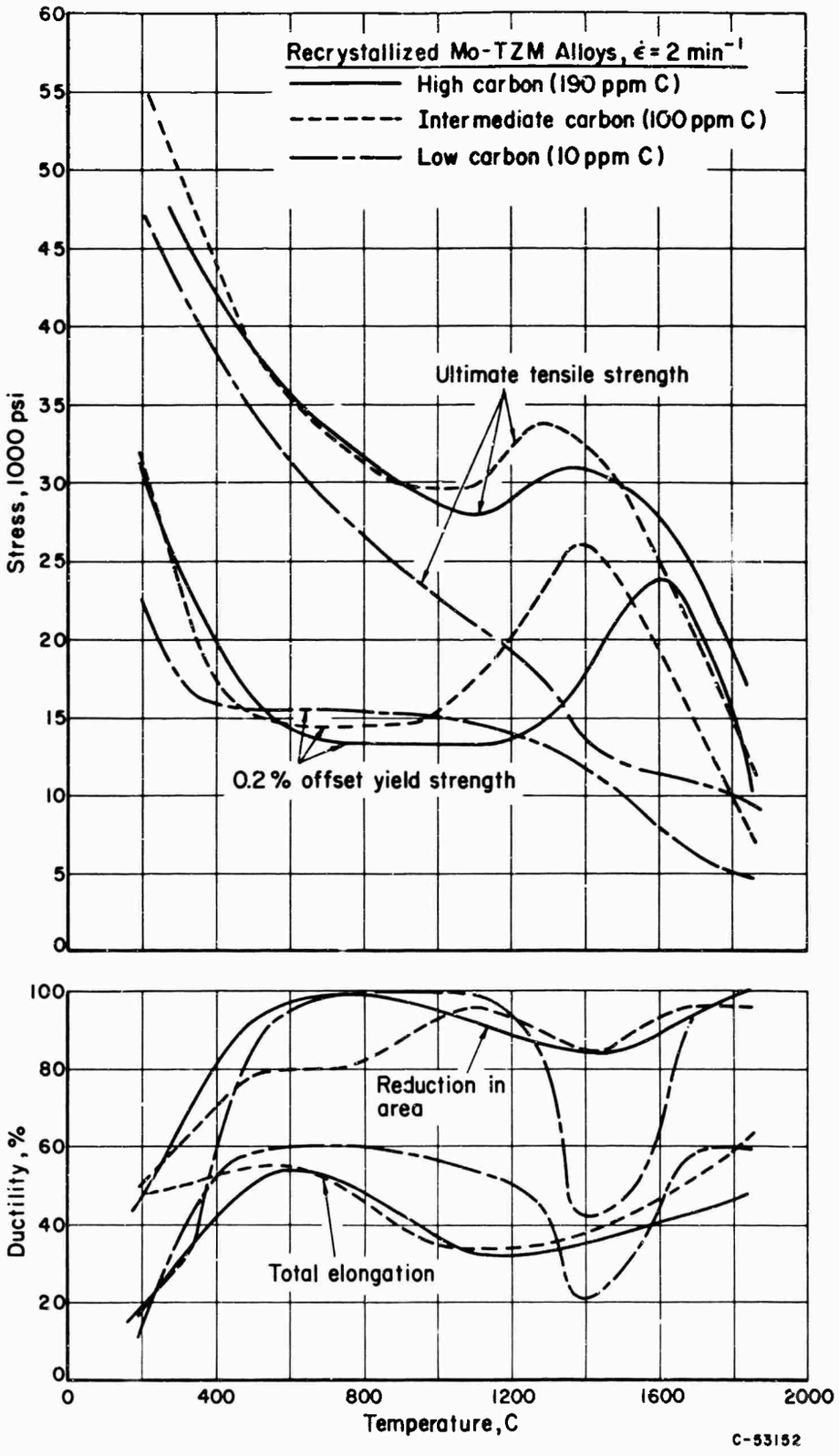

FIGURE 23. EFFECT OF CARBON CONTENT ON MECHANICAL PROPERTIES OF RECRYSTALLIZED Mo-TZM ALLOYS, TESTED AT $\dot{\epsilon}$ = 2 MIN^{-1}

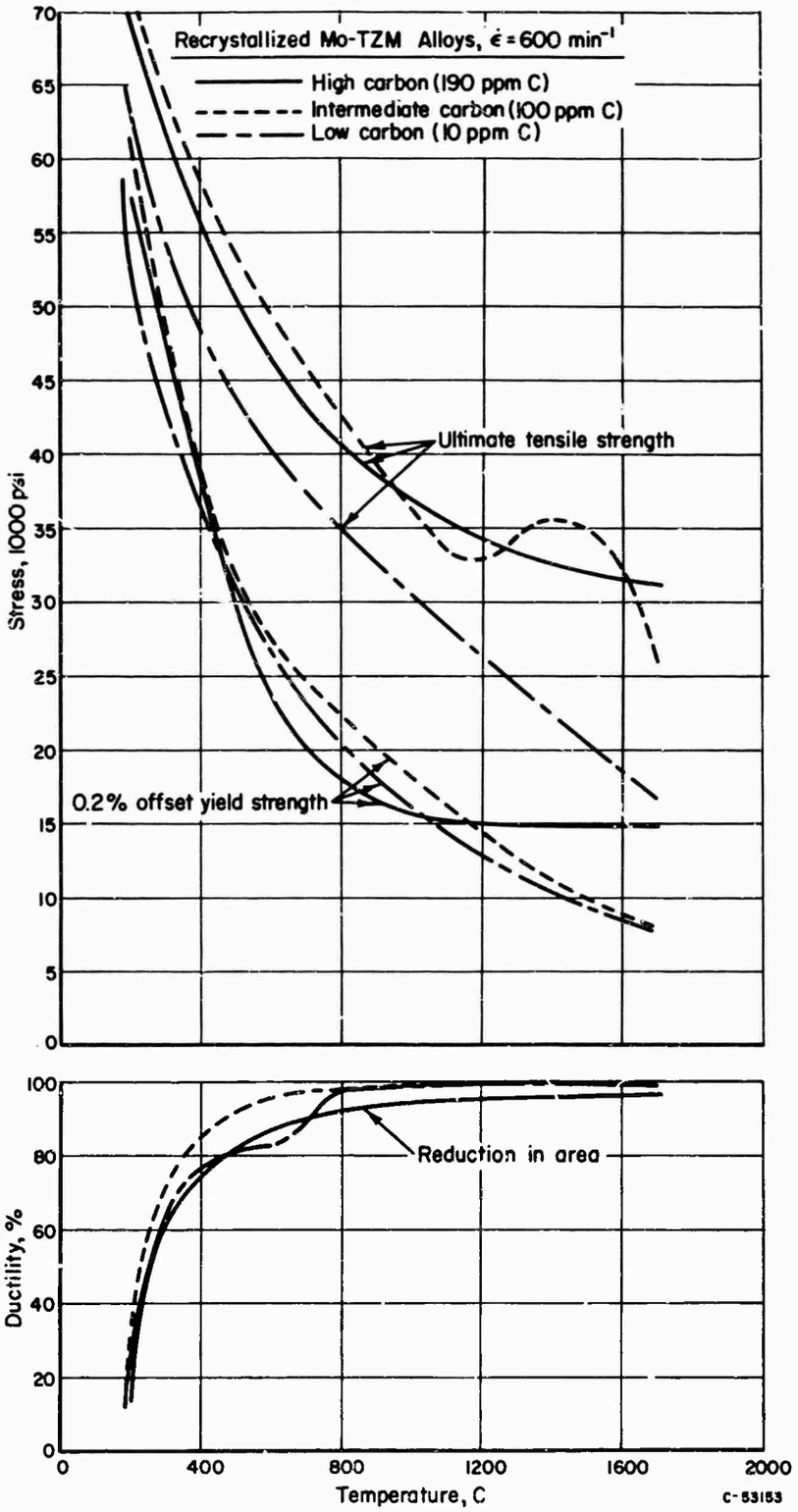

FIGURE 24. EFFECT OF CARBON CONTENT ON MECHANICAL PROPERTIES OF RECRYSTALLIZED Mo-TZM ALLOYS, TESTED AT $\dot{\epsilon}$ = 600 MIN^{-1}

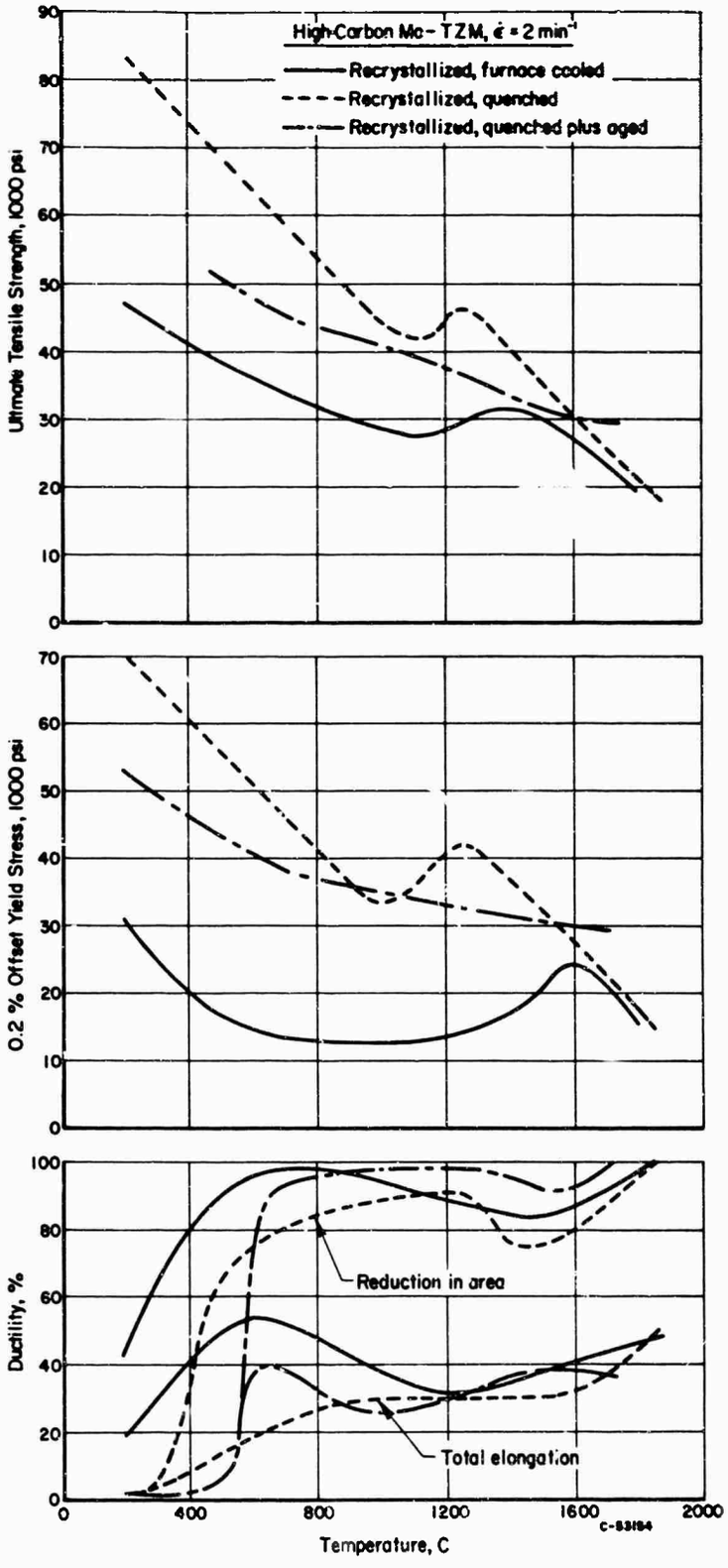

FIGURE 25. EFFECT OF HEAT TREATMENT ON MECHANICAL PROPERTIES OF RECRYSTALLIZED HIGH-CARBON (190 PPM CARBON) Mo-TZM, TESTED AT $\dot{\epsilon}$ = 2 MIN^{-1}

In order to investigate the effect of interstitial content, tungsten of two carbon levels was tested. Carbon was selected since Schnitzel[30] identified an internal friction peak in tungsten at ~400 C as a Snoek peak due to carbon. It was originally intended to aim for nominal carbon levels of ~10 ppm and ~75 ppm. However during fabrication from the ingot, the carbon content of the high carbon tungsten was reduced from 75 to ~35 ppm (see Table II). In addition, fabrication of the high-carbon tungsten proved very difficult, with much of the material being lost because of pronounced cracking and fracture during swaging. Thus, because of a shortage of usable bar stock only a limited number of tests were made on this material.

Wrought-Stress-Relieved Tungsten

The effect of strain rate on wrought-stress-relieved low-carbon tungsten (10 ppm C) is summarized in Figure 11 (see also Appendix III, Table X, Figures 40, 41, and 42). Figure 11 shows the normal rate sensitivity behavior, i.e., an increase in yield stress and an increase in the ductile-to-brittle transition temperature with increasing strain rate.

For strain rates of 0.01 and 2 min^{-1} the total elongation curves show an apparent "ductility minimum" over the temperature range ~800-1300 C. However this can be rationalized by noting the character of the deformation curves (Table X). There are two temperature regions where the deformation curves show some degree of work hardening (e.g., ~400 to 700 C and ~1400 to 1850 C) and the data points here are plotted as open points in Figures 40 and 41. The high-temperature region is probably a result of recovery (and possibly recrystallization) during testing. However the low-temperature region probably reflects the operation of some thermally activated dynamic strengthening mechanism since the total elongation "peak" is shifted from ~400 C for $\dot{\epsilon}$ = 0.01 min^{-1} to ~650 C for $\dot{\epsilon}$ = 2 min^{-1}. The strengthening effect, however, is relatively small, since no peaks are observed in the plots of yield strength versus temperature. Specimens deformed in the intermediate-temperature range (~800-1300 C), exhibit plastic instability, i.e., necking, immediately after yielding, and these results are plotted as solid points in Figures 40 and 41. This behavior results in lower total elongations, but should not be interpreted as a true decrease in ductility, since the reductions in area are ~95-100 per cent.

Recrystallized Tungsten

The effect of strain rate on the mechanical properties of recrystallized low-carbon tungsten (10 ppm C) is summarized in Figure 12, and the influence of carbon content is shown in Figure 13 (see also Appendix III, Tables XI and XII, Figures 43, 44, 45, and 46). Total elongation is not included in Figures 12 and 13 for clarity, since a great deal of scatter was apparent for all strain rates.

As in the case of wrought-stress-relieved low-carbon tungsten, the strength (both yield strength and ultimate tensile strength) is increased with increasing strain rate (Figure 12). There is no difference in the ductile-to-brittle transition temperature (~500-600 C) for strain rates of 0.01 and 2 min^{-1}. However raising the strain rate to 60 min^{-1} increases the ductile-brittle transition temperature to ~850 C. In both recrystallized tungsten materials there is no evidence of intermediate-temperature dynamic strengthening, nor is there any tendency for reduced ductility at temperatures above the ductile-brittle transition temperature.

Figure 13 indicates that there is no significant effect of carbon content on the strength of recrystallized tungsten tested at $\dot{\epsilon} = 2\ min^{-1}$. Increasing the carbon level from 10 to 35 ppm causes a slight increase in yield strength, but the ultimate tensile strength is somewhat lower for the high-carbon material. It is surprising that the ductile-brittle transition temperature of the low-carbon tungsten is higher than that of the high-carbon material (Figure 13), since the latter proved the more difficult to fabricate. However it is seen in Figures 44 and 46 that the ductile-brittle transition temperature is poorly defined and the apparent difference is of the same magnitude as the experimental scatter. It is concluded, then, that there is little difference in the mechanical behavior of 10 ppm and 35 ppm carbon recrystallized tungsten.

Mo-TZM

As the inception of this program, data in the literature[5-8] indicated that the total elongation of wrought-stress-relieved Mo-TZM sheet decreased from ~20 percent at room temperature to ~3-10 per cent over a wide temperature range of ~500-1200 C. However the only previous work which measured reduction in area (also on sheet) showed only a very slight decrease in percent reduction in area from room temperature to 1200 C[6]. These same investigators[6] found that recrystallized Mo-TZM sheet had a significant minimum in percent reduction in area at ~1200 C.

Wrought-Stress-Relieved Mo-TZM

The effect of strain rate on the deformation behavior of wrought-stress-relieved low-carbon Mo-TZM is summarized in Figure 14 (see also Table XIII, Figures 47, 48, and 49). Similar plots are made for high-carbon Mo-TZM in Figure 15 (see also Table XVI, Figures 56, 57, and 58). For both alloys the usual strain-rate sensitivity of the yield stress is apparent. The rapid drop in strength and increase in total elongation at ~1300-1400 C is probably due to dynamic recovery (and possibly recrystallization) during the course of testing. The reductions in area are ~90-100 percent for all strain rates at test temperatures above ~350 C. Although, for both materials, the total elongation decreases somewhat with increasing test temperature (to ~1000 C), this does not really constitute a true ductility minimum since the reductions in area are relatively unaffected by test temperature, strain rate, or carbon content.

Figures 16, 17, and 18 show the influence of carbon content on the mechanical properties (at constant strain rate). The high-carbon Mo-TZM (190 ppm carbon) is ~15-40,000 psi stronger than the low-carbon (10 ppm carbon) material over the temperature range 200-1200 C. Although the high-carbon alloy is somewhat more worked (see Figure 3), the chief strengthening probably occurs from the greatly increased amount of carbide (see Figure 4). The presence of carbides in the high-carbon Mo-TZM could strengthen in the classical fashion by blocking dislocation movement during testing. However, perhaps more important, the carbides might contribute to the stabilization of a finer substructure during the course of fabrication, i.e., promote a finer subgrain size.

In order to investigate the effect of interstitial content, tungsten of two carbon levels was tested. Carbon was selected since Schnitzel[30] identified an internal friction peak in tungsten at ~400 C as a Snoek peak due to carbon. It was originally intended to aim for nominal carbon levels of ~10 ppm and ~75 ppm. However during fabrication from the ingot, the carbon content of the high carbon tungsten was reduced from 75 to ~35 ppm (see Table II). In addition, fabrication of the high-carbon tungsten proved very difficult, with much of the material being lost because of pronounced cracking and fracture during swaging. Thus, because of a shortage of usable bar stock only a limited number of tests were made on this material.

Wrought-Stress-Relieved Tungsten

The effect of strain rate on wrought-stress-relieved low-carbon tungsten (10 ppm C) is summarized in Figure 11 (see also Appendix III, Table X, Figures 40, 41, and 42). Figure 11 shows the normal rate sensitivity behavior, i.e., an increase in yield stress and an increase in the ductile-to-brittle transition temperature with increasing strain rate.

For strain rates of 0.01 and 2 min^{-1} the total elongation curves show an apparent "ductility minimum" over the temperature range ~800-1300 C. However this can be rationalized by noting the character of the deformation curves (Table X). There are two temperature regions where the deformation curves show some degree of work hardening (e.g., ~400 to 700 C and ~1400 to 1850 C) and the data points here are plotted as open points in Figures 40 and 41. The high-temperature region is probably a result of recovery (and possibly recrystallization) during testing. However the low-temperature region probably reflects the operation of some thermally activated dynamic strengthening mechanism since the total elongation "peak" is shifted from ~400 C for $\dot{\epsilon} = 0.01$ min^{-1} to ~650 C for $\dot{\epsilon} = 2$ min^{-1}. The strengthening effect, however, is relatively small, since no peaks are observed in the plots of yield strength versus temperature. Specimens deformed in the intermediate-temperature range (~800-1300 C), exhibit plastic instability, i.e., necking, immediately after yielding, and these results are plotted as solid points in Figures 40 and 41. This behavior results in lower total elongations, but should not be interpreted as a true decrease in ductility, since the reductions in area are ~95-100 per cent.

Recrystallized Tungsten

The effect of strain rate on the mechanical properties of recrystallized low-carbon tungsten (10 ppm C) is summarized in Figure 12, and the influence of carbon content is shown in Figure 13 (see also Appendix III, Tables XI and XII, Figures 43, 44, 45, and 46). Total elongation is not included in Figures 12 and 13 for clarity, since a great deal of scatter was apparent for all strain rates.

As in the case of wrought-stress-relieved low-carbon tungsten, the strength (both yield strength and ultimate tensile strength) is increased with increasing strain rate (Figure 12). There is no difference in the ductile-to-brittle transition temperature (~500-600 C) for strain rates of 0.01 and 2 min^{-1}. However raising the strain rate to 600 min^{-1} increases the ductile-brittle transition temperature to ~850 C. In both recrystallized tungsten materials there is no evidence of intermediate-temperature dynamic strengthening, nor is there any tendency for reduced ductility at temperatures above the ductile-brittle transition temperature.

Comparison of This Work With Results of Previous Investigations on Wrought-Stress-Relieved Mo-TZM Sheet. Figure 26 compares the ductility of wrought-stress-relieved Mo-TZM sheet[5-8] with results of this investigation on the high-carbon bar. The general trend in total elongation is the same for both sheet and bar, i. e., the elongation decreases from ~20 percent (sheet) and ~50 percent (bar) at room temperature to ~3-10 percent (sheet) and ~25 percent (bar) over a wide temperature range of ~500-1200 C. At temperatures greater than ~1200-1400 C the total elongation then increases, and again this increase is probably associated with dynamic recovery and possibly some recrystallization occurring during the course of testing. However the intermediate temperature decrease in total elongation should not be misconstructed as a decrease in true ductility, since for both sheet[6] and bar (this work), it is found that the reduction in area is relatively unaffected over the temperature range room temperature to 1200 C (see Figure 26).

The decrease in total elongation from room temperature to 1200 C can be rationalized simply by noting the nature of the deformation curves. For example, Figure 27 illustrates two stress-strain curves for wrought-stress-relieved high-carbon Mo-TZM bar tested at $\dot{\epsilon} = 0.01$ min^{-1} (Curve A, T = 200 C, total elongation = 38.4 percent; Curve B, T = 650 C, total elongation 22.8 percent). At 200 C some work hardening occurs, whereas at 650 C plastic instability (i.e., necking) occurs immediately after yielding. This of course means that at 650 C uniform elongation is negligible, and thus the measured total elongation is less than that of the specimen tested at 200 C. However the reduction in area values for both specimens are ~94 percent, and thus the true ductility is very nearly the same for both specimens. A similar argument can be made for wrought-stress-relieved Mo-TZM sheet, and in fact Dotson[19] has made such observations.

Thus on the basis of the above discussion, it is concluded that there is no true intermediate-temperature ductility minimum in wrought-stress-relieved Mo-TZM bar or sheet.

Recrystallized Mo-TZM

Summary plots of the mechanical-property data of recrystallized Mo-TZM alloys are shown in Figures 19-25, for the purpose of making the following comparisons:

(a) The effect of strain rate

Figure 19, low-carbon Mo-TZM
Figure 20, intermediate-carbon Mo-TZM
Figure 21, high-carbon Mo-TZM

(b) The effect of carbon content

Figure 22, $\dot{\epsilon} = 0.01$ min^{-1}
Figure 23, $\dot{\epsilon} = 2$ min^{-1}
Figure 24, $\dot{\epsilon} = 600$ min^{-1}

(c) The effect of heat treatment, for high-carbon Mo-TZM

Figure 25.

The data from which these graphs were plotted are given in Appendix III.

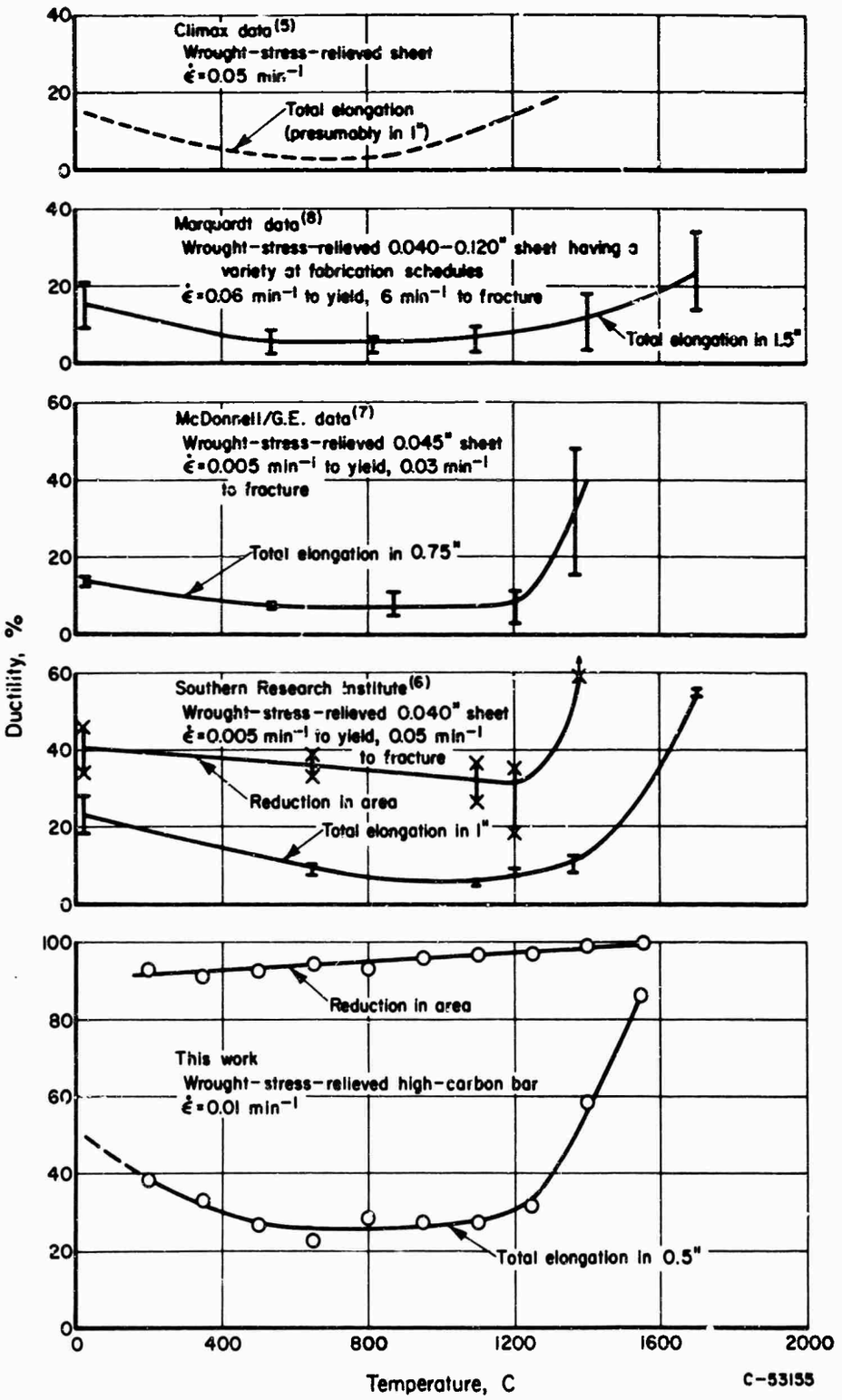

FIGURE 26. COMPARISON OF TOTAL ELONGATION AND REDUCTION IN AREA FOR WROUGHT-STRESS-RELIEVED Mo-TZM SHEET (PREVIOUS WORK) AND BAR (THIS WORK)

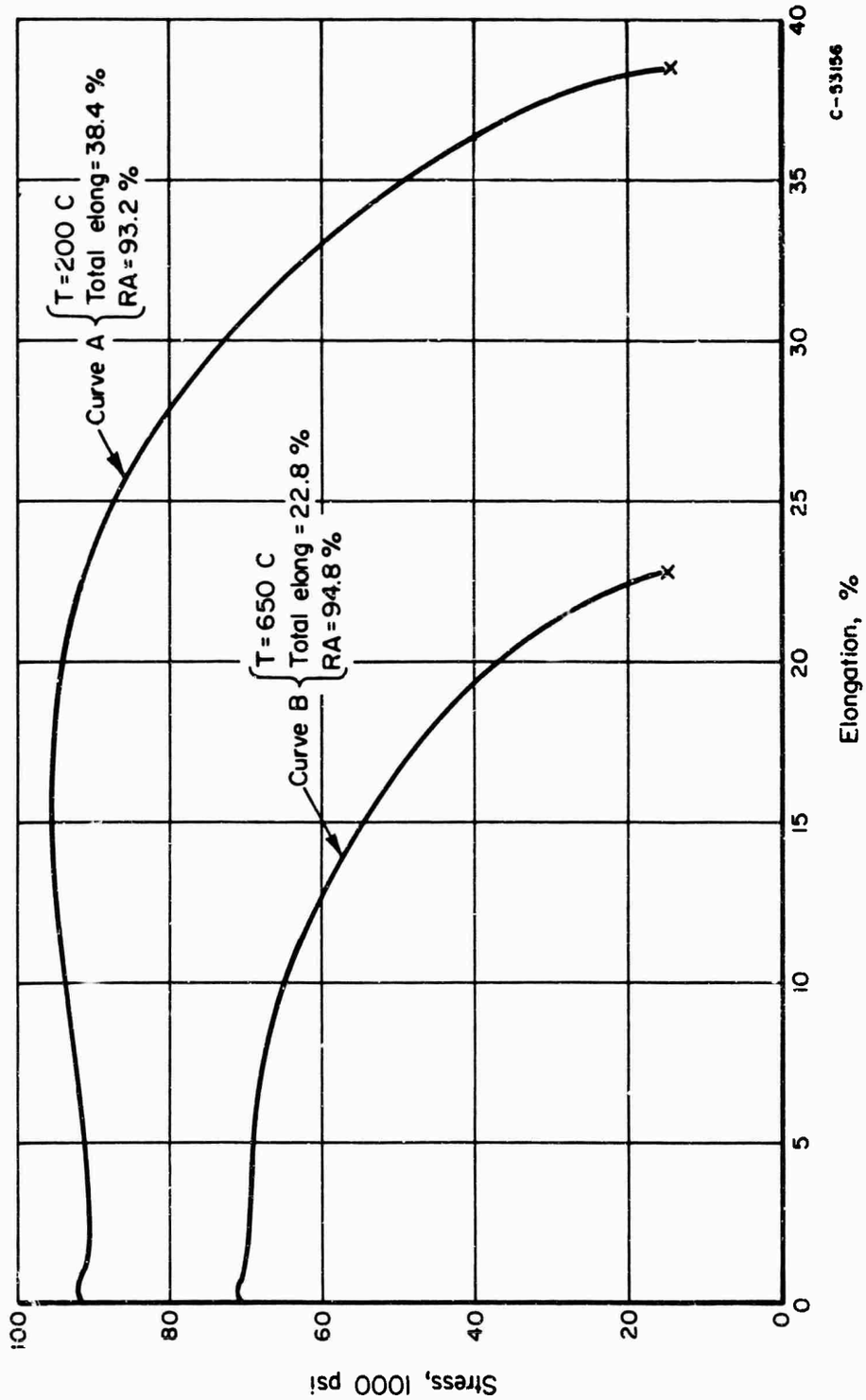

FIGURE 27. DEFORMATION CURVES OF WROUGHT-STRESS-RELIEVED HIGH-CARBON (190 PPM C) Mo-TZM ($\dot{\epsilon}$ = 0.01 MIN^{-1})

Illustrating how lower total elongation can arise (Curve B) as a result of plastic instability occurring shortly after yielding.

It is seen in Figures 19, 20, and 21 that the usual strain-rate sensitivity of the yield and ultimate strengths is obtained for all three alloys. Figures 22, 23, 24 show that increasing the carbon (i.e., carbide) content of these recrystallized (and furnace cooled) alloys does not result in the same degree of strengthening as was observed for wrought-stress-relieved Mo-TZM (see Figures 16, 17, and 18). The greater "carbide" strengthening in the wrought materials may be associated with the fact that in the higher carbon alloys the carbides contribute to strengthening by stabilizing a finer substructure during the mechanical working processes used in fabrication, as already suggested.

Several other general features are observed in Figures 19-25: (a) There are pronounced peaks in strength (except for the low-carbon alloy) over the general temperature range ~1000-1500 C; such strength peaks have also been observed by Chang[20-22] on similar alloys such as Mo-TZM and Mo-TZ; (b) In the same general temperature range (except for tests at a strain rate of 600 min^{-1}) there is a significant decrease in ductility (both reduction in area and total elongation). This coincides with previous observations on recrystallized Mo-TZM sheet[6].

This intermediate-temperature ductility decrease does in fact represent a true ductility minimum, and it is associated with the occurrence of pronounced grain-boundary cracking during tensile testing.

Grain-Boundary Cracking. During the course of this study it became apparent that there was a definite correlation between the intermediate temperature ductility decrease and the occurrence of grain-boundary cracking in recrystallized Mo-TZM alloys. The cracking phenomenon is illustrated by the macrophotos of broken tensile specimens in Figure 28. These are recrystallized low-carbon Mo-TZM specimens tested at a strain rate of 2 min^{-1}, and the same features were observed for the intermediate- and high-carbon alloys. It is seen that the specimens tested at 800 and 1850 C show no grain-boundary surface cracks and both have ~95 percent reduction in area. However the specimen tested at 1400 C has pronounced cracking at most of the grain boundaries and has a greatly reduced macroscopic ductility, i.e., 43 percent reduction in area. Figure 29 illustrates that the grain-boundary cracks occur in the interior of the susceptible specimens as well as at the surface.

Once formed, the grain-boundary cracks propagate slowly during continued deformation. The fracture surfaces are characterized by numerous striations apparently caused by slip bands intersecting the grain-boundary surfaces. These are illustrated by the optical fractograph in Figure 30, and the replica electron fractographs in Figure 31 (all on recrystallized low-carbon Mo-TZM). Figure 31c shows that on occasion the amount of shear in such slip bands can be very large — of the order of several hundred percent. Such large accommodation strains provide stress concentrations necessary for nucleation of grain-boundary cracks.

For comparison, Figure 32a shows a grain-boundary replica fractograph of a low-carbon Mo-TZM specimen which fractured in a completely brittle fashion at room temperature. Here the fracture occurred by mixed cleavage (Figure 32b) and grain boundary parting (Figure 32a), and the grain boundary facets showed no striations. In both the high temperature fracture (Figures 30, 31) and the room-temperature fracture (Figure 32) the grain-boundary facets contain some imbedded precipitates. The fine striations associated with the large particle embedded in the grain boundary in

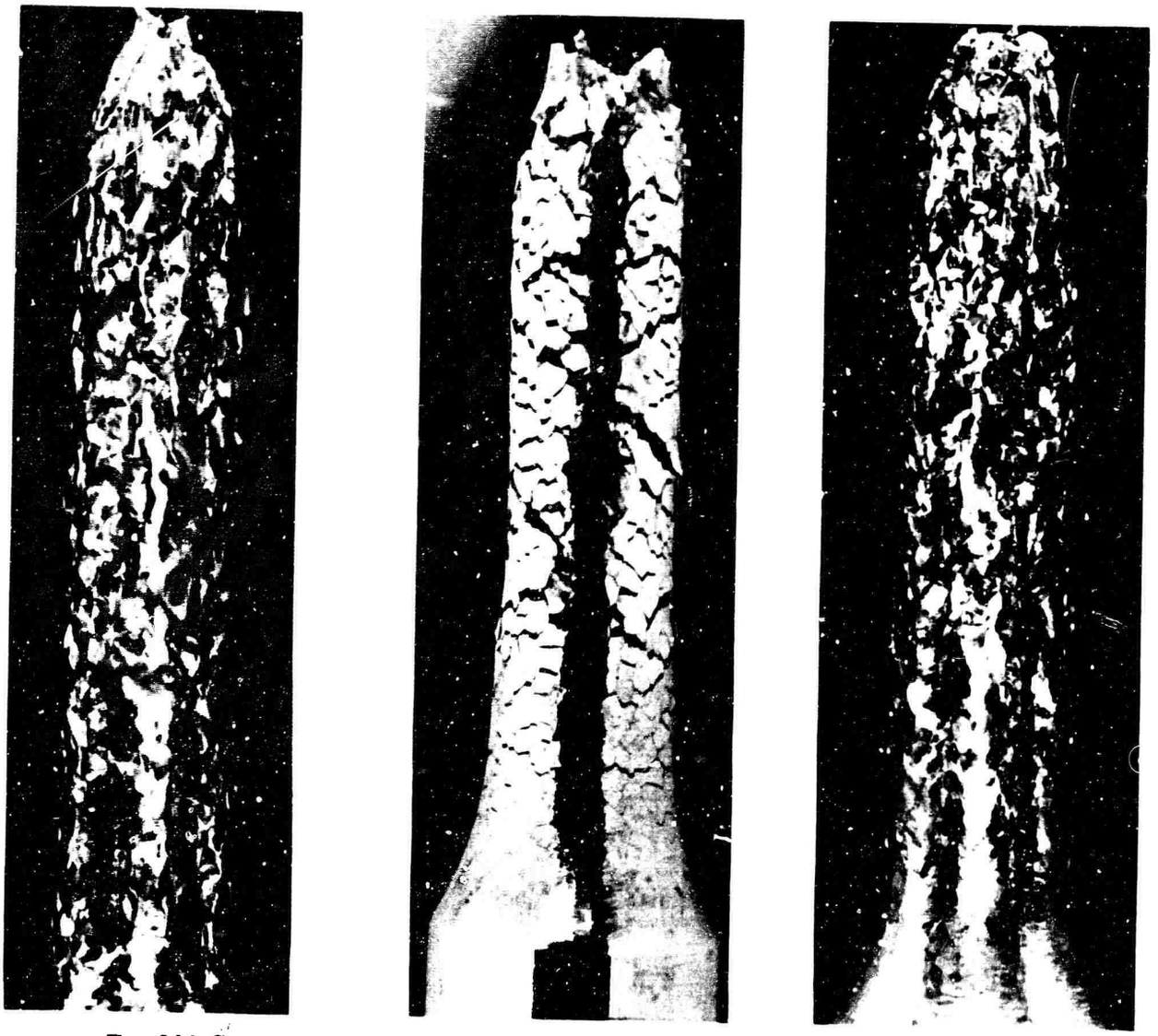

a. T = 800 C, 97% RA

b. T = 1400 C, 43% RA

c. T = 1850 C, 95% RA

FIGURE 28. FRACTURED SPECIMENS OF RECRYSTALLIZED LOW-CARBON Mo-TZM (10 PPM CARBON) TESTED AT $\dot{\epsilon}$ = 2 MIN^{-1}, 10X

75X 22141 250X 22143

a. Interior b. Surface (Nickel Plated)

FIGURE 29. GRAIN BOUNDARY CRACKS IN RECRYSTALLIZED LOW-CARBON Mo-TZM, TESTED AT 1400 C AND $\dot{\epsilon}$ = 0.01 MIN^{-1}

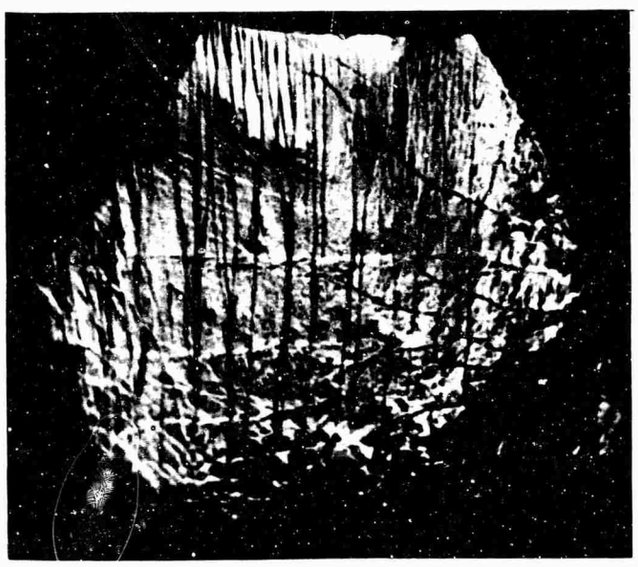

250X 25092

FIGURE 30. OPTICAL FRACTOGRAPH SHOWING GRAIN-BOUNDARY FACET ON FRACTURE SURFACE OF RECRYSTALLIZED LOW-CARBON (10 PPM C) Mo-TZM SPECIMEN TESTED AT $\dot{\epsilon}$ = 2 MIN^{-1} AND T = 1400 C

4300X E1644A

a.

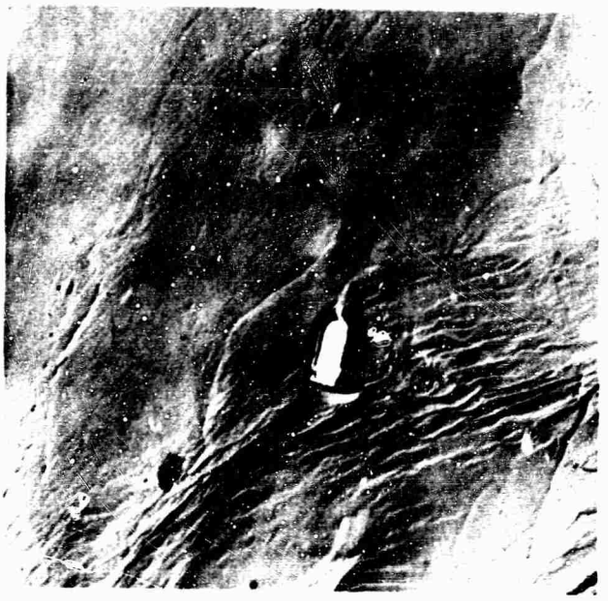

8400X E1643B

b.

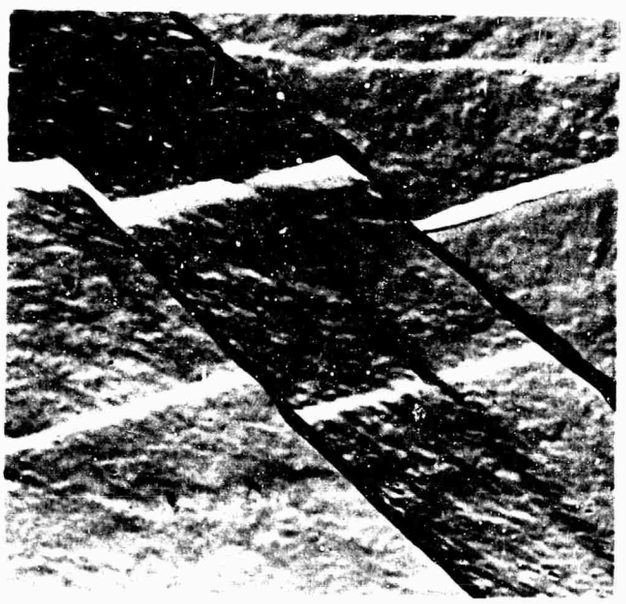

6200X E1642C

c.

FIGURE 31. REPLICA ELECTRON FRACTOGRAPHS OF GRAIN-BOUNDARY FACETS ON FRACTURE SURFACE OF RECRYSTALLIZED LOW-CARBON (10 PPM) Mo-TZM SPECIMEN TESTED AT $\dot{\epsilon}$ = 2 MIN^{-1} AND T = 1400 C

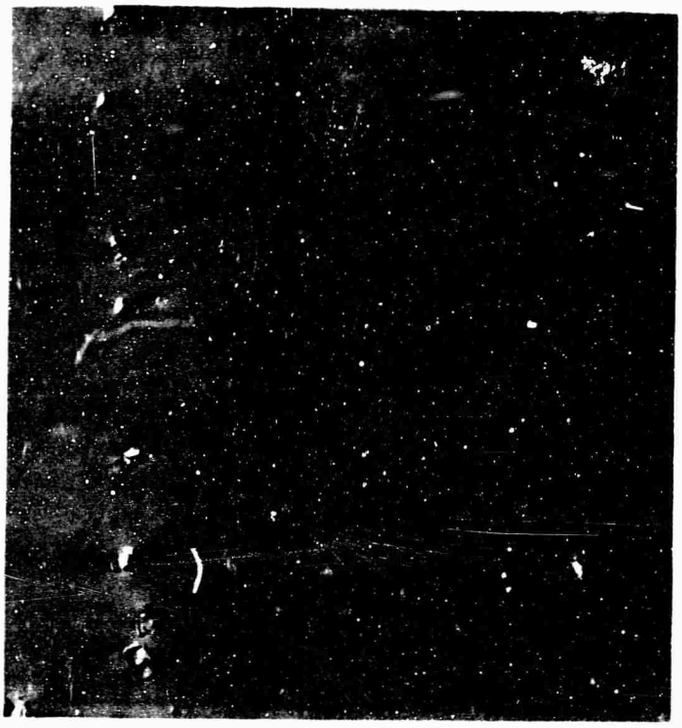

11,100X E1821C

a. Grain-Boundary Facet With Imbedded Precipitates

11,100X E1822E

b. Cleavage Facet – With Precipitates Marked by Arrows

FIGURE 32. REPLICA ELECTRON FRACTOGRAPHS OF RECRYSTALLIZED LOW-CARBON (10 PPM C) Mo-TZM FRACTURED AT ROOM TEMPERATURE

Figure 31b suggests that the precipitate promoted localized slip and enhanced cross-slip at some stage during the high-temperature test. No such effect, however, was observed on the grain-boundary facets of the specimen fractured at room temperature.

The photographs of the room-temperature fracture surfaces shown in Figure 32 again provide information about the precipitate particles. In Figure 32a, the regular array of precipitates on the exposed grain-boundary suggests a retention of the chemical heterogeneities introduced by the thermomechanical treatments used in the primary fabrication process. Such a "memory" effect implies that details of the fabrication procedure may affect the deformation and fracture properties of subsequently recrystallized material unless such material is given an effective solution treatment. In Figure 32b, another effect of the particles is seen at the location of the arrows, where the particles have perturbed the cleavage fracture path as indicated by the deflection of the river line above and to the left of the particles. It has been suggested[23] previously that particles such as these may be important in converting a grain-boundary crack to the cleavage mode by virtue of the stress concentrations existing in their vicinity.

An Explanation of Grain-Boundary Cracking and Reduced Intermediate-Temperature Ductility. At the test temperatures where grain-boundary cracking was observed, the deformation curves were frequently serrated. This was most pronounced at the lowest strain rate, and an example of such serrated flow is shown in Figure 33. This deformation behavior is commonly observed in tests where some dynamic strengthening mechanism is operative, e.g., strain aging, or precipitation during deformation. This dynamic strengthening is also reflected by peaks in the yield and ultimate strengths (see Figures 20-25).

In the present recrystallized Mo-TZM alloys the dynamic strengthening is probably associated with precipitation during deformation rather than classical strain aging. Chang[20-22] has offered reasonable arguments to support this explanation, based upon studies of similar Mo-base alloys (e.g., Mo-TZC and Mo-TZ).

Thus coincident with a minimum in ductility are three phenomena:

- Grain-boundary cracking
- Serrated flow
- Strength peaks.

Table VI summarizes the temperature ranges where the above phenomena occur in the various alloys. The following observations from Table VI and Figures 19-25 are relevant to a discussion of the nature of intermediate-temperature reduced ductility caused by grain-boundary cracking.

(a) The ductility minima temperatures lie within the temperature ranges where grain-boundary cracking, serrated yielding, and dynamic strengthening occur. Thus, there is evidence to suppose that these phenomena are related.

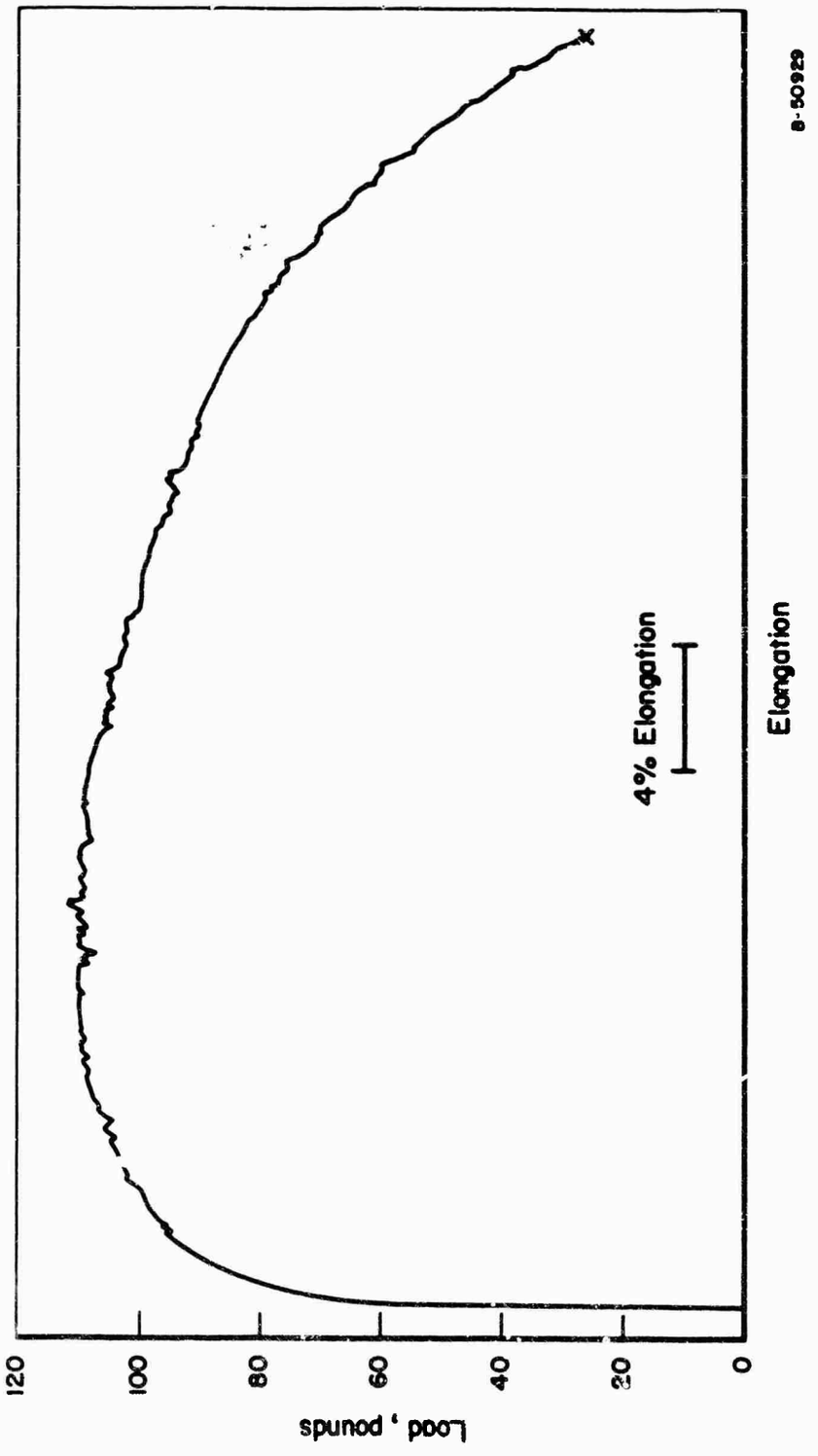

FIGURE 33. SERRATED DEFORMATION CURVE OF RECRYSTALLIZED LOW-CARBON Mo-TZM, TESTED AT 1400 C AND $\dot{\epsilon} = 0.01$ MIN^{-1}

TABLE VI. SUMMARY OF PHENOMENA ASSOCIATED WITH INTERMEDIATE-TEMPERATURE DECREASE IN DUCTILITY IN RECRYSTALLIZED Mo-TZM ALLOYS

	Low Carbon, Furnace Cooled	Intermediate Carbon, Furnace Cooled	High Carbon, Furnace Cooled	High Carbon, Quenched	High Carbon, Quenched and Aged
Intermediate temperature at which there is a minimum in % RA					
$\dot{\epsilon}$ = 0.01 min^{-1}	≥ 1550 C	1400 C	1250 C	--	--
$\dot{\epsilon}$ = 2 min^{-1}	1400	1400	1400	1400 C	1550 C
$\dot{\epsilon}$ = 600 min^{-1}	Absent	Absent	Absent	--	--
Temperature range where grain-boundary cracking was observed					
$\dot{\epsilon}$ = 0.01 min^{-1}	1100-1550[a]	1100-1550[a]	1100-1550[a]	--	--
$\dot{\epsilon}$ = 2 min^{-1}	1400-1700	1400-1550	1100-1550	800-1550	1250-1550[b]
$\dot{\epsilon}$ = 600 min^{-1}	Absent	Absent	Absent	--	--
Temperature range where serrated flow was observed					
$\dot{\epsilon}$ = 0.01 min^{-1}	500-1550[a]	500-1550[a]	650-1550[a]	--	--
$\dot{\epsilon}$ = 2 min^{-1}	(c)	(c)	(c)	800-1250	Absent
$\dot{\epsilon}$ = 600 min^{-1}	(d)	(d)	(d)	--	--
Temperature range where dynamic strengthening was observed (i.e., specifically - peaks in yield and ultimate strengths)					
$\dot{\epsilon}$ = 0.01 min^{-1}	Not well defined	950-1250	1100-1350	--	--
$\dot{\epsilon}$ = 2 min^{-1}	Not well defined	1100-1650	1250-1700	1100-1400	Absent
$\dot{\epsilon}$ = 600 min^{-1}	Not well defined	1250-1600	Not well defined	--	--

(a) The highest temperature tested was 1550 C. Grain-boundary cracking and serrated flow possibly could have persisted to higher temperatures.

(b) Grain-boundary cracking in quenched plus aged material was very slight.

(c) Some deformation curves at intermediate temperatures (~950-1200 C) showed a tendency for serrated flow. However this was not well defined since the Instron pen response was inadequate.

(d) Oscillograph traces were not sensitive enough to detect serrated flow.

(b) For a given material there is a general tendency (with some exceptions) for these phenomena to occur at higher temperatures as the strain rate is increased. This is most noticeable in the case of strength peaks, and is further indicated by the absence of grain-boundary cracking and reduced ductility in specimens tested at $\dot{\epsilon} = 600\ min^{-1}$

(c) The most severe grain-boundary cracking (i.e., where pronounced cracking occurred over the widest temperature range) was noted in the quenched high-carbon Mo-TZM tested at $\dot{\epsilon} = 2\ min^{-1}$ (see Table VI). This condition should be the most susceptible to precipitation during deformation.

(d) In the quenched-plus-aged high-carbon Mo-TZM (tested at $\dot{\epsilon} = 2\ min^{-1}$) the cracking was very slight, with fractured specimens having only one or two cracks in the gage length. This condition should be the least susceptible to precipitation during deformation, and in fact no serrated flow or strength peaks were observed.

(e) For a given strain rate, increasing the carbon content had little effect on these phenomena, except for the fact that the strength peaks in low-carbon Mo-TZM were not well defined (see Figure 19).

Considering the above points, it is possible to suggest a phenomenological explanation for the intermediate-temperature grain-boundary cracking. Recourse can be made to the concept of an "equicohesive temperature", and this is schematically shown in Figure 34. This figure shows that at lower temperatures and at very high temperatures the "strength" of grain boundaries is greater than that of the matrix. However at intermediate temperatures, precipitation during deformation raises the strength of the matrix. Coincident with the matrix strengthening, which Chang[22] has shown to be the result of TiC precipitation, there is grain-boundary depletion and partial dissolution of preexisting Mo_2C. This could result in a "weakening" of the grain boundaries and this is shown schematically in Figure 34. The grain-boundary cracking then results in lower macroscopic ductility, i.e., a ductility minimum temperature. At very high temperatures ($\gtrsim$ 1800 C) TiC is no longer stable[22], which removes both the matrix strengthening and grain-boundary weakening. Accordingly, grain-boundary cracking is no longer evident at very high temperatures.

The Effect of Heat Treatment on the Properties of Recrystallized High-Carbon Mo-TZM. As noted in Table III, recrystallized high-carbon Mo-TZM was tested in three heat-treated conditions:

(1) Annealed 1 hour at 2100 C, furnace cooled

(2) Annealed 1 hour at 2100 C, quenched into molten tin at 250 C

(3) Annealed 1 hour at 2100 C, quenched into molten tin at 250 C, aged 100 hours at 1300 C.

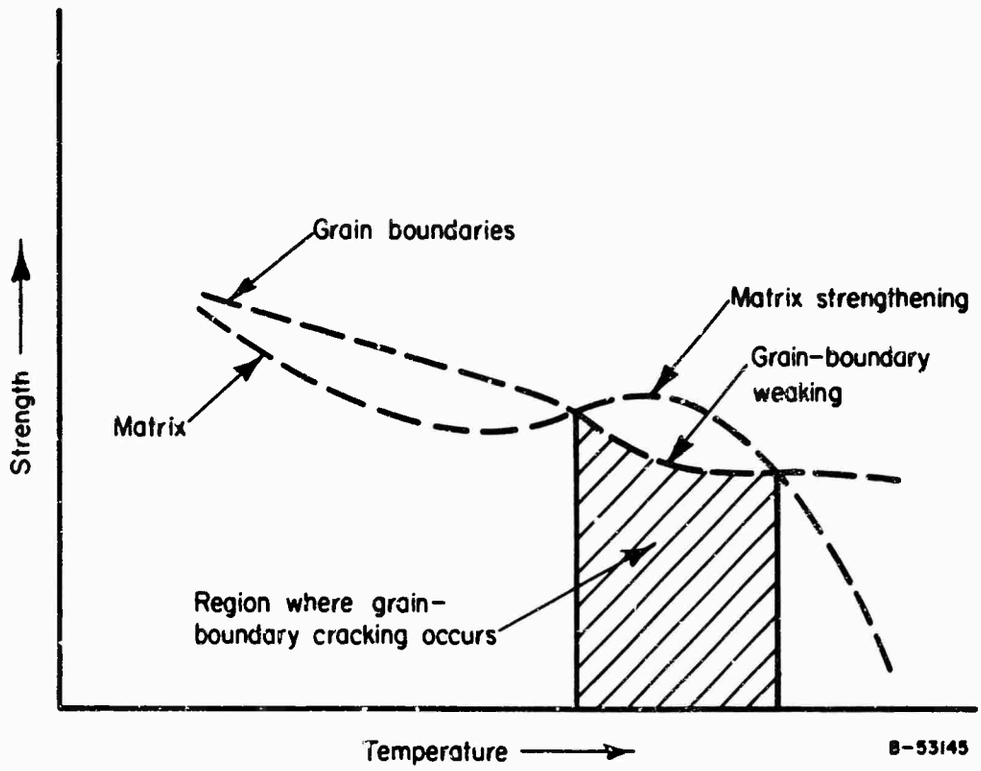

FIGURE 34. SCHEMATIC DRAWING SHOWING PHENOMENOLOGICAL DESCRIPTION OF INTERMEDIATE-TEMPERATURE GRAIN-BOUNDARY CRACKING MECHANISM OBSERVED IN RECRYSTALLIZED Mo-TZM ALLOYS

The effect of these treatments on intermediate-temperature grain-boundary cracking was discussed above, where it was noted that the quenched material was the most susceptible, and the quenched-plus-aged material was the least susceptible.

It was also observed, however, that there was a pronounced effect of heat treatment on the strength of this alloy (see Figure 25). For example, over the temperature range of ~200-800 C, the yield and ultimate tensile strengths of quenched specimens are 20-40,000 psi greater than those of furnace-cooled specimens. The strength of quenched-plus-aged specimens at a given test temperature is seen to be intermediate between those of the quenched and furnace-cooled specimens.

The strength improvement achieved by quenching can be explained in terms of the microstructures obtained by the various heat treatments. Furnace cooling from 2100 C resulted in very coarse carbides which were easily observed at 100X (see Figure 5a). However quenching resulted in a very finely dispersed precipitate about 500 Å in diameter (Figures 6a and 6b); and aging caused the carbide to coarsen somewhat to ~2000-3000 Å (see Figures 6c and 6d).

The increase in initial strength (approximated by the 0.2 percent yield stress) of the quenched high-carbon Mo-TZM over that of the furnace-cooled specimens can be roughly accounted for by considering the Orowan concept of strengthening by nondeforming particles – in this case the very fine carbides. The shear strength, τ, is given by the sum of the yield stress of the matrix τ_s, and the increment in shear stress caused by the precipitates, τ_p:

$$\tau = \tau_s + \tau_p \quad . \tag{5}$$

The Orowan stress increment, τ_p, is given approximately by[13, 24]*:

$$\tau_p \approx \frac{Gb}{4\pi} \cdot \frac{1}{d/2 - r_s} \cdot \ln\left(\frac{d/2 - r_s}{b}\right) \tag{6}$$

G = shear modulus of molybdenum at the test temperature, estimated from data on the temperature dependence of Young's modulus[25]

b = Burgers vector

d/2 = one-half of the mean planar center-to-center particle separation = 1565 Å*

r_s = mean planar particle radius = $\sqrt{2/3}\ r_v$ = 230 Å.

Taking τ_s to be the yield (shear) stress of specimens which were furnace cooled from the annealing temperature of 2100 C and tested at $\dot{\epsilon}$ = 2 min^{-1}**, and calculating τ_p from Equation (6), gives values of τ which agree closely with experimental yield stress measurements of the quenched specimens tested at $\dot{\epsilon}$ = 2 min^{-1} (refer to Tables XVII and XVIII for the raw tensile data). Several examples showing the good agreement between calculated and measured τ values are listed on the following page.

*See discussion on page 12 for a description of how the average precipitate size and spacing were determined.

**The actual values of τ_s and the experimental τ values used were assumed to be one-half the 0.2 percent tensile yield strength. The furnace-cooled specimens were selected as the base for comparison, since the very coarse carbides (see Figure 5a) should not contribute significantly to the strength.

Test Temp, C	τ_s, psi	τ_p (from Eq. 6), psi	Calculated $\tau = \tau_s + \tau_p$, psi	Experimental τ (Quenched High-Carbon Mo-TZM), psi
200	14,750	17,000	31,750	34,500
500	6,900	16,400	23,300	25,300

In applying Equation (6) to calculate the Orowan contribution to the shear stress, several minor contributions to the initial flow stress were neglected. These are caused by: (a) elastic strain in the matrix surrounding precipitates, and (b) the difference in shear modulus between precipitate and matrix. For a discussion of how these factors influence the Orowan stress see Reference (13). However, Ashby[13] has noted that these contributions are minor in most cases and for simplification they were neglected in the present calculations.

CONCLUSIONS

(1) There is no significant effect of strain rate or carbon content on the intermediate temperature reductions in area of recrystallized or wrought-stress-relieved tungsten.

(2) An apparent minimum in total elongation over the temperature range ~600-1200 C was noted for both wrought-stress-relieved tungsten and wrought-stress-relieved Mo-TZM. This does not indicate a true decrease in ductility, but is simply a reflection of the fact that in this temperature range plastic instability occurs immediately after yielding. Reduction in area values remained ~90-100 percent over this temperature range.

(3) In recrystallized Mo-TZM alloys, a temperature region of reduced ductility (~1100-1500 C) was caused by pronounced grain-boundary cracking. This was associated with dynamic strengthening of the matrix as a result of precipitation during deformation.

(4) Quenching the highest carbon Mo-TZM (190 ppm carbon) from 2100 C into molten tin resulted in a very fine distribution of carbides (560 Å average diameter and ~3000 Å spacing). The strength of such material was significantly greater than that of the furnace-cooled condition, and the strength increase was rationalized in terms of the Orowan mechanism of hardening by nondeforming particles.

FUTURE WORK

The preceding discussion on the strengthening of recrystallized high-carbon Mo-TZM by a heat treatment which produces very finely dispersed carbides, suggests that this may be a very potent way to improve the strength of this commercial alloy.

However, rather than relying solely on the precipitates to strengthen by blocking dislocation motion, it is now recognized that suitable thermomechanical processing can be very effective in further increasing the strength by a large amount. The technique is essentially as follows. In an alloy which contains a fine, stable, uniformly distributed precipitate or dispersion (~100-500 Å in diameter and having a spacing of ~1000-4000 Å), the precipitate can be utilized to stabilize a very fine grain and/or subgrain size. This can be achieved by repetitious light working followed by recovery annealing. During annealing, the dislocations introduced by working rearrange themselves in a cell structure pinned by the precipitate. Gradually a cell structure builds up with repeated working-annealing cycles, until finally a very stable grain or subgrain structure is achieved, with a size approximately equal to that of the interparticle spacing. A material with such a fine effective grain size should be very strong, and the structure should be stable at high temperatures if the processing is done correctly. This technique has been successfully exploited by Du Pont and Sherritt-Gordon Mines, Ltd., in producing Ni-ThO_2 alloys having good strength and excellent high-temperature stability.

In a preliminary investigation on quenched high-carbon Mo-TZM (which has carbides ~500 Å in diameter, spaced ~3000 Å apart - see Figures 6a and 6b) this thermomechanical processing technique was very successful in producing high-strength wires. The fabrication procedure was essentially as follows:

(a) After quenching 1/4-inch-diameter rods from 2100 C, the specimens were canned in stainless steel.

(b) Working was accomplished by hot swaging (at ~1050 C) and warm wire drawing (at ~500 C), with intermediate anneals of 1/2 hour at 1050 C after each 15 percent reduction. In the final stages of wire drawing, the intermediate anneals were omitted and the drawing was done at room temperature.

Wire specimens of different diameters were tested at a strain rate of 2 min^{-1} to compare with the properties of as-quenched Mo-TZM (from Table XVIII), and the results are listed in Table VII. The excellent improvement in strength with swaging and wire drawing lends support to the concepts discussed above, although at present the high-temperature structural stability has not been investigated. Transmission electron microscopy studies on the wires are presently under way to determine the effect of working on the structure, i.e., the cell size and general dislocation structure.

TABLE VII. PROPERTIES OF HIGH-CARBON Mo-TZM, AS-QUENCHED FROM 2100 C, SWAGED, AND WIRE DRAWN ($\dot{\epsilon}$ = 2 MIN^{-1})

	Room Temperature			200 C		
Condition	0.2% YS, psi	UTS, psi	% RA	0.2% YS, psi	UTS, psi	% RA
As-quenched, 0.25" diameter bar	~80,000[a]	~95,000[a]	--	69,000	81,000	17.5
Hot swaged to 0.080"	194,000	194,000	37	178,000	178,000	65
Warm wire drawn to 0.045"	320,000	320,000	59	239,000	239,000	66
Warm wire drawn to 0.028"	351,000	351,000	41			
Ditto	353,000	353,000	46			
Cold wire drawn to 0.017"	418,000	418,000	39			

(a) Extrapolated to room temperature from Figure 62.

The highest room-temperature strength achieved to date (418,000 psi on 17-mil wire) is approximately three times stronger than commercial wrought-stress-relieved Mo-TZM sheet or bar (120-140,000-psi ultimate tensile strength[26]. It is anticipated that further wire drawing, to say ~5 mil, would produce strengths greater than 500,000 psi. For example Embury and Fisher[27] have measured strengths of ~600,000 psi on 3-mil drawn pearlitic steel. Here a stable, elongated cell-type substructure was achieved by wire drawing, with the cell size decreasing with decreasing wire diameter.

The success achieved in this preliminary investigation has suggested several avenues of research aimed at further exploiting this technique of strengthening. For example such high-strength wires are likely candidates for reinforcing filaments in fiber-reinforced composites. However before such applications can be made much additional research is needed to fully evaluate the properties of Mo-TZM wires produced by this technique. Of particular importance are such studies as

(a) An investigation of different heat-treating procedures to determine the optimum treatment for producing the finely dispersed carbides. For example the present treatment employing a quench from 2100 C may not result in the optimum dispersion.

(b) The effect of varying the fabrication process (e.g., working and annealing temperature, swaging and wire-drawing reductions, etc.) on the mechanical properties.

(c) The high-temperature structural stability of wires produced by this technique, particularly the recovery and recrystallization characteristics as well as elevated-temperature mechanical properties.

(d) A detailed investigation relating the properties to the structure, particularly the substructure developed by different heat treatments and the swaging and wire-drawing operations.

APPENDIX I

CALIBRATION FOR ELEVATED-TEMPERATURE TENSILE TESTING IN AN ELECTRON-BEAM FURNACE

Although electron-beam heating of tensile or compression specimens has been done in the past, previous investigators[28, 29] have made the specimen the anode, and heating was accomplished by direct impingement of electrons on the specimen test section.

Applied this way, however, the technique has the following disadvantages:

(1) Since the specimen is heated by electrons accelerated in the field directly over the specimen surface, and the strength of this field is inversely proportional to the radius of curvature of the specimen, then the rate of heating is proportional to the specimen radius. As necking of a tensile specimen begins and causes a local reduction in radius, the specimen is preferentially heated in the necked region. This effect is autocatalytic and can lead to ductility data (e. g., reduction in area and total elongation), relating not to the temperature at which the test is nominally performed, but, to some temperature higher by an unknown amount.

(2) In addition, determination of the specimen temperature even prior to necking is extremely difficult. Thermocouples attached to the specimen surface generally give erroneous readings because of the preferential attraction of electrons by the small-diameter thermocouple leads, the bead of which need not necessarily be in thermal equilibrium with the specimen. Melting-point determinations on wires of different materials wound round the specimen are inaccurate for the same reason. Optical pyrometry is also faulty because usually the specimen radiates under conditions far removed from a black body, and reflection of the high-temperature filament from the specimen surface can give optical readings much in error.

In order to circumvent these difficulties, the electron-beam test chamber shown in Figure 35 was designed which permits accurate temperature calibration and eliminates local heating associated with necking. The system was made for use in a 6-kw electron-beam furnace manufactured by the Gilliland Instrument Co., Inc., of Oakland, California (see Figure 9) and adapted to an Instron testing machine. As seen in Figure 35, the specimen is surrounded by a tantalum tube (3/32-inch wall thickness) which is open at the bottom and screws onto the specimen at the top. This tube becomes the anode heated by the electron beam, and the specimen is heated by radiation from the tantalum. The specimen is thus electrically shielded, which permits the use of thermocouples for direct temperature measurement, and also permits calibration by melting-point determinations. It is also shielded optically from the filament and radiates under conditions more closely approximating black-body conditions.

During a tensile test, the specimen temperature is measured with a calibrated Leeds and Northrup optical pyrometer by sighting on the specimen gage length through the hole in the tantalum radiation anode. The specimen surface brightness readings

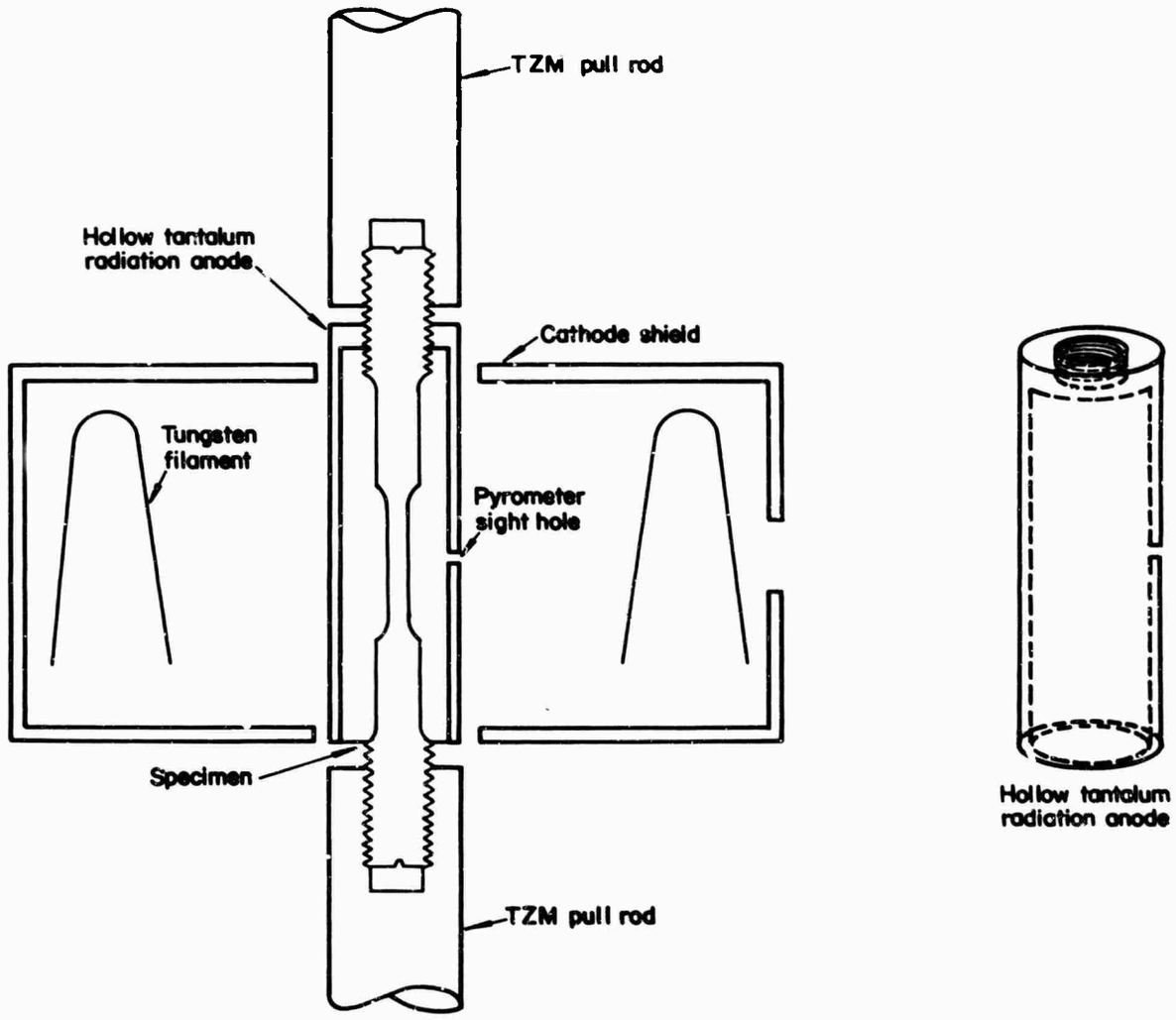

FIGURE 35. SCHEMATIC ELECTRON-BEAM TENSILE TESTING CHAMBER

were calibrated against true temperature in the following way. A 1/16-inch-diameter hole was spark machined axially in an electropolished tungsten tensile specimen (1/2-inch gage length, 1/8-inch gage diameter) to the center of the gage length and fitted with an insulated Pt-Pt/10Rh thermocouple which is in contact with the specimen (Figure 36). Another hole, 1/32 inch in diameter (length-to-radius ratio = 6) was spark machined in the gage length perpendicular to the specimen axis for black-body optical pyrometer readings.

Table VIII lists the results from a typical temperature calibration, comparing the thermocouple and black-body temperatures with optical pyrometer readings on the specimen surface. At temperatures $\gtrsim$1200 C there is complete agreement between black-body and thermocouple readings. For temperatures below 1200 C, however, black-body readings deviated from the thermocouple readings and reliance was placed on the latter. At temperatures >1400 C it was necessary to remove the thermocouple because evaporation from the alumina insulator coated the specimen surface, thereby changing the emissivity, and it was necessary to check the accuracy of the black-body readings by a melting-point determination. A wire of A-nickel (liquidus temperature = 1446 C) was wound tightly around the specimen directly below the black-body hole. On heating, the nickel was observed to melt at a temperature of 1446 C as measured by the optical pyrometer black-body reading. Thus, the true temperature (shown in Table VIII) was taken to be that of the thermocouple readings below 1400 C, and as given by black-body readings above 1400 C.

TABLE VIII. RESULTS FROM TYPICAL TEMPERATURE CALIBRATION (REFER TO FIGURE 36)

Pt-Pt/10Rh Thermocouple at A (Specimen Center), C	Optical Pyrometer[a]	
	at B (Black-Body), C	at C (Specimen Surface)[b], C
800[c]	904	1104 C
972[c]	1021	1240
1090[c]	1113	1328
1191[c]	1194[c]	1395
1315[c]	1317[c]	1486
1398[c]	1400[c]	1554
--	1471[c]	1597
--	1580[c]	1692
--	1729[c]	1815
--	1785[c]	1859
--	1942[c]	2004
--	2085[c]	2139

(a) Optical pyrometer readings are corrected for sight glass losses.
(b) Specimen surface was electropolished as in tensile tests.
(c) "True temperature".

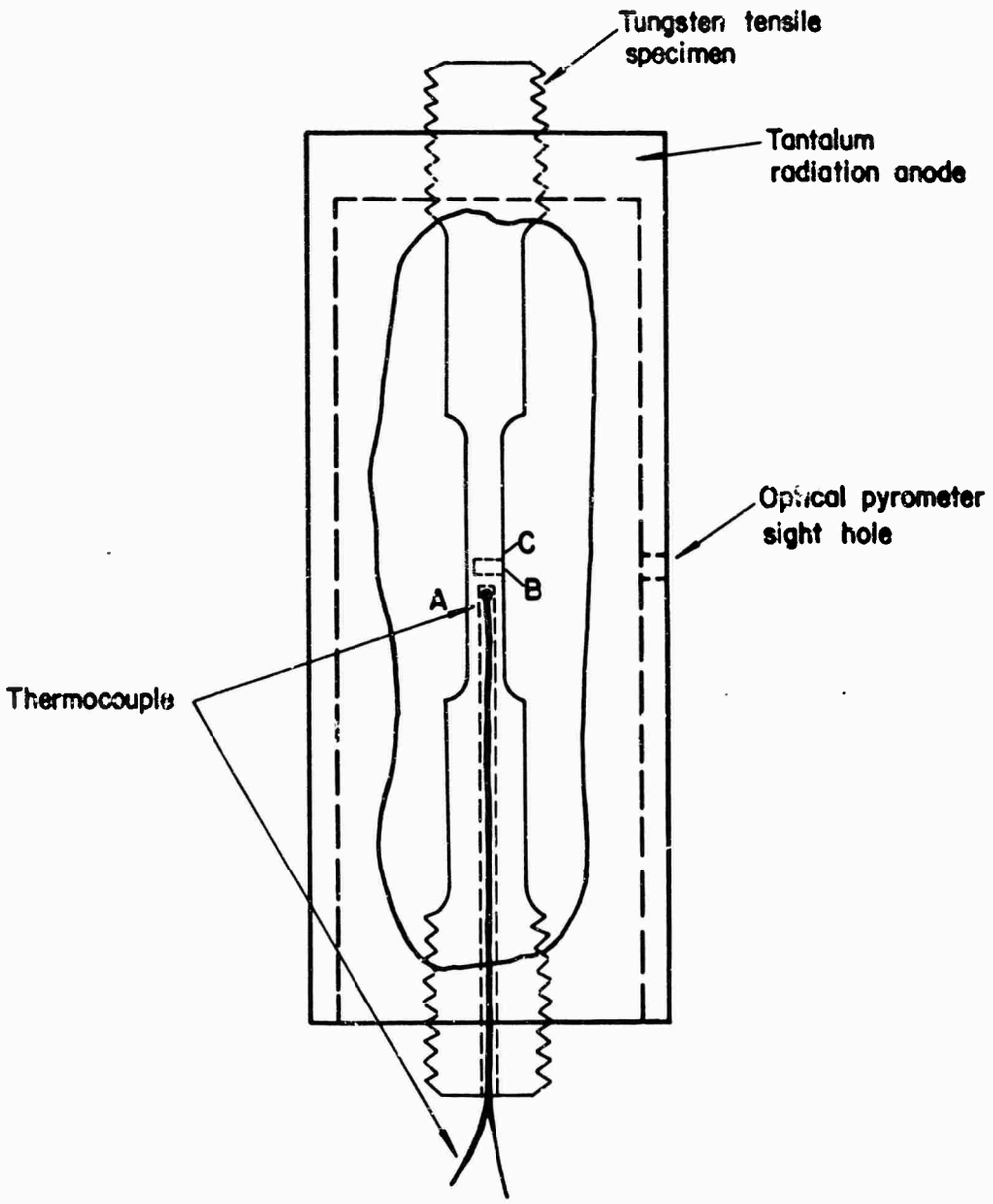

FIGURE 36. SCHEMATIC DRAWING OF ARRANGEMENT USED FOR TEMPERATURE CALIBRATION

APPENDIX II

HIGH-TEMPERATURE TESTING APPARATUS FOR USE WITH THE KRAFFT-HAHN DYNAMIC LOADER

Krafft-Hahn Dynamic Loader

High strain rates in tension were provided by a Krafft-Hahn Dynamic Loader, Model Dul. II-B, Serial No. 7 (see Figure 10). The machine operates by direction expansion of a volume of cold, pressurized gas acting on a driving piston. It is hydraulically stiffened by requiring the piston, in addition to loading the specimen, to force a gas-free liquid through a controllable restrictive orifice. The design results in a machine of high stiffness, rapid speed-response characteristics, and a wide speed range of 0.001 to 10 inches per second. Details of this machine and its operation are given in Reference (15). A crosshead speed of 5 inches per second was used and gave a strain rate of 600 per minute on the 0.5-inch-long reduced section of the specimens.

Furnaces

Test temperatures of 25-650 C were satisfactorily attained by one or two flexible electric heater tapes wired in parallel. The latter measured 1/2 x 24 inches (Briskeat No. 115) and handled 144 watts each. The specimen was held by two TZM pull rods attached to the dynamic loader and covered by the heater tapes. Tests were conducted in air up to 350 C. A stream of argon protected the specimens tested at 500 and 650 C, at which temperature surface oxidation became appreciable. Temperature was controlled by varying the voltage on the heater tape, and was measured by a Chromel-Alumel thermocouple. Its bead was wired directly to the center of the specimen reduced section.

The high-temperature furnace had to meet the following requirements:

(1) Produce specimen temperatures of 650-1700 C

(2) Fit into a space of 6-inch-diameter x 20 inches high, without undue heating of the dynamic loader

(3) Protect the specimens from oxidation

Vacuum-induction heating, satisfied the requirements. Heating was done by a 4-kw Lepel spark-gap converter at 125-450 kilocycles. Fine adjustment of the power output was achieved by varying a resistance (0-11.2 ohms, 2000 watts) in parallel with the work coil.

A compact vacuum system held the specimen which was gripped by two 1/2-inch-diameter TZM pull rods (see Figure 37). A 1/2-inch-ID, 0.020-inch wall, tantalum susceptor surrounded the specimen. The vertical specimen and susceptor were axially surrounded by a 25-mm-ID clear quartz tube, 12 inches long, and connected to two vacuum unions. The upper fitting contained a bellows assembly capable of a 5/8-inch stroke being distributed 75% compression 25% tension on the bellows. The latter was

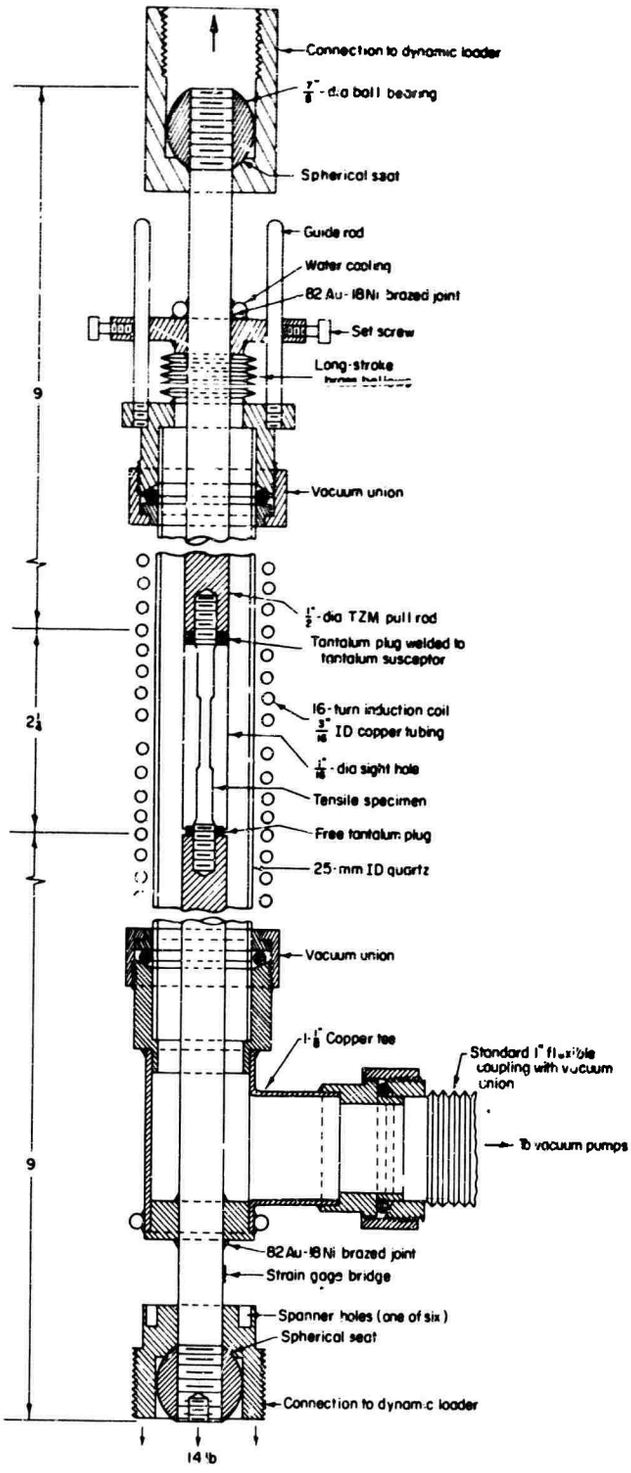

FIGURE 37. VACUUM-INDUCTION FURNACE FOR HIGH-STRAIN-RATE TENSILE TESTS IN KRAFFT-HAHN DYNAMIC LOADER

1-1/8-inch-OD, 5/8-inch-ID, single ply, 0.0042-inch brass made by Robertshaw Controls Company. The bellows was silver soldered (Easy Flo No. 45, 620 C) to the brass O-ring seat and 302 stainless steel top plate. The latter contained holes for positioning of the bellows with two guide rods and set screws. The top plate was vacuum brazed to the TZM pull rod with 82Au-18Ni at 950 C. The bottom O-ring seat was silver soldered to a copper tee which, in turn, was silver soldered to a flexible connection to the vacuum pumps and stainless steel plug. The latter was brazed to the TZM pull rod. Water cooling was provided by copper coils soft soldered near the two brazed joints and kept the extremities of the pull rods under about 100 C.

To obtain axial loading, the extremities of the TZM pull rods were threaded into two annealed 7/8-inch-diameter ball bearings. The balls rested in spherical seats in fixtures which screwed directly into the dynamic loader.

A platform holding 14 pounds of weights hung from the bottom pull rod. This weight just offset the compressive force on the specimen introduced by evacuation.

Since the specimen and pull rods extended about 0.1 inch on heating, the lower fitting was provided with six spanner holes. These enabled gentle tightening with a Lucite wrench during induction heating just before the test.

Vacuum was attained by a 2-inch vacuum system attached to the lower brass fitting. Pumps consisted of a 1402 B Welsh, 5-cfm mechanical pump in series with a PMC-115 145-liter/second oil-diffusion pump. Operating vacuums were about 0.1 micron or less as measured by a cold-cathode Philips gage. Two 0.022-inch-diameter radial holes at the bottom of the 1/2-20 internal threads of the TZM pull rods assured proper evacuation around the specimen threads.

Temperature Measurement

Specimen temperatures in tests performed in the vacuum furnace at 650-1700 C were estimated optically to ±25 C. Apparent surface temperatures were measured by sighting through a 1/16-inch-diameter hole in the tantalum susceptor and on the reduced section of the specimens. The major adjustment was the black-body correction. The latter was measured by determining the temperature difference between the surface and bottom of a 0.022-inch-diameter radial hole spark machined ~0.1 inch deep at the center of the reduced section of a dummy specimen. The difference amounted to a maximum of 200 C as presented in Figure 38. This difference did not appear to be significantly different for TZM and tungsten specimens.

Four other complications arose. In similar tests, the as-read hole temperature was higher than that indicated by a thermocouple for specimen temperatures lower than about 1200 C (see Appendix I). This discrepancy was as high as 100 C and could have been caused by the low level of radiation coming from the susceptor. The curved quartz tube introduced attenuation which amounted to as much as 70 C, as indicated in Figure 38. During initial outgassing runs, deposits formed on the inside of the quartz tube and reduced readings as much as 100 C. After these preliminary runs, the deposits were minor and barely detectable, even after tests near 1700 C. Lastly, it was necessary to allow for cooling, since it was necessary to turn off the induction before making the test, because the rf caused drastic distortions of the oscillogram. Attempts to shield the oscilloscope and introduce correction circuitry were inadequate. It was found that the specimen cooled from about 1350 to 1100 C (hole temperatures) within

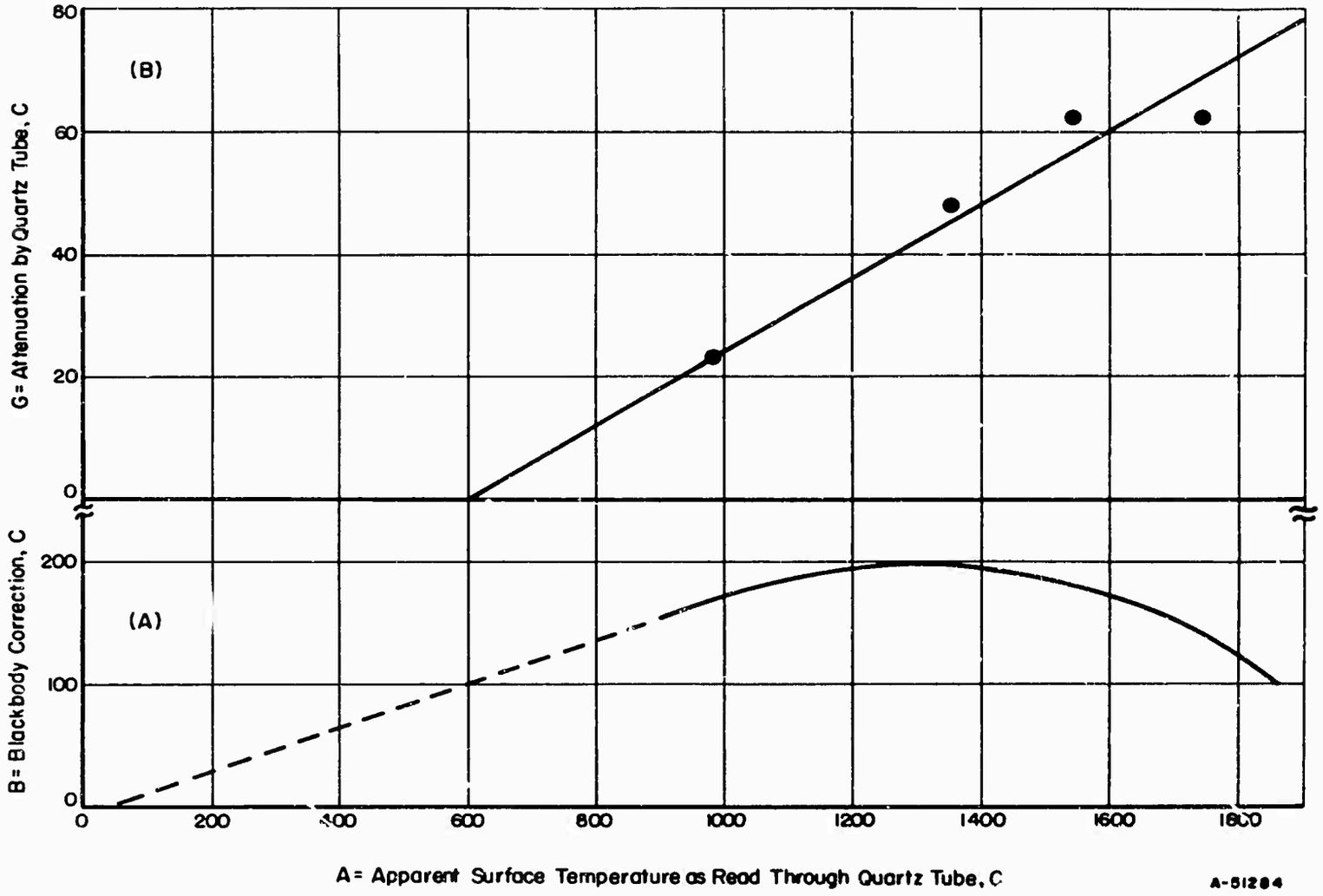

FIGURE 38. CORRECTIONS USED FOR SPECIMEN TEMPERATURE MEASUREMENT IN VACUUM-INDUCTION FURNACE ATTACHED TO KRAFFT-HAHN DYNAMIC LOADER

6 seconds, or roughly 25 C/second. With improved manual techniques, it was estimated the test was completed 1 second after the induction was shut off. The duration of the test (about 50 milliseconds) was small in comparison. Cooling corrections were estimated for each test temperature.

In summary, the average true specimen temperature during the test can be expressed by

$$T = A - B - X - C + G + D, \tag{7}$$

where

A = apparent surface temperature as measured optically

B = black-body correction = T(surface) - T(hole)

X = additional adjustment for T < 1200 C

C = allowance for 1 second of cooling

G = attenuation caused by the quartz tube

D = attenuation caused by deposits on the quartz.

Equation (7) is evaluated for the range of test temperatures used as indicated in Table IX.

TABLE IX. ADJUSTMENTS USED TO DETERMINE SPECIMEN TEMPERATURE ACCORDING TO EQUATION (7)*

Temperature, C						
T	A	B	X	C	G	D
650	900	150	~100	20	20	0
800	1070	180	100	20	30	0
950	1190	200	50	20	30	0
1100	1310	200	20	30	40	0
1250	1430	190	0	30	50	0
1400	1550	180	0	30	60	0
1550	1690	160	0	~40	60	~0
1700	1800	120	0	~50	70	~0

(a) A = apparent surface temperature as measured optically, B = black-body correction = T(surface) - T(hole), X = additional adjustment for T < 1200 C, C = allowance for 1 second of cooling, G = attenuation caused by the quartz tube, and D = attenuation caused by deposits on the quartz.

Load Measurement

Signals from strain gage network provided the vertical displacement of oscilloscope trace which, in turn, was used to measure tensile loads. For tests involving the vacuum furnace, strain gages (EA-06-031-DE-120, GF = 2.0, Micro Measurement Company) were attached (epoxy cement, maximum operating temperature 100 C) to the

lower TZM pull rod. The network consisted of a 4-gage bridge, two longitudinal (tension) and two interposed circumferential (compression), and arranged in a simple Wheatstone bridge circuit connected to a Tektronix Type 502 A oscilloscope, according to Figure 39. A d-c voltage was impressed on the bridge. The oscilloscope trace was positioned by R. During loading, resistance changes in the gages caused changes in voltage seen by the oscilloscope and resulted in vertical movement of the scope trace. For tests involving heater tapes, a similar bridge was used which consisted of strain gages (SR4 A-5, GF 2.0) mounted to the steel draw bar of the dynamic loader.

Loads were calibrated using an Instron tensile machine. Its load cell was clamped to the movable table of the dynamic loader. The member containing the strain gages was pulled at a low speed and stopped at at least six loads ranging from 0-4500 pounds as indicated on the Instron recorder. A convenient fast sweep of 5 msec/cm was used. A Polaroid photograph was taken of each load series, with at least three series being taken for each strain-gage network and oscilloscope sensitivity setting. Loads were calibrated to the vertical displacement measured on the photograph. Calibrations remained linear and essentially constant on the basis of three checks during a 3-month testing period and were

Sensitivity, mv/cm	Calibration, lb per cm	
	1-Inch-Diameter Steel Draw Bar	0.5-Inch-Diameter TZM Pull Rod
0.2	350 ±5	134 ±5
0.5	874 ±5	335 ±5

As a further indication of linearity, the ratio of sensitivities and calibration for a given load member are equal. As expected, the TZM pull rod gave about a factor of two more sensitivity than the steel draw bar. The fourfold reduction in cross-sectional area was partially affected by the higher elastic modulus of the TZM.

Strain Measurement

The horizontal sweep of the oscilloscope provided a measure of strain. Plastic extension of the specimen was calculated from

$$\Delta L = f \times t \, s \ , \tag{8}$$

where x = plastic extension measured on the oscillogram in cm, t = oscilloscope sweep time in sec/cm, s = average cross head speed in in./sec, and f is a scale factor of 1.09 relating the measured lengths to the equivalent lengths on the oscilloscope screen. Calculated values of total plastic extension agreed to within 20 percent of those measured on broken specimens with s ~5 in./sec. For elongations under 0.25 inch (i.e., <50 percent strain) the agreement was better.

Calculated total elongations were generally greater than those measured on the broken specimens. This suggests the cross head slowed down during the test. In an effort to minimize this, the high-pressure charge in the dynamic loader was set relatively high (1200 psi) to make the machine stiffer.

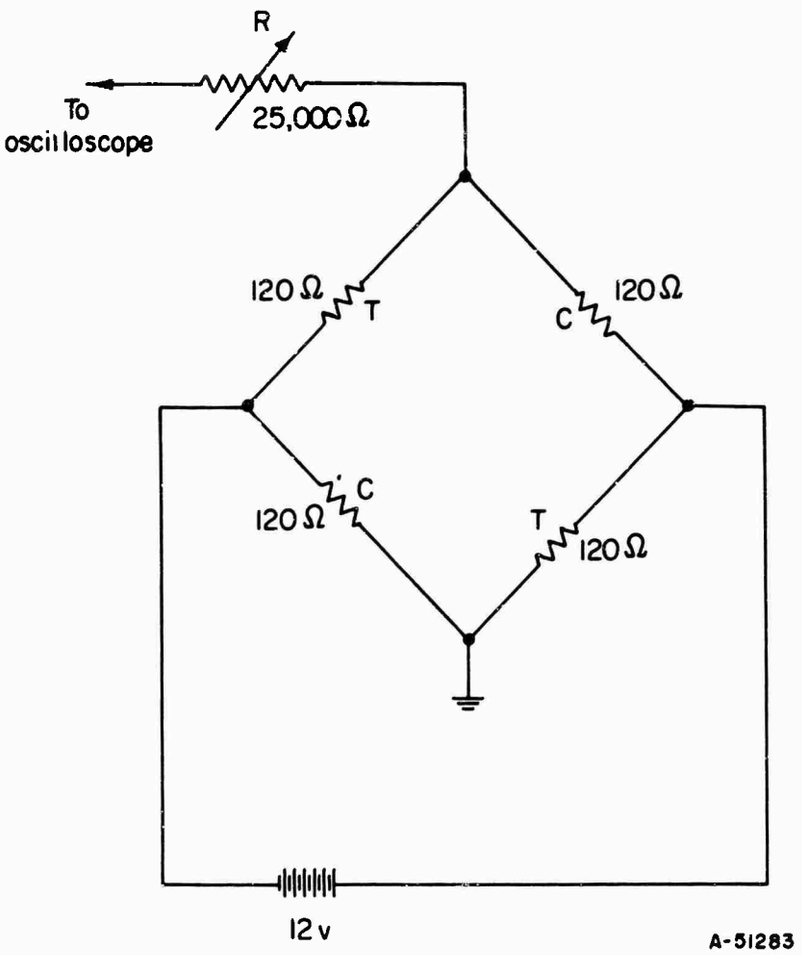

FIGURE 39. STRAIN-GAGE BRIDGE USED TO MEASURE LOADS

APPENDIX III

MECHANICAL-PROPERTY DATA FOR MATERIALS TESTED

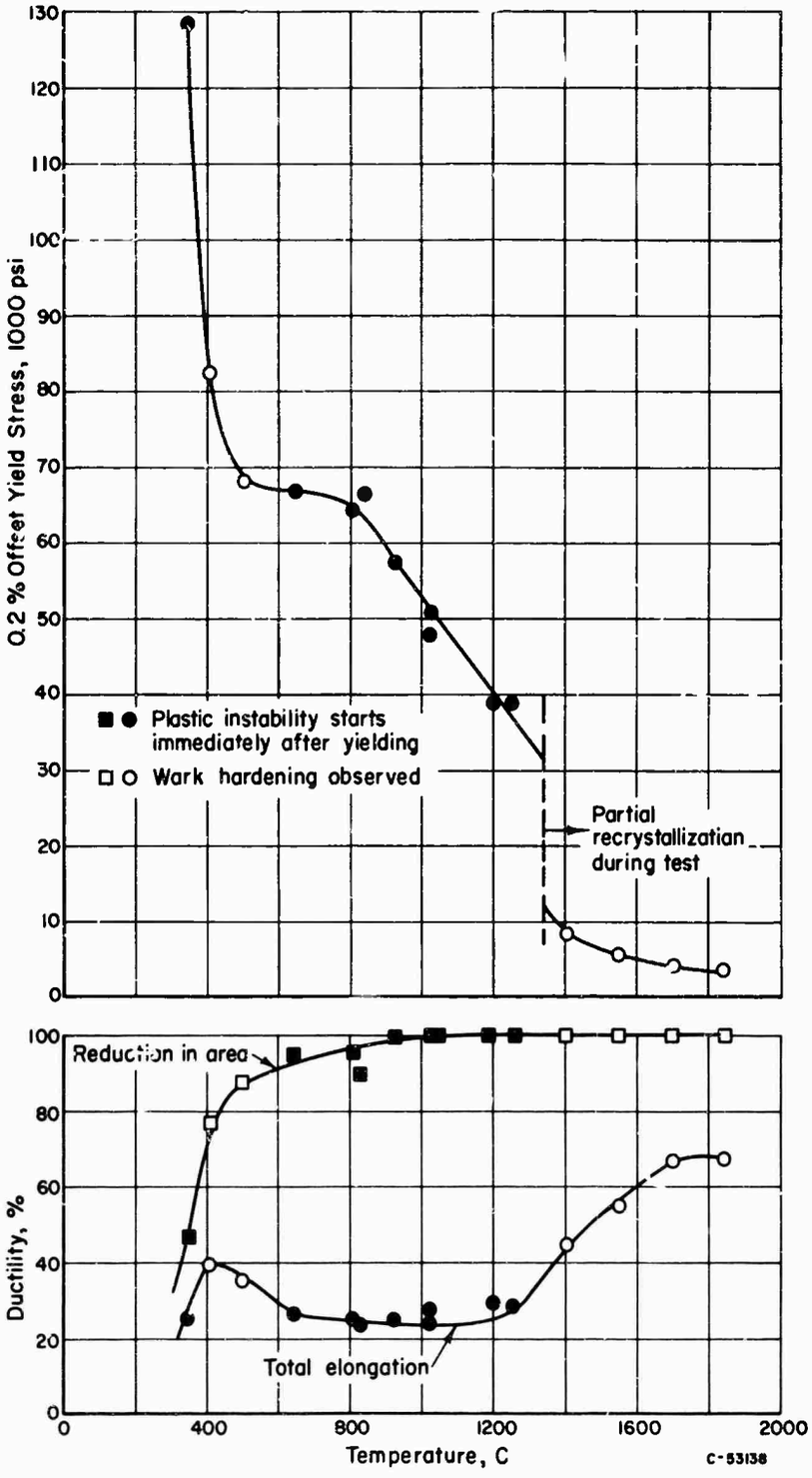

FIGURE 40. MECHANICAL PROPERTIES OF WROUGHT-STRESS-RELIEVED LOW-CARBON TUNGSTEN (10 PPM CARBON), TESTED AT $\dot{\epsilon}$ = 0.01 MIN^{-1}

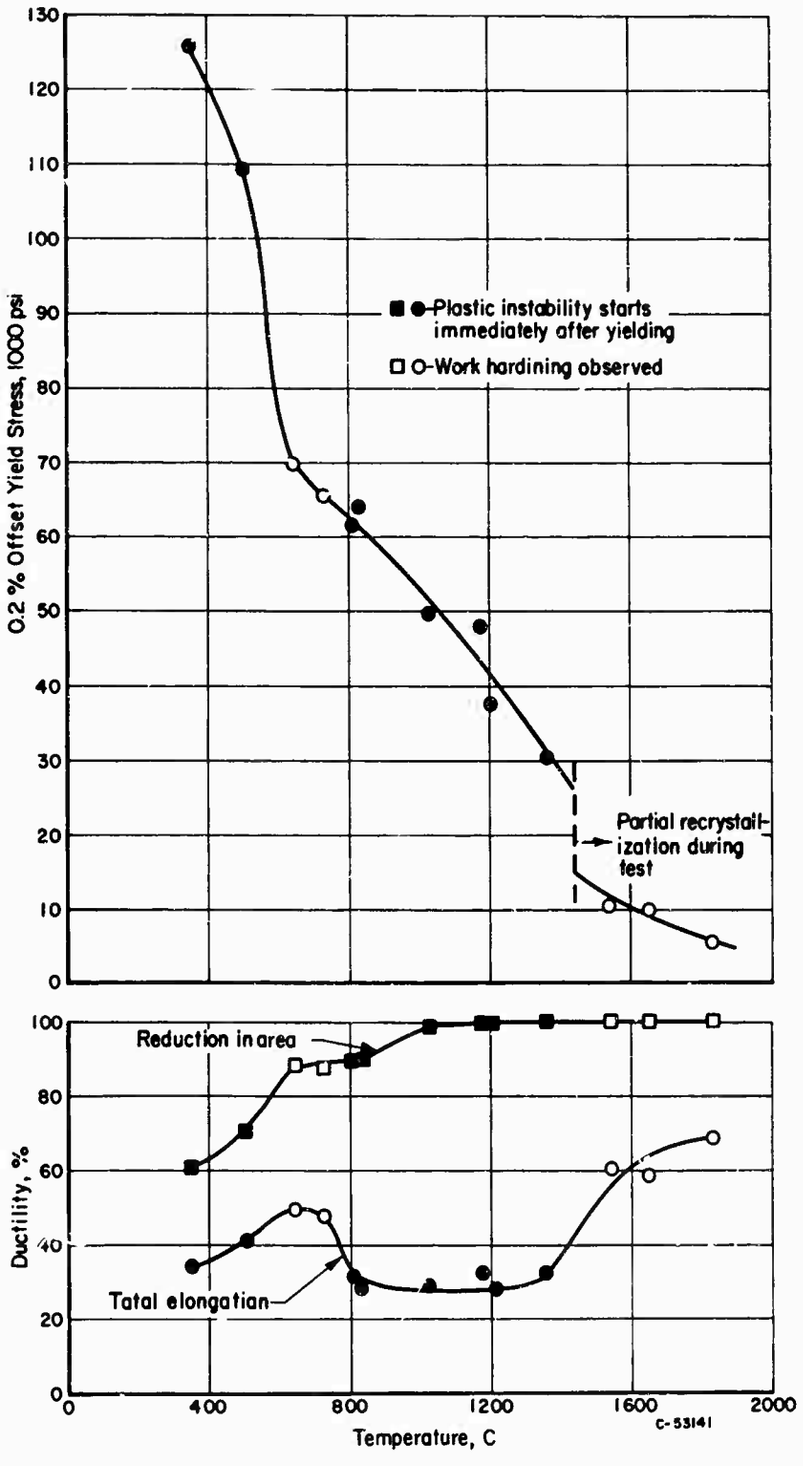

FIGURE 41. MECHANICAL PROPERTIES OF WROUGHT-STRESS-RELIEVED LOW-CARBON TUNGSTEN (10 PPM CARBON), TESTED AT $\dot{\epsilon}$ = 2 MIN^{-1}

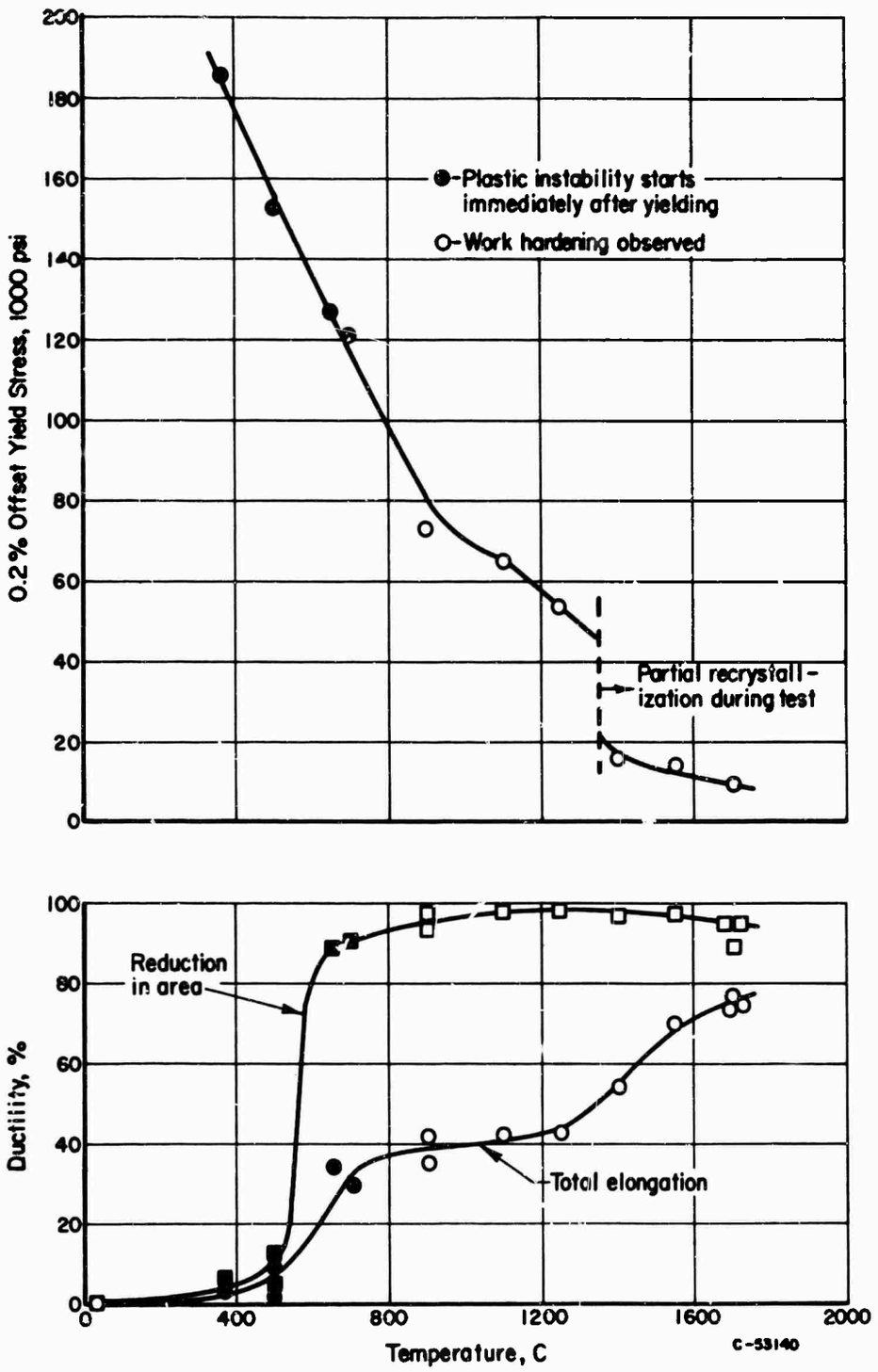

FIGURE 42. MECHANICAL PROPERTIES OF WROUGHT-STRESS-RELIEVED LOW-CARBON TUNGSTEN (10 PPM CARBON), TESTED AT $\dot{\epsilon} = 600\ \text{MIN}^{-1}$

TABLE X. MECHANICAL-PROPERTY DATA FOR WROUGHT-STRESS-RELIEVED LOW-CARBON TUNGSTEN (10 PPM CARBON)

Test Temperature, C	Total Elongation, percent	Reduction in Area, percent	0.2% Offset Yield Strength, ksi	Ultimate Tensile Strength, ksi	True Fracture Stress, ksi	Deformation Characteristics
			$\dot{\epsilon}$ = 0.01 Min^{-1}			
350	25.1	46.3	128.5(a)	130.0(b)	189	Yield drop, immediate plastic instability
410	39.9	76.6	82.2	85.3	224	Yield drop, slight work hardening
500	35.1	87.6	68.1	71.7	255	Ditto
645	26.9	95.0	66.7(a)	69.5(b)	286	Yield drop, immediate plastic instability
807	25.2	95.1	64.4(a)	67.3(b)	186	Ditto
830	23.8	89.9	66.7(a)	71.9(b)	286	"
925	25.4	~100	57.6(a)	57.9(b)	--	"
1025	27.4	~100	51.0(a)	51.8(b)	--	"
1028	26.0	~100	47.9(a)	48.6(b)	--	"
1200	29.0	~100	38.9(a)	39.1(b)	--	"
1250	28.2	~100	39.3(a)	39.9(b)	--	"
1405	44.6	100	8.2	20.5	--	No yield drop, strong work hardening
1550	55.0	~100	5.5	14.2	--	Ditto
1770	67.0	~100	4.2	10.3	--	"
1845	68.0	~100	3.7	10.0	--	"
			$\dot{\epsilon}$ = 2 Min^{-1}			
351	34.5	60.7	125.7(a)	124.0(b)	216	Yield drop, immediate plastic instability
504	41.0	70.1	112.9(a)	113.6(b)	227	Ditto
647	49.5	88.7	69.7	74.9	302	Yield drop, slight work hardening
730	47.5	87.2	65.7	69.7	258	No yield drop, slight work hardening
810	31.5	89.2	61.4	63.9	212	No yield drop, immediate plastic instability
830	28.9	90.3	64.2(a)	66.2(b)	259	Yield drop, immediate plastic instability
1024	29.7	~100	49.7(a)	50.4(b)	--	Ditto
1174	32.8	~100	47.8(a)	47.9(b)	--	"
1210	28.8	100	37.8	38.5	--	No yield drop, immediate plastic instability
1365	32.2	~100	30.3	31.4	--	Ditto
1542	60.4	~100	10.9	20.8	--	No yield drop, strong work hardening
1650	59.0	~100	10.0	20.2	--	Ditto
1835	68.8	~100	5.7	17.6	--	"
			$\dot{\epsilon}$ = 600 Min^{-1}			
25	0.0	0.0	--	>115	>115	Brittle fracture
370	4.2	6.4	186	186(b)	~173	Yield drop, immediate plastic instability
500	10.0	12.5	153	153(b)	~148	Ditto
500	3.0	4.0	--	--	--	"
650	34.8	88.4	127	127(b)	~280	"
700	29.9	90.3	121.8	121.8(b)	--	"
900	41.6	94.0	71.6	73.6	--	Yield drop, slight work hardening
900	35.0	96.8	--	--	--	Ditto
1100	42.4	98.0	65.5	65.7	--	"
1250	42.4	98.2	54.0	54.0	--	"
1400	54.0	97.0	15.5	39.0	--	Yield drop, strong work hardening
1550	70.0	97.0	14.2	32.8	--	Ditto
1700	74.2	88.6	~10	27.9	--	Strong work hardening
1700	76.8	94.8	--	--	--	Ditto
1700	74.0	95.0	--	--	--	"

(a) The 0.2 percent strain was less than the strain at the upper yield point.
(b) The maximum load in these tests was the upper yield point.

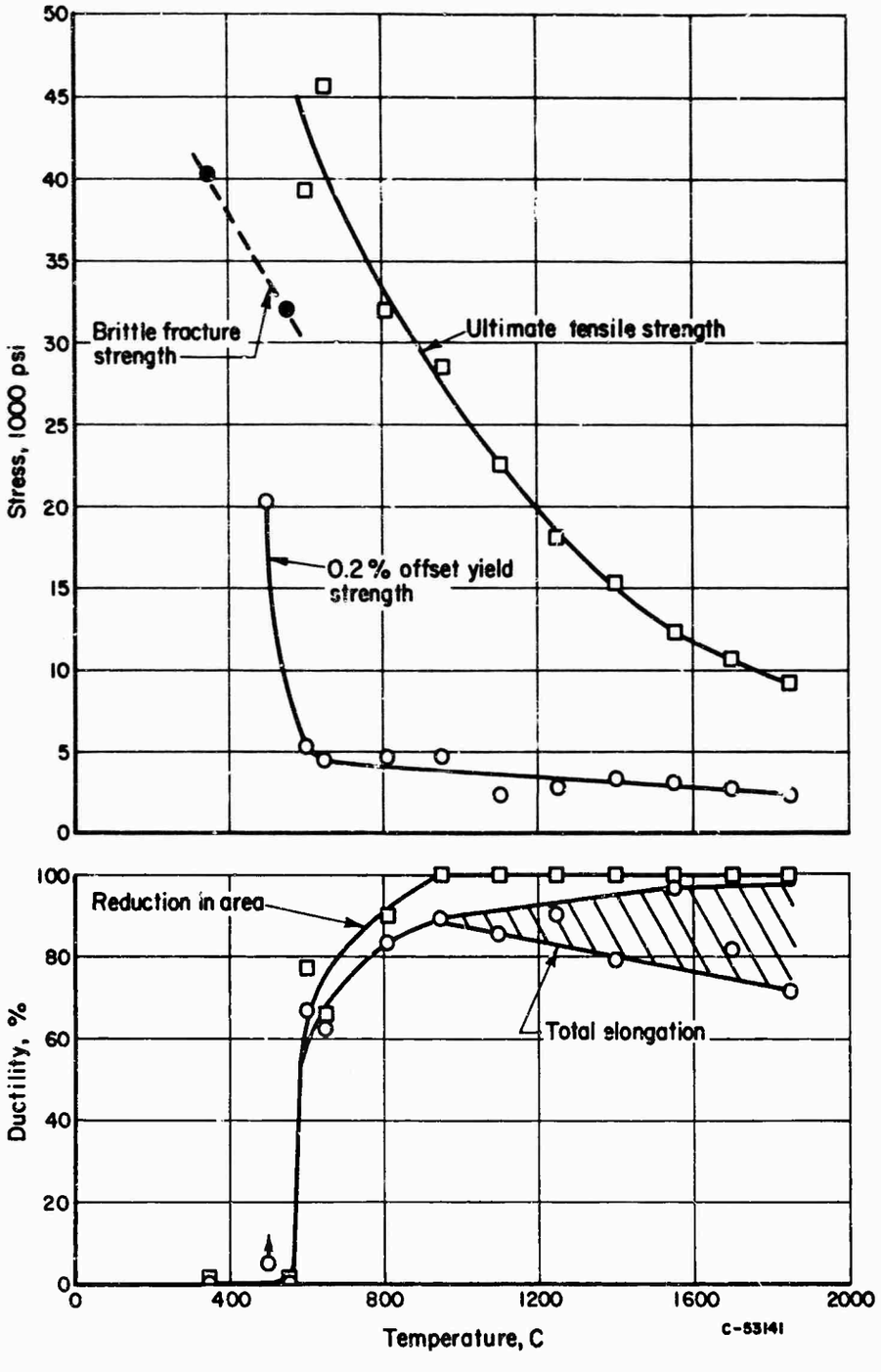

FIGURE 43. MECHANICAL PROPERTIES OF RECRYSTALLIZED LOW-CARBON TUNGSTEN (10 PPM CARBON), TESTED AT $\dot{\epsilon} = 0.01\ \text{MIN}^{-1}$

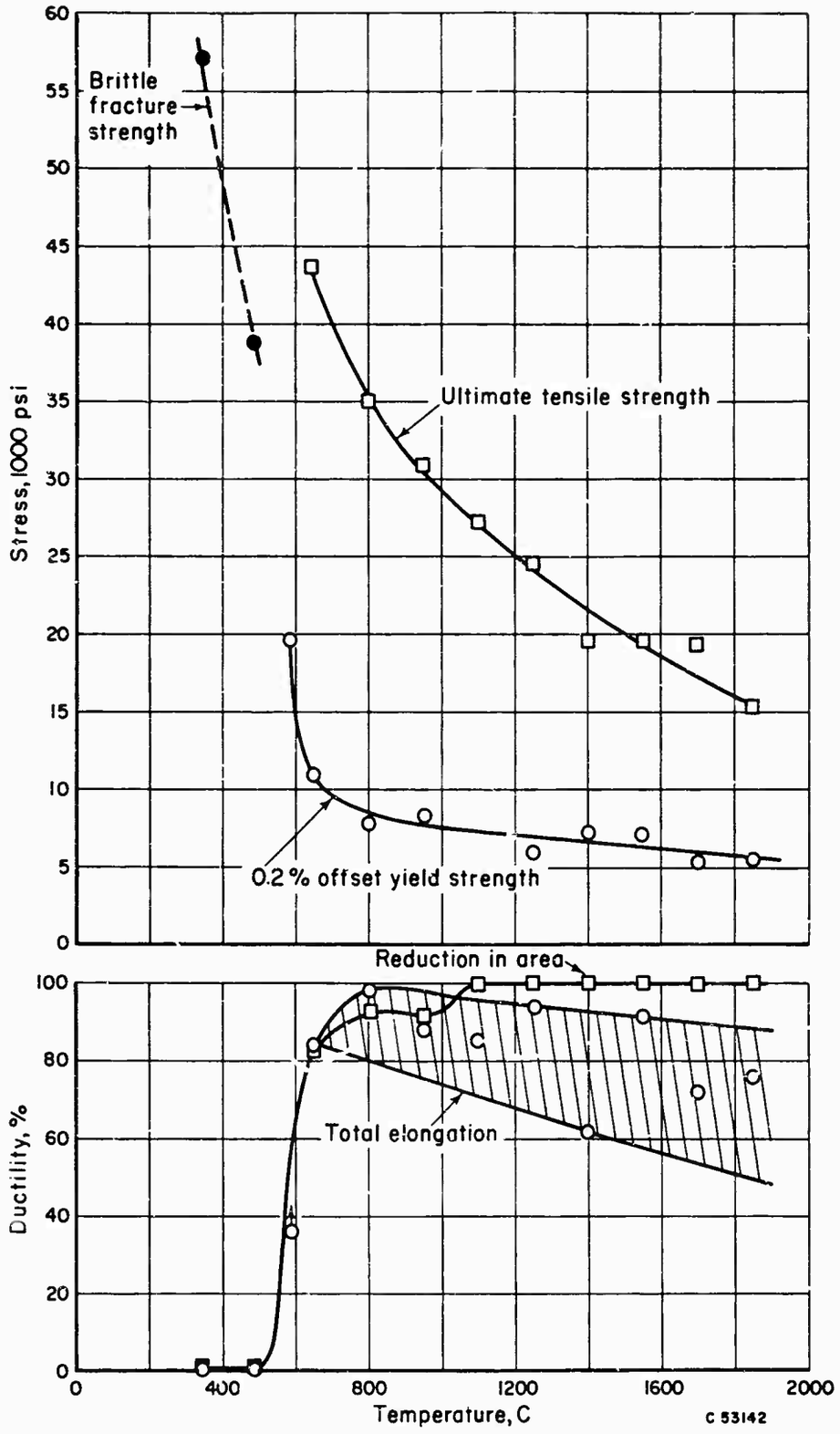

FIGURE 44. MECHANICAL PROPERTIES OF RECRYSTALLIZED LOW-CARBON TUNGSTEN (10 PPM CARBON), TESTED AT $\dot{\epsilon}$ = 2 MIN^{-1}

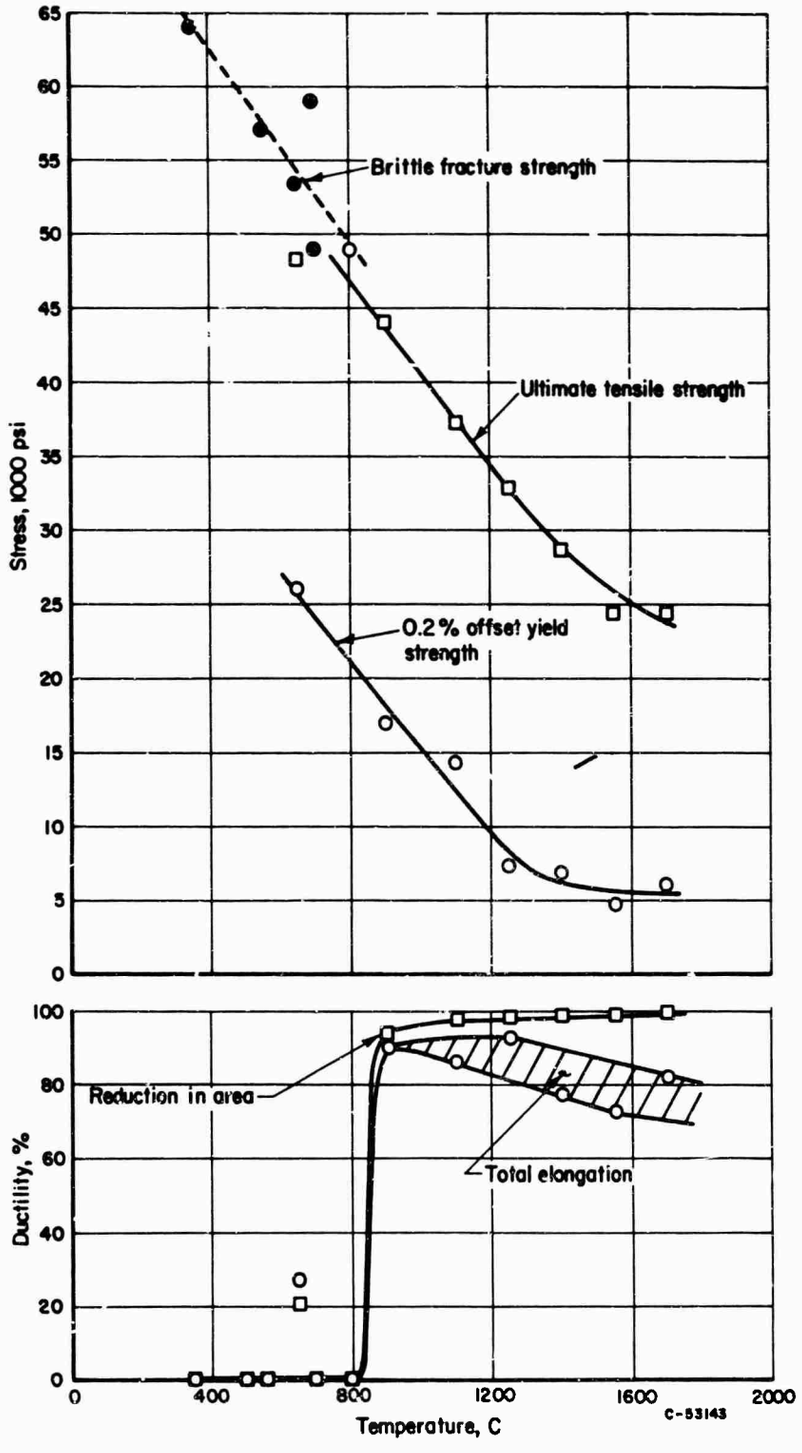

FIGURE 45. MECHANICAL PROPERTIES OF RECRYSTALLIZED LOW-CARBON TUNGSTEN (10 PPM CARBON), TESTED AT $\dot{\epsilon}$ = 600 MIN^{-1}

TABLE XI. MECHANICAL PROPERTY DATA FOR RECRYSTALLIZED LOW-CARBON TUNGSTEN (10 PPM CARBON)

Test Temperature, C	Total Elongation, percent	Reduction in Area, percent	0.2% Offset Yield Strength, ksi	Ultimate Tensile Strength, ksi	True Fracture Stress, ksi	Deformation Characteristics
			$\dot{\epsilon} = 0.01\ Min^{-1}$			
354	0	0	--	--	40	Brittle fracture
500	>5.3	--	20.4	--	--	Yield drop, strong work hardening, broke in shoulder
550	0.1	0.1	--	--	32	Fractured at upper yield point
600	66.8	77.3	5.2	39.4	~114	No yield point, strong work hardening
646	62.5	66.6	4.4	45.7	~109	Ditto
808	83.6	89.8	4.7	32.0	~103	"
946	89.0	~100	4.8	28.6	--	"
1100	85.6	~100	2.4	22.6	--	"
1250	90.6	~100	2.9	18.2	--	"
1400	79.6	~100	3.3	15.3	--	"
1550	97.2	~100	3.1	12.4	--	"
1700	81.0	~100	2.8	10.9	--	"
1850	70.5	~100	2.4	9.3	--	"
			$\dot{\epsilon} = 2\ Min^{-1}$			
350	0	0	--	--	57	Brittle fracture
492	0	0	--	--	38	Ditto
590	>36	--	19.2	-	--	Yield drop, strong work hardening, broke in threads
647	84.0	82.5	10.8	43.7	~143	Yield drop, strong work hardening
805	98.8	93.0	7.9	35.0	~149	No yield drop, strong work hardening
949	88.0	91.6	8.2	30.9	--	Ditto
1100	85.0	~100	--	27.2	--	"
1250	93.6	~100	5.9	24.5	--	"
1400	61.6	~100	7.5	19.5	--	"
1550	91.2	~100	7.0	19.7	--	"
1700	72.0	~100	5.4	19.4	--	"
1850	75.2	~100	5.5	15.3	--	"
			$\dot{\epsilon} = 600\ Min^{-1}$			
350	0.0	0.0	--	--	65	Brittle fracture
500	0.0	0.0	--	--	--	Ditto
550	0.0	0.0	--	--	57	"
650	27.2	20.3	~26.0	45.4	53	No yield drop, strong work hardening
700	0.0	0.0	--	--	49	Brittle fracture
700	0.0	0.0	--	--	59	Ditto
800	0.0	0.0	--	--	49	"
900	90.6	93.4	17.1	43.0	--	No yield drop, strong work hardening
1100	86.8	97.5	~14.0	37.3	--	Ditto
1250	92.8	97.9	7.2	32.8	--	"
1400	77.6	98.0	6.8	28.6	--	"
1550	72.6	98.5	4.6	24.4	--	Yield drop, strong work hardening
1700	81.4	99.1	6.0	24.3	--	Ditto

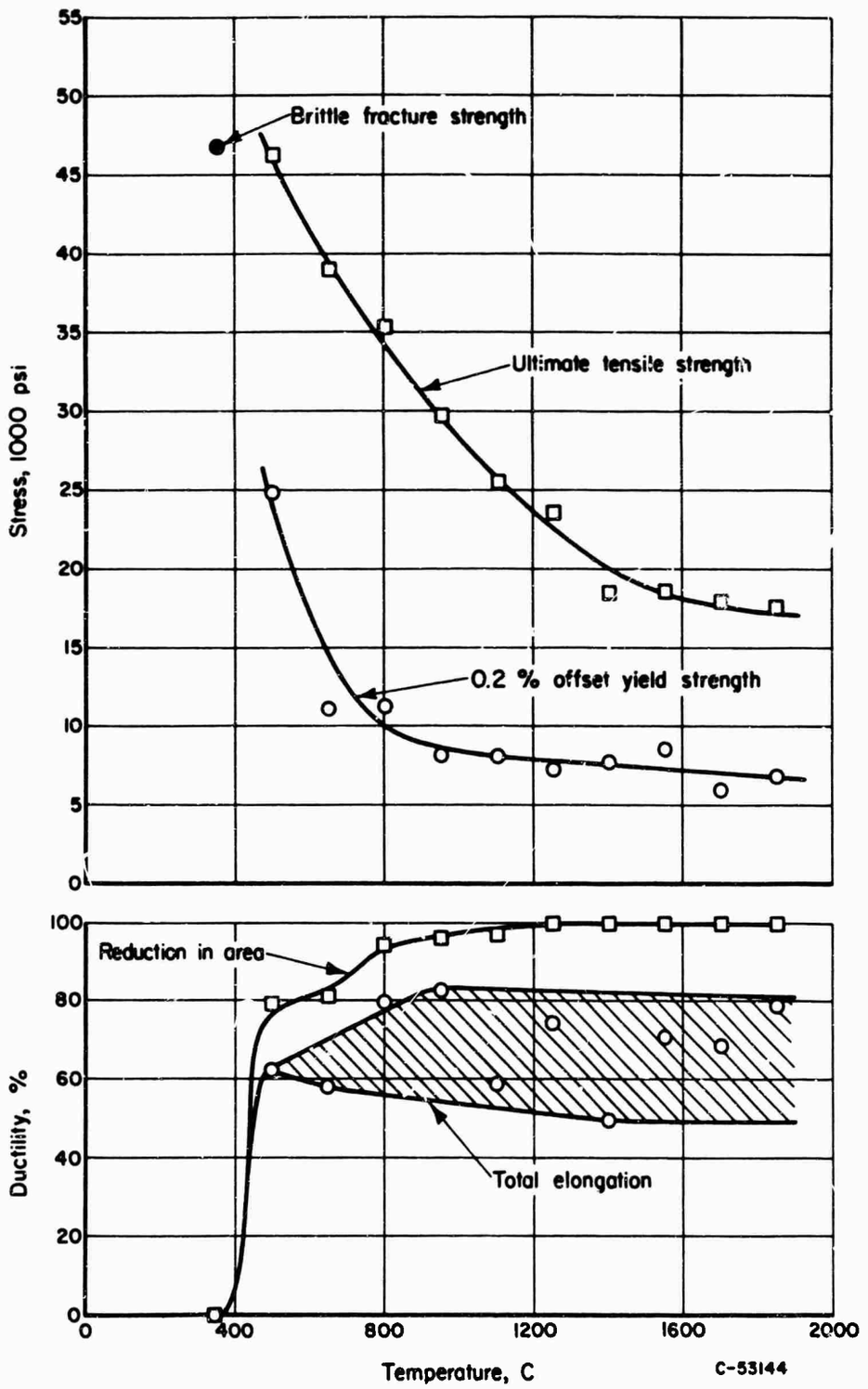

FIGURE 46. MECHANICAL PROPERTIES OF RECRYSTALLIZED HIGH-CARBON TUNGSTEN (35 PPM CARBON) TESTED AT $\dot{\epsilon} = 2\ \text{MIN}^{-1}$

TABLE XII. MECHANICAL-PROPERTY DATA FOR RECRYSTALLIZED HIGH-CARBON TUNGSTEN (35 PPM CARBON)

Test Temperature, C	Total Elongation, percent	Reduction in Area, percent	0.2% Offset Yield Strength, ksi	Ultimate Tensile Strength, ksi	True Fracture Stress, ksi	Deformation Characteristics
				$\dot{\epsilon} = 2\ \text{Min}^{-1}$		
350	0.0	0.0	--	--	46	Brittle fracture
500	62.8	79.9	24.9	46.2	191	Yield drop, strong work hardening
650	58.2	81.2	11.1	39.0	--	No yield drop, strong work hardening
800	80.0	95.0	11.3	35.3	--	Ditto
950	82.8	96.1	8.4	29.9	--	"
1100	58.8	97.0	8.1	25.6	--	"
1250	74.8	~100	7.2	23.6	--	"
1400	49.6	~100	7.7	18.5	--	"
1550	71.2	~100	8.6	18.6	--	"
1700	68.4	~100	6.0	18.0	--	"
1850	79.6	~100	6.7	17.7	--	"

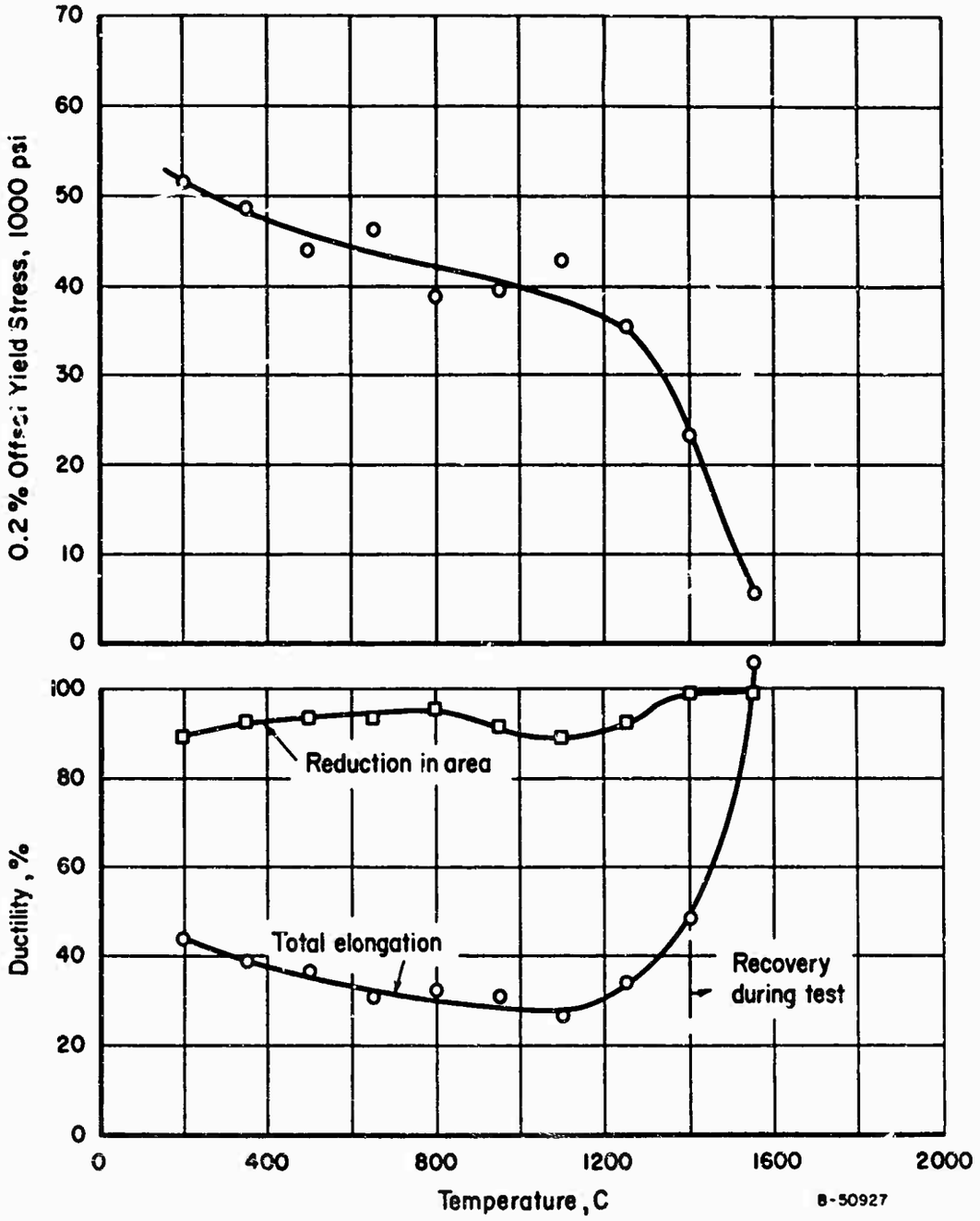

FIGURE 47. MECHANICAL PROPERTIES OF WROUGHT, STRESS-RELIEVED LOW-CARBON Mo-TZM (10 PPM CARBON), TESTED AT $\dot{\epsilon} = 0.01$ MIN^{-1}

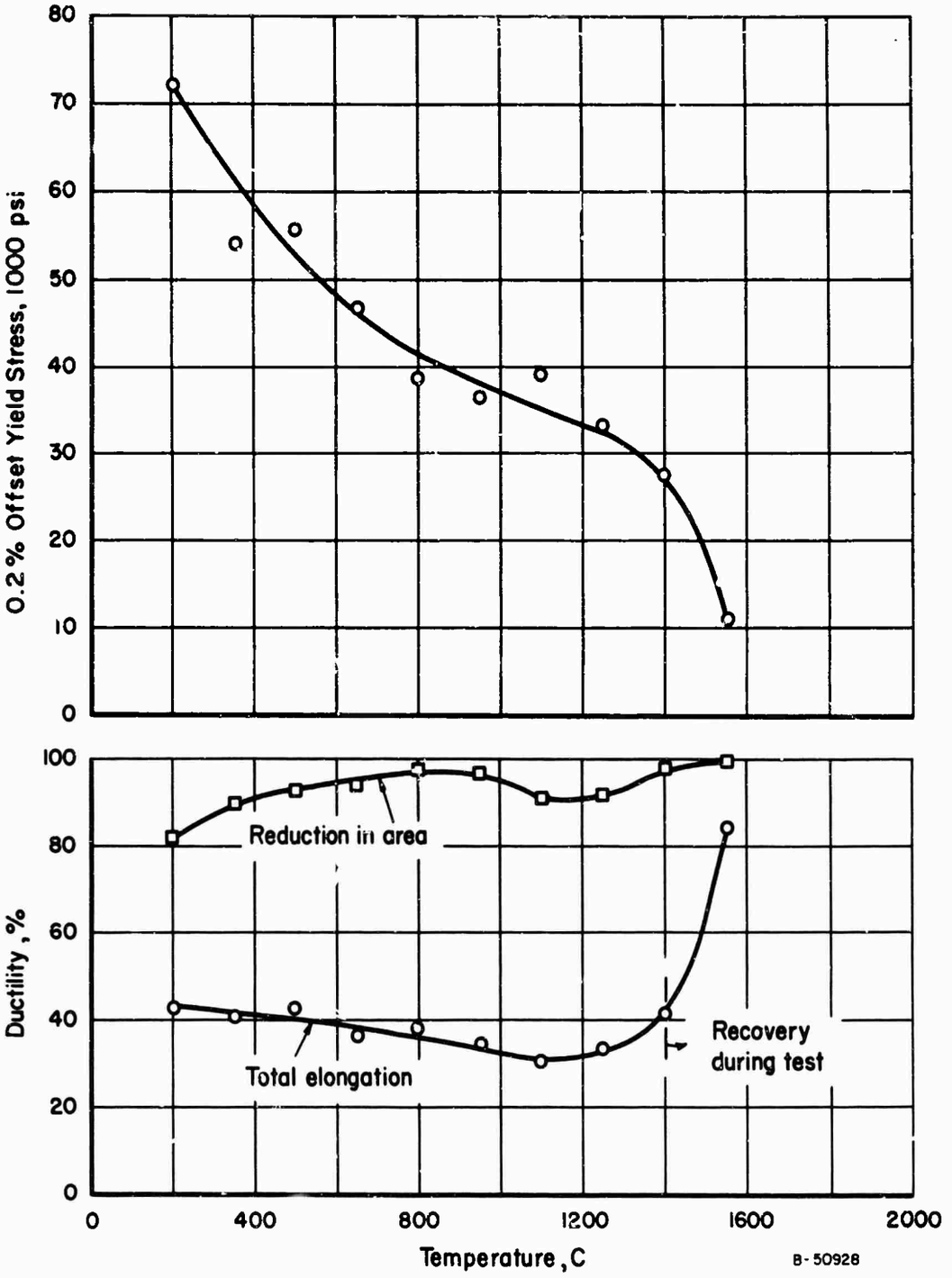

FIGURE 48. MECHANICAL PROPERTIES OF WROUGHT, STRESS-RELIEVED LOW-CARBON Mo-TZM (10 PPM CARBON), TESTED AT $\dot{\epsilon}$ = 2 MIN^{-1}

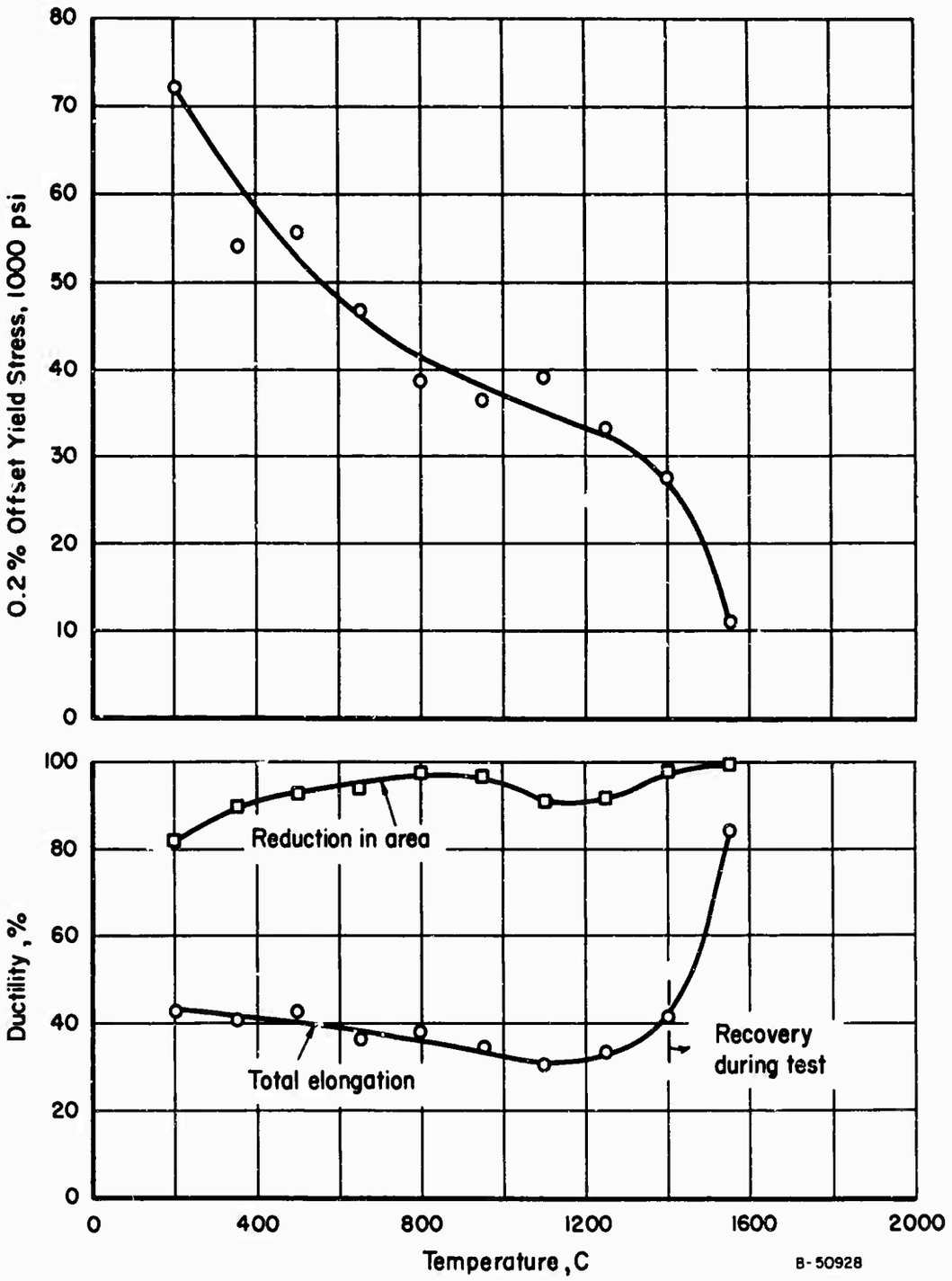

FIGURE 48. MECHANICAL PROPERTIES OF WROUGHT, STRESS-RELIEVED LOW-CARBON Mo-TZM (10 PPM CARBON), TESTED AT $\dot{\epsilon}$ = 2 MIN^{-1}

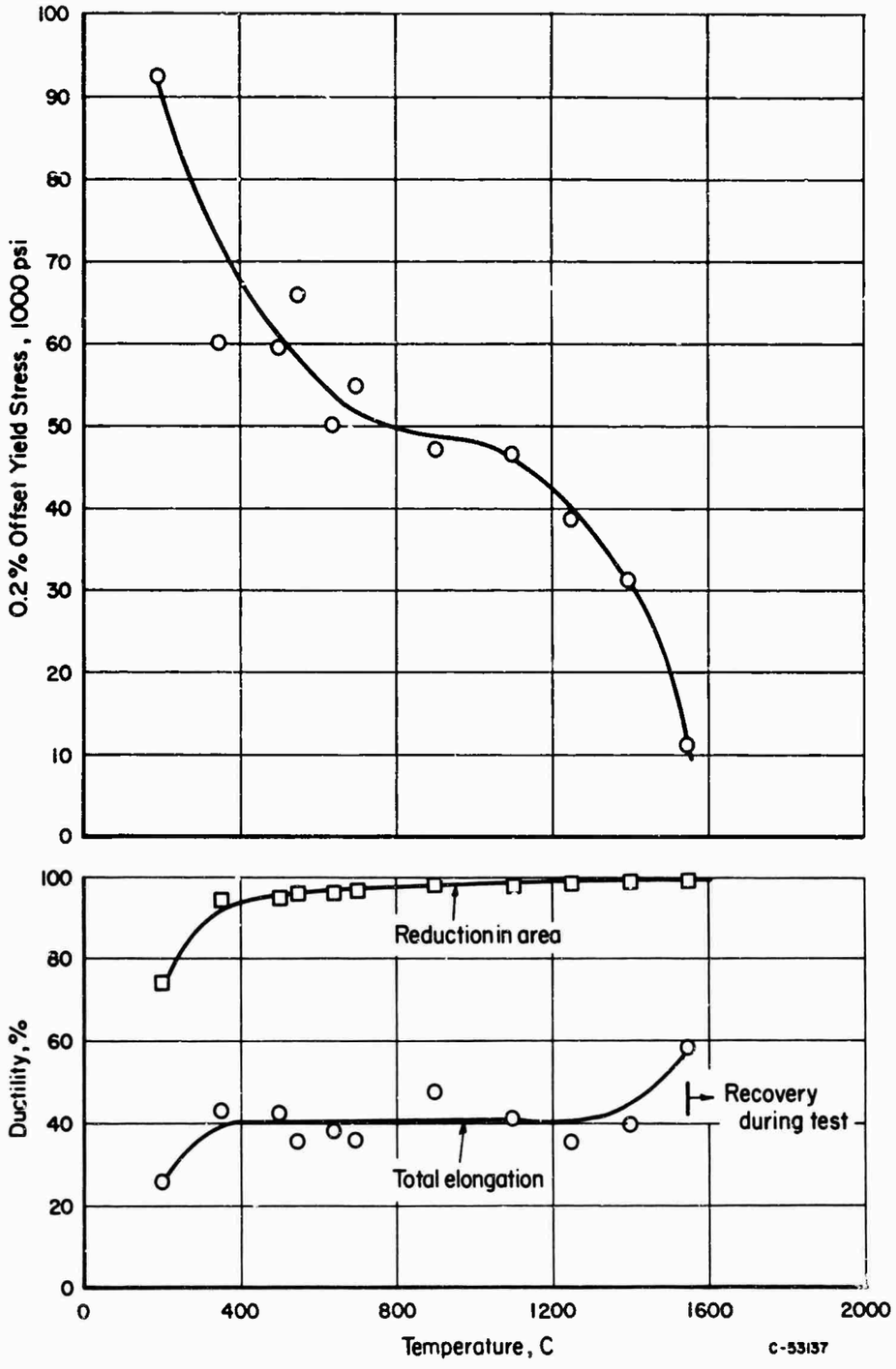

FIGURE 49. MECHANICAL PROPERTIES OF WROUGHT, STRESS-RELIEVED LOW-CARBON Mo-TZM (10 PPM CARBON), TESTED AT $\dot{\epsilon}$ = 600 MIN^{-1}

TABLE XIII. MECHANICAL-PROPERTY DATA FOR WROUGHT, STRESS-RELIEVED LOW-CARBON Mo-TZM (10 PPM CARBON)

Test Temperature, C	Total Elongation, percent	Reduction, in Area, percent	0.2% Offset Yield Strength, ksi	Ultimate Tensile Strength, ksi	True Fracture Stress, ksi	Deformation Characteristics
			$\dot{\epsilon}$ = 0.01 Min $^{-1}$			
200	43.8	89.7	51.4	68.6	~290	No yield drop, slight work hardening
350	38.2	92.3	48.8	54.8	~200	Ditto
500	36.5	93.5	44.0	50.8	~180	"
650	31.0	93.5	46.4	48.5	--	"
800	32.6	95.7	38.7	42.2	--	"
950	31.0	91.7	39.8	43.2	--	"
1100	26.8	89.3	43.0	43.8	--	"
1250	34.2	92.3	35.4	36.2	--	Immediate plastic instability, serrated flow
1400	48.8	~100	23.3	23.5	--	Ditto
1550	106.0	~100	5.7	8.1	--	"
			$\dot{\epsilon}$ = 2 Min $^{-1}$			
200	42.2	81.5	73.2	75.8	~226	No yield drop, slight work hardening
350	40.7	89.9	54.2	64.3	~258	Ditto
500	43.3	92.3	55.8	61.5	~287	Yield drop, slight work hardening
650	36.8	94.2	46.7	48.5	~218	Ditto
800	38.4	97.1	38.9	39.6	--	"
950	34.0	96.2	36.6	37.0	--	"
1100	30.8	90.9	39.4	39.9	--	"
1250	33.2	91.3	33.3[a]	34.4[b]	--	Yield drop, immediate plastic instability
1400	41.6	98.0	27.6[a]	27.7[b]	--	Ditto
1550	84.1	~100	10.8	15.4	--	No yield drop, slight work hardening
			$\dot{\epsilon}$ = 600 Min $^{-1}$			
200	25.8	74.2	92.5	93.6	~177	No yield drop, slight work hardening
350	43.0	94.4	~60.0	68.6	~294	Ditto
500	42.6	94.6	59.6	67.1	--	"
550	35.8	96.0	66.0	71.4	--	"
640	38.0	96.3	50.0	59.9	--	"
700	36.2	96.4	55.9	69.5	--	"
900	47.8	98.0	47.0	51.5	--	Small yield drop, slight work hardening
1100	41.4	97.9	46.6	49.5	--	Ditto
1250	35.2	98.4	38.7	43.6	--	"
1400	39.8	98.8	31.5	35.1	--	"
1550	58.6	99.0	11.1	25.0	--	"

(a) The strain at 0.2 percent offset was less than the strain at the upper yield point.
(b) The maximum load in these tests was the upper yield point.

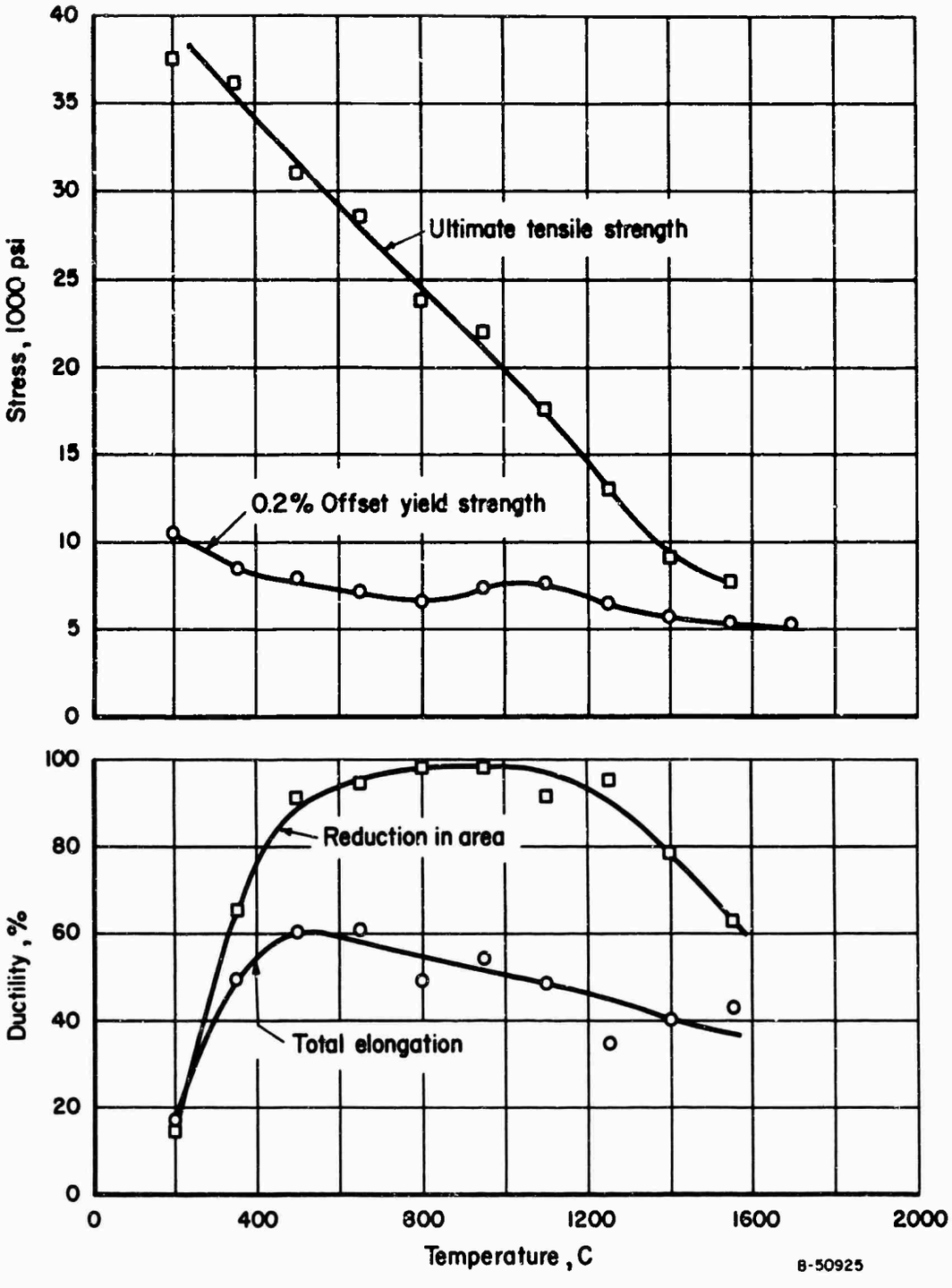

FIGURE 50. MECHANICAL PROPERTIES OF RECRYSTALLIZED LOW-CARBON Mo-TZM (10 PPM CARBON), TESTED AT $\dot{\epsilon} = 0.01$ MIN^{-1}

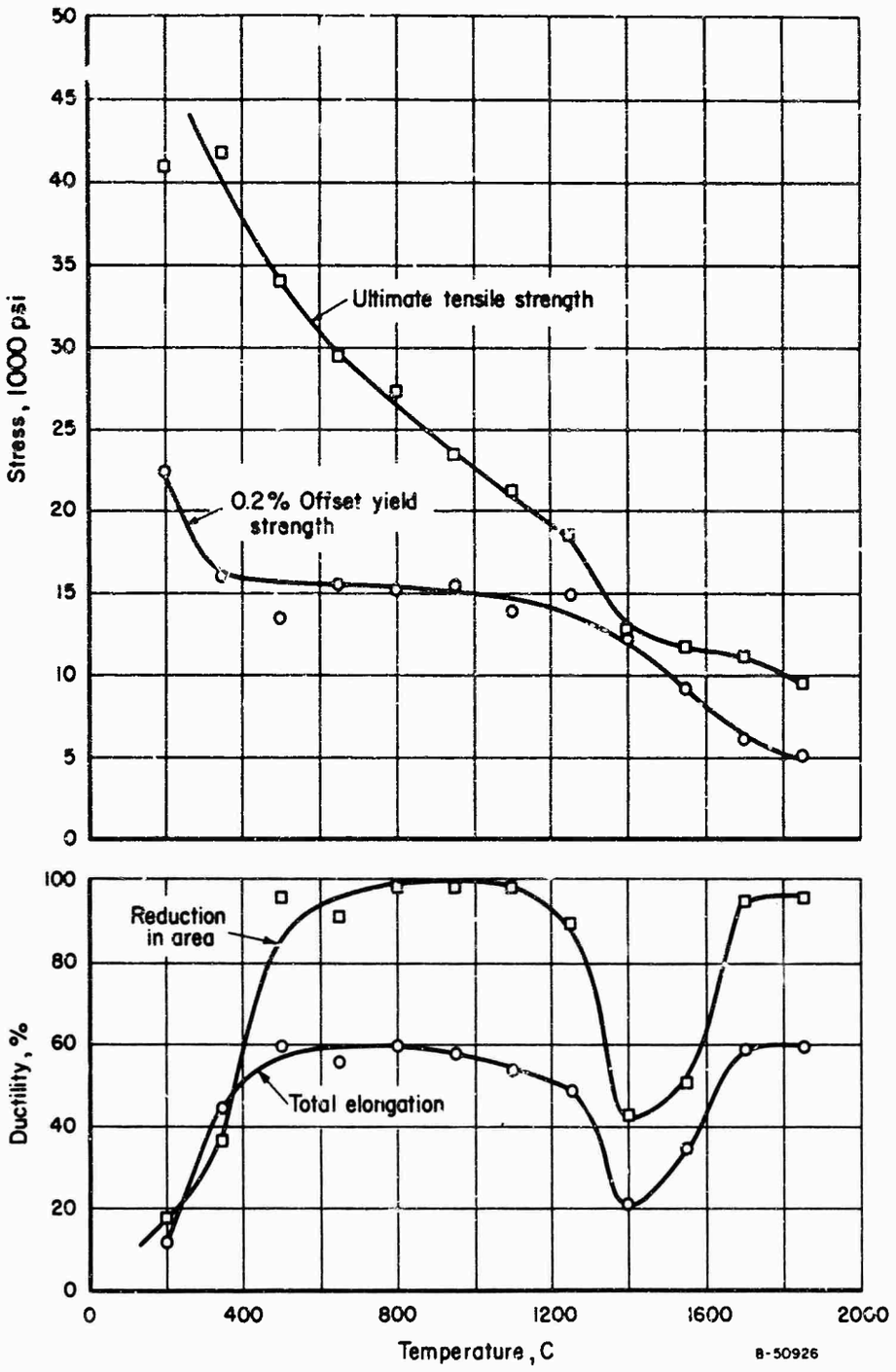

FIGURE 51. MECHANICAL PROPERTIES OF RECRYSTALLIZED LOW-CARBON Mo-TZM (10 PPM CARBON), TESTED AT $\dot{\varepsilon}$ = 2 MIN^{-1}

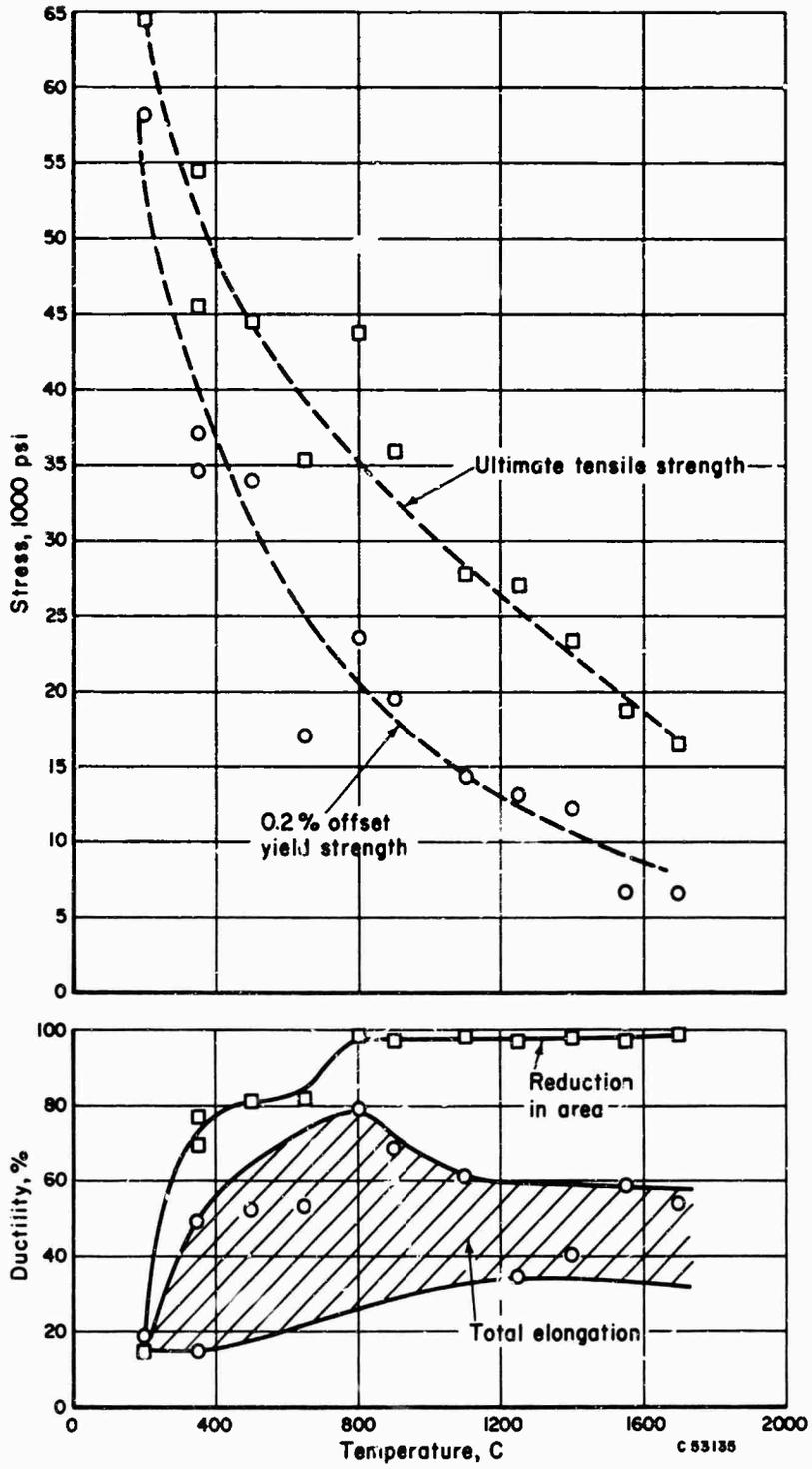

FIGURE 52. MECHANICAL PROPERTIES OF RECRYSTALLIZED LOW-CARBON Mo-TZM (10 PPM CARBON), TESTED AT $\dot{\epsilon}$ = 600 MIN^{-1}

TABLE XIV. MECHANICAL-PROPERTY DATA FOR RECRYSTALLIZED LOW-CARBON Mo-TZM (10 PPM CARBON)

Test Temperature, C	Total Elongation, percent	Reduction in Area, percent	0.2% Offset Yield Strength, ksi	Ultimate Tensile Strength, ksi	True Fracture Stress, ksi	Deformation Characteristics
			$\dot{\epsilon}$ = 0.01 Min^{-1}			
200	17.1	14.7	10.5	37.5	~44	No yield drop, strong work hardening
350	49.0	65.5	8.4	36.1	~75	Ditto
500	60.4	91.1	7.8	31.0	~108	No yield drop, strong work hardening, slight serrated flow
650	60.8	94.8	7.2	28.5	--	Ditto
800	49.2	~100	6.6	23.8	--	"
950	54.6	~100	7.4	22.0	--	"
1100	48.6	91.7	7.6	17.7	--	No yield drop, strong work hardening, serrated flow, grain-boundary cracks
1250	34.8	95.0	6.3	13.0	--	Ditto
1400	40.0	78.8	5.7	9.0	--	"
1550	43.0	62.8	5.2	7.6	--	"
1700	--	--	5.3	--	--	Poor temperature control after yielding
			$\dot{\epsilon}$ = 2 Min^{-1}			
200	11.1	17.6	22.4	41.0	~49	Yield drop, strong work hardening
350	44.8	36.7	16.0	41.7	~66	No yield drop, strong work hardening
500	59.1	95.8	13.2	34.0	--	Ditto
650	55.2	91.5	15.5	29.5	~107	"
800	59.2	97.0	15.2	27.3	--	"
950	57.6	~100	15.3	23.2	--	"
1100	53.6	~100	14.0	21.2	--	"
1250	48.4	89.5	14.9	18.7	--	"
1400	21.2	42.7	12.2	12.3	--	Yield drop, immediate plate instability, grain-boundary cracks
1550	34.4	50.3	9.1	11.6	--	No yield drop, slight work hardening, grain-boundary cracks
1700	58.4	95.0	6.1	11.2	--	No yield drop, slight work hardening, very few grain-boundary cracks
1850	59.2	95.0	5.1	9.4	--	No yield drop, slight work hardening
			$\dot{\epsilon}$ = 600 Min^{-1}			
200	18.8	14.8	58.1	64.6	~73	Yield drop, strong work hardening
350	49.8	76.9	34.7	45.6	~84	Ditto
350	17.6	69.5	37.2	54.4	~178	"
500	52.4	80.9	34.0	44.6	--	"
650	56.6	81.9	17.0	35.4	--	"
800	79.0	98.4	23.6	43.8	--	"
900	68.2	97.5	19.6	36.2	--	"
1100	61.4	99.2	14.2	27.8	--	"
1250	35.0	97.5	13.2	27.1	--	"
1400	40.6	98.3	12.3	23.4	--	"
1550	59.4	97.1	6.8	17.6	--	"
1700	54.6	98.9	6.8	16.5	--	"

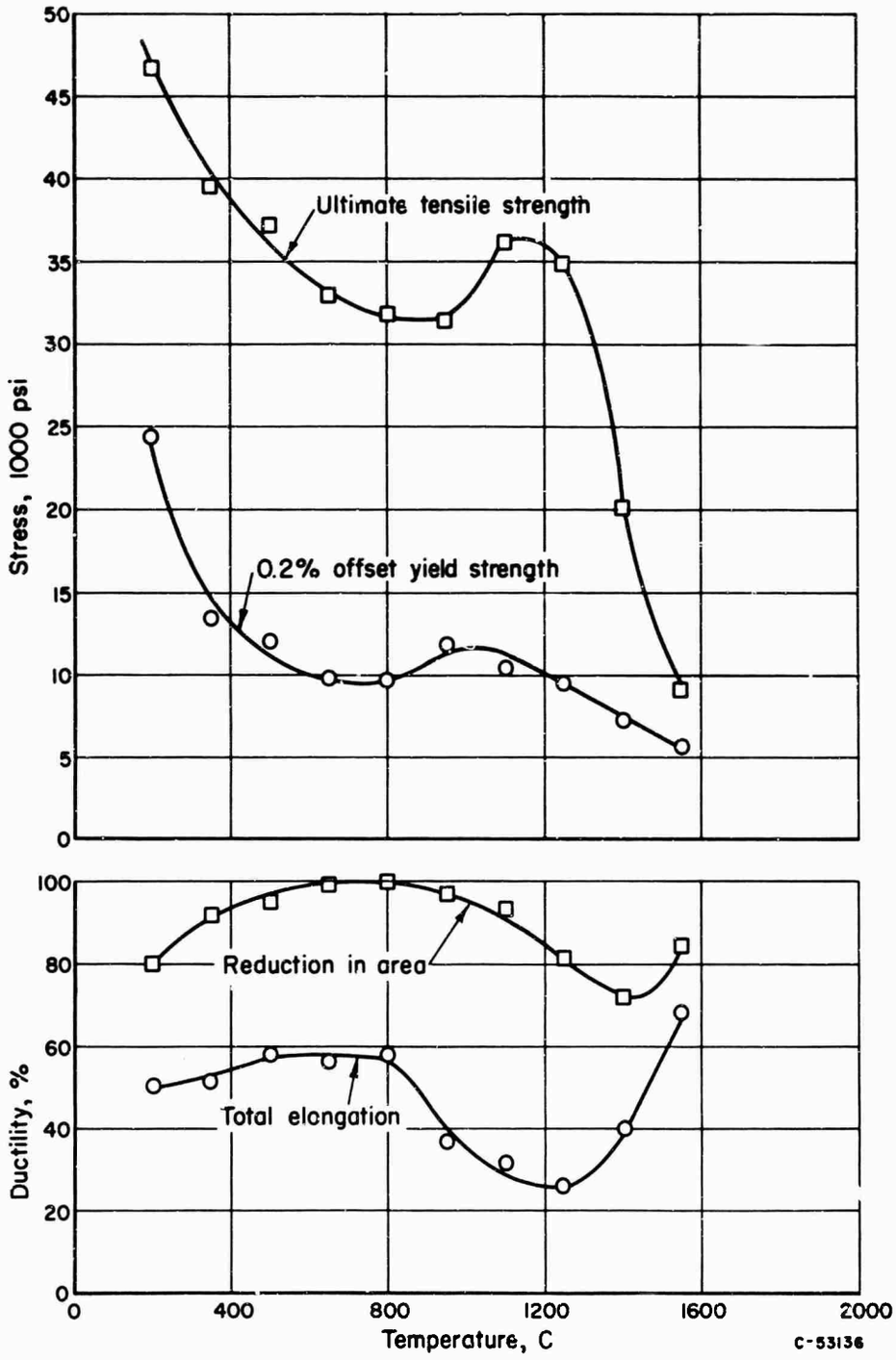

FIGURE 53. MECHANICAL PROPERTIES OF RECRYSTALLIZED INTERMEDIATE-CARBON Mo-TZM (100 PPM CARBON), TESTED AT $\dot{\epsilon}$ = 0.01 MIN^{-1}

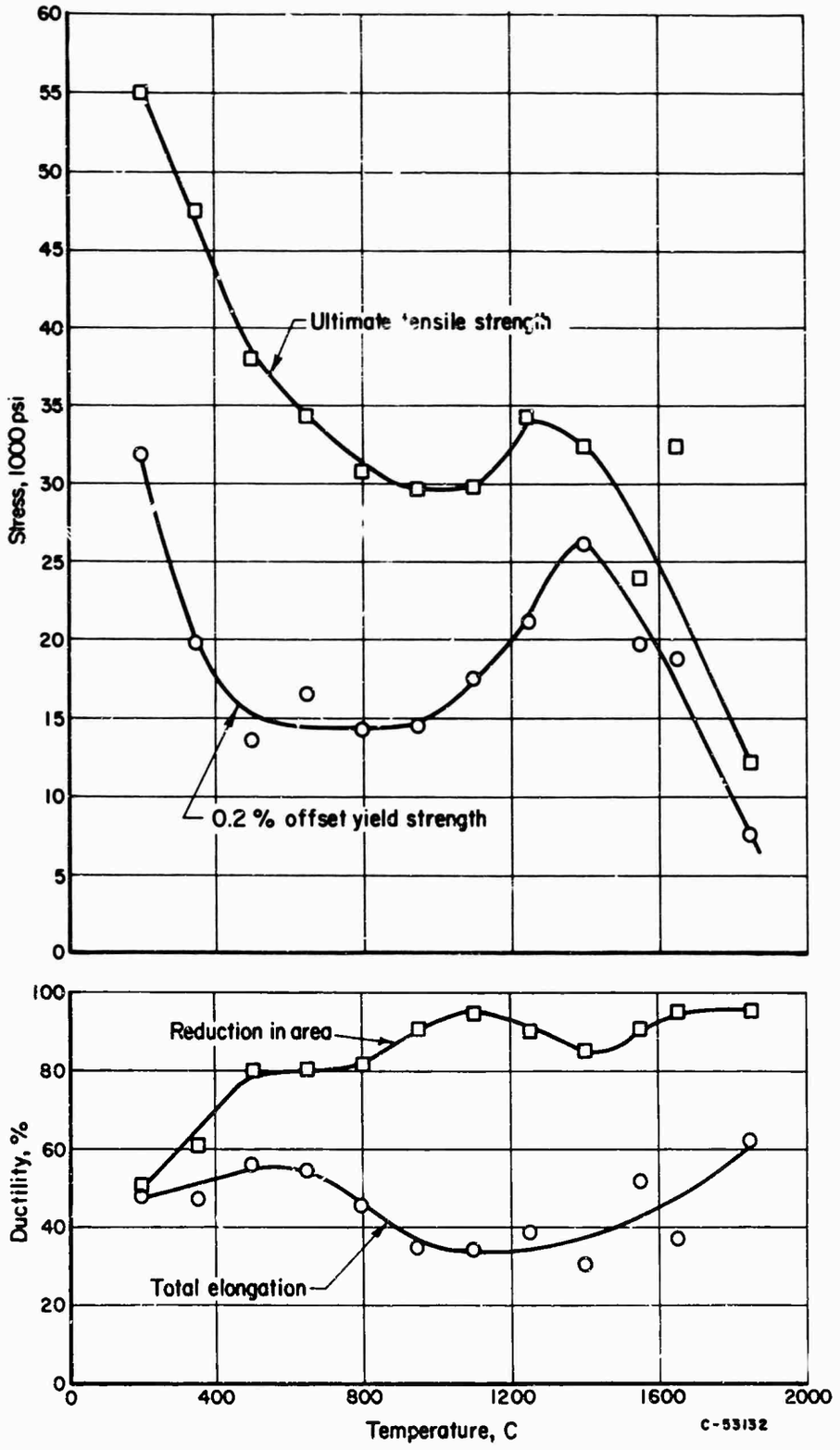

FIGURE 54. MECHANICAL PROPERTIES OF RECRYSTALLIZED INTERMEDIATE-CARBON Mo-TZM (100 PPM CARBON), TESTED AT $\dot{\epsilon}$ = 2 MIN^{-1}

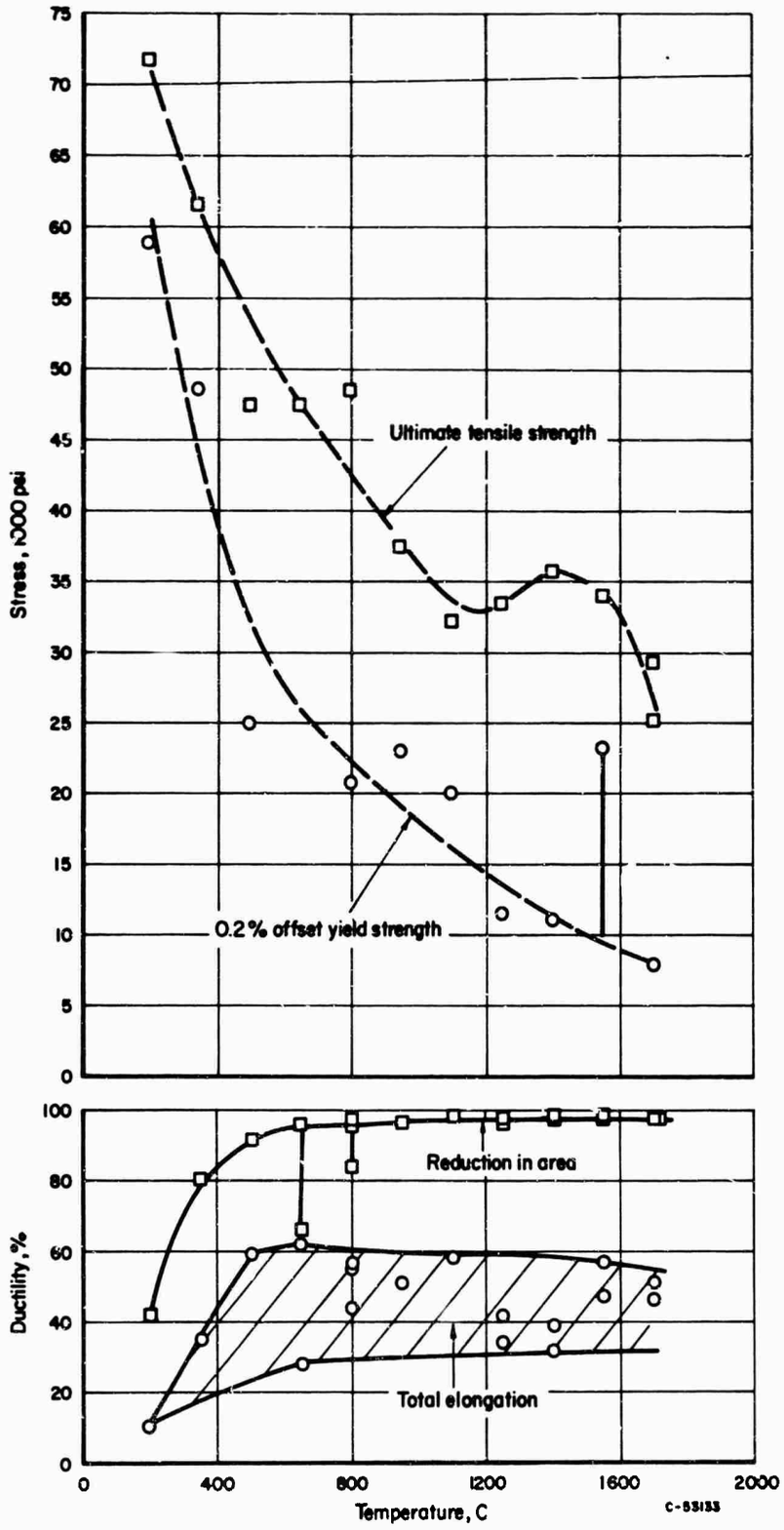

FIGURE 55. MECHANICAL PROPERTIES OF RECRYSTALLIZED INTERMEDIATE-CARBON Mo-TZM (100 PPM CARBON), TESTED AT $\dot{\epsilon}$ = 600 MIN^{-1}

TABLE XV. MECHANICAL-PROPERTY DATA FOR RECRYSTALLIZED INTERMEDIATE-CARBON Mo-TZM (100 PPM CARBON)

Test Temperature, C	Total Elongation, percent	Reduction in Area, percent	0.2% Offset Yield Strength, ksi	Ultimate Tensile Strength, ksi	True Fracture Stress, ksi	Deformation Characteristics
			$\dot{\epsilon}$ = 0.01 Min^{-1}			
200	50.0	80	24.2	46.5	196	Yield drop, strong work hardening
350	51.0	92	13.3	39.5	--	Ditto
500	58.0	95	12.0	37.3	--	Yield drop, strong work hardening, slight serrated flow
650	56.1	~100	9.7	32.9	--	Ditto
800	57.8	~100	9.7	31.8	--	No yield drop, strong work hardening, serrated flow
950	37.0	97	11.9	31.4	--	Ditto
1100	31.6	93	10.2	36.1	--	No yield drop, strong work hardening, serrated flow, grain-boundary cracks
1250	26.4	81	9.3	34.8	--	Ditto
1400	40.0	72	7.2	20.0	--	"
1550	68.0	84	5.6	9.1	--	"
			$\dot{\epsilon}$ = 2 Min^{-1}			
200	50.0	49.7	31.8	55.0	94	Yield drop, strong work hardening
350	47.6	60.5	19.7	47.4	101	Ditto
500	56.0	80.7	13.5	38.0	134	No yield drop, strong work hardening
650	54.4	80.8	16.4	34.2	106	Ditto
800	46.0	81.5	14.2	30.7	~117	"
950	34.8	90	14.6	29.8	--	"
1100	34.4	95	17.5	29.7	--	"
1250	39.0	90	21.1	34.2	--	"
1400	30.7	85	26.2	32.4	--	No yield drop, strong work hardening, grain-boundary cracks
1550	52.0	91	19.7	23.8	--	Ditto
1650	38.0	95	18.8	32.2	--	No yield drop, strong work hardening
1850	62.0	95	7.7	12.2	--	Ditto
			$\dot{\epsilon}$ = 600 Min^{-1}			
200	10.6	41.5	59.0	71.7	~123	Yield drop, strong work hardening
350	35.2	80.4	48.6	61.6	~244	Ditto
500	59.0	91.7	24.9	47.4	--	"
650	62.0	96.0	--(a)	52.0	--	--
650	28.0	65.8	--(a)	--	--	--
800	43.4	84.0	20.6	48.4	~120	No yield drop, strong work hardening
800	56.2	96.0	--(a)	--	--	--
800	55.0	97.5	--(a)	--	--	--
950	50.8	96.7	23.0	37.3	--	Ditto
1100	57.6	98.3	20.0	32.0	--	"
1250	34.0	97.4	11.2	33.3	--	"
1250	41.4	96.6	--(a)	--	--	--
1400	38.6	98.0	10.9	35.6	--	"
1400	31.6	97.2	--(a)	--	--	"
1550	47.0	97.0	23.1	33.9	--	Possible yield drop, strong work hardening
1550	56.4	98.4	--(a)	--	--	--
1700	46.0	97.6	7.7	29.0	--	No yield drop, slight work hardening
1700	50.8	97.8	--(a)	25.0	--	--

(a) Obtained no (or only partial) oscillograph trace.

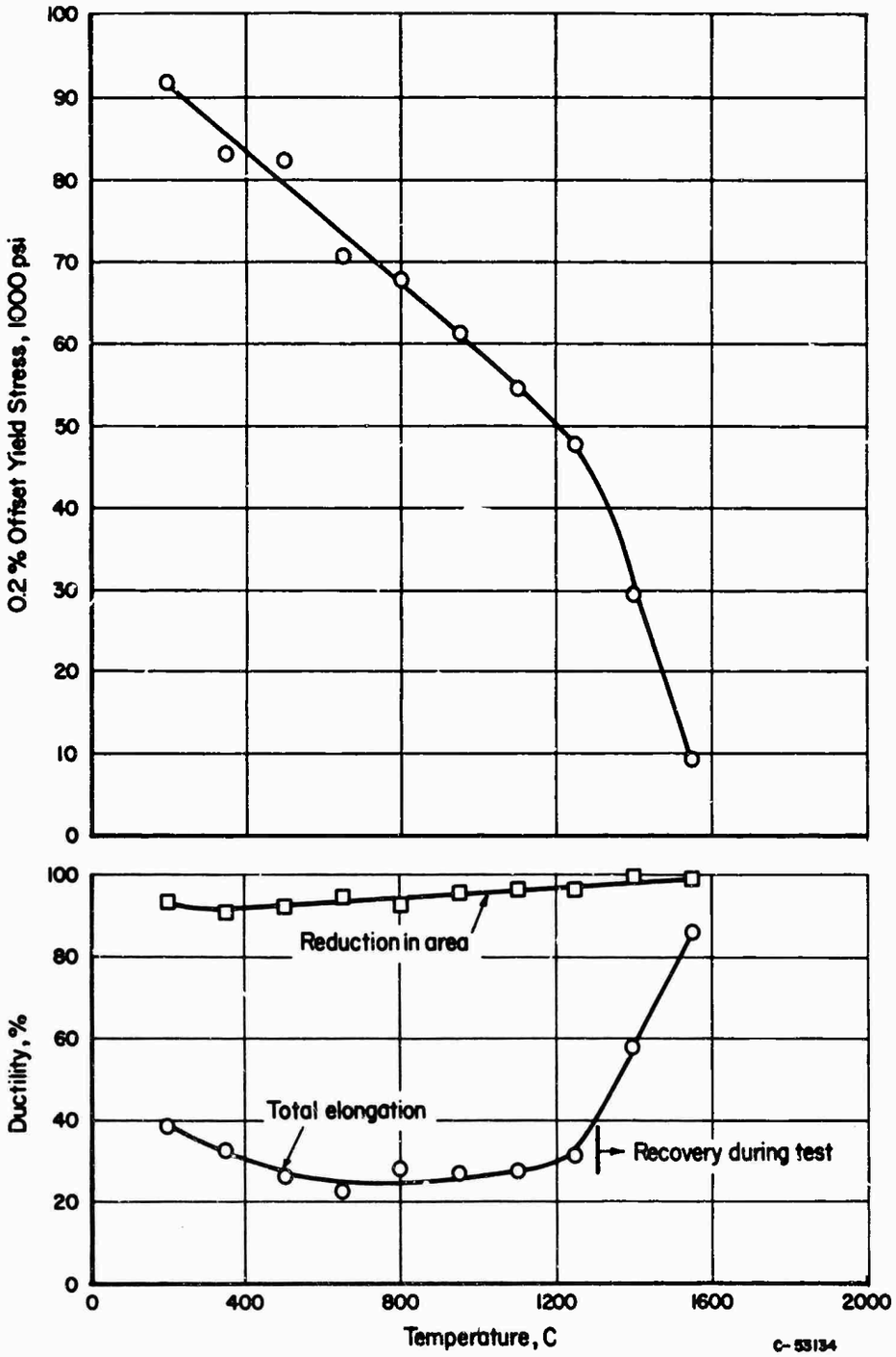

FIGURE 56. MECHANICAL PROPERTIES OF WROUGHT-STRESS-RELIEVED HIGH-CARBON Mo-TZM (190 PPM CARBON), TESTED AT $\dot{\epsilon} = 0.01\ \text{MIN}^{-1}$

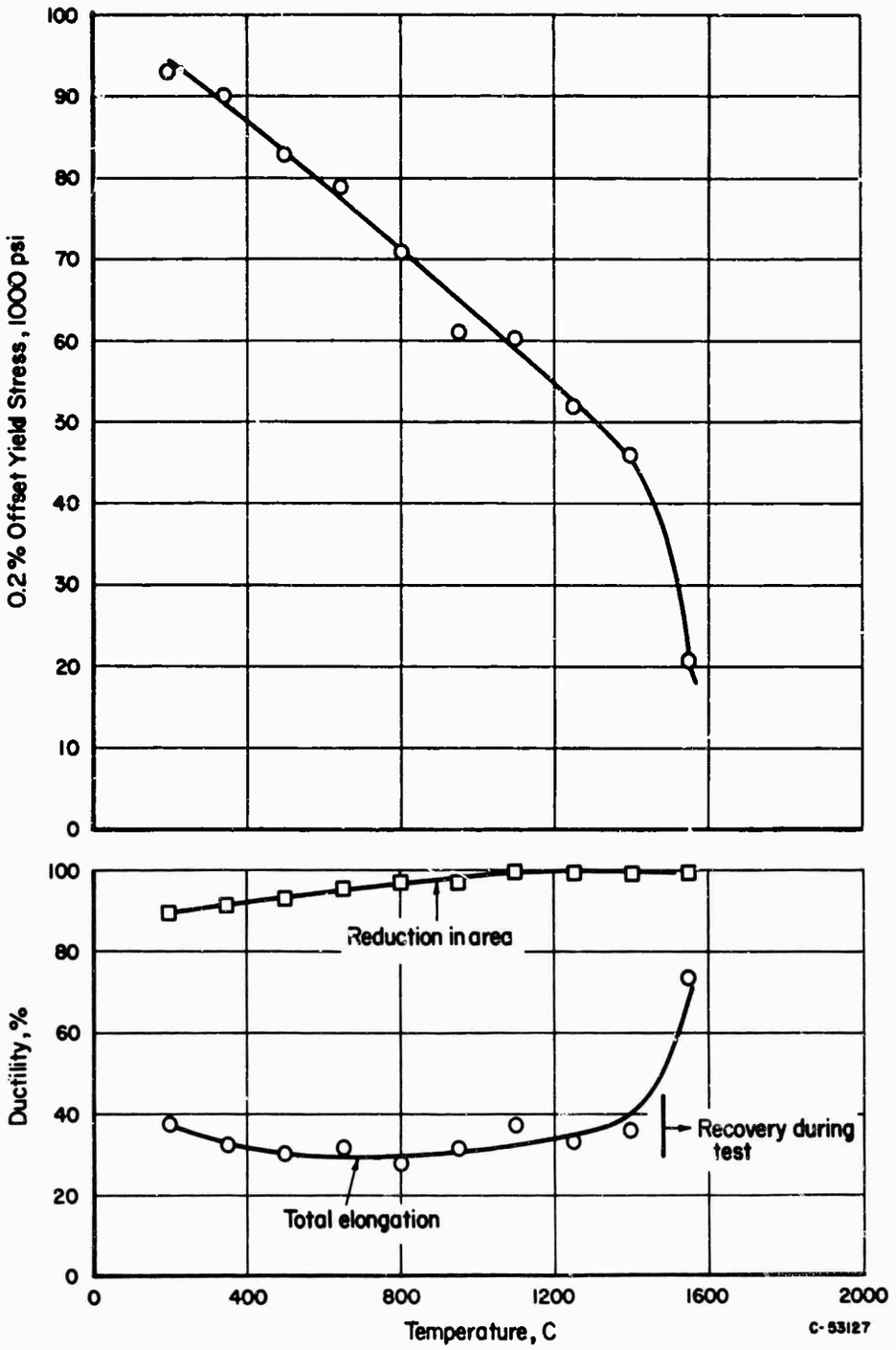

FIGURE 57. MECHANICAL PROPERTIES OF WROUGHT-STRESS-RELIEVED HIGH-CARBON Mo-TZM (190 PPM CARBON), TESTED AT $\dot{\epsilon} = 2\ \text{MIN}^{-1}$

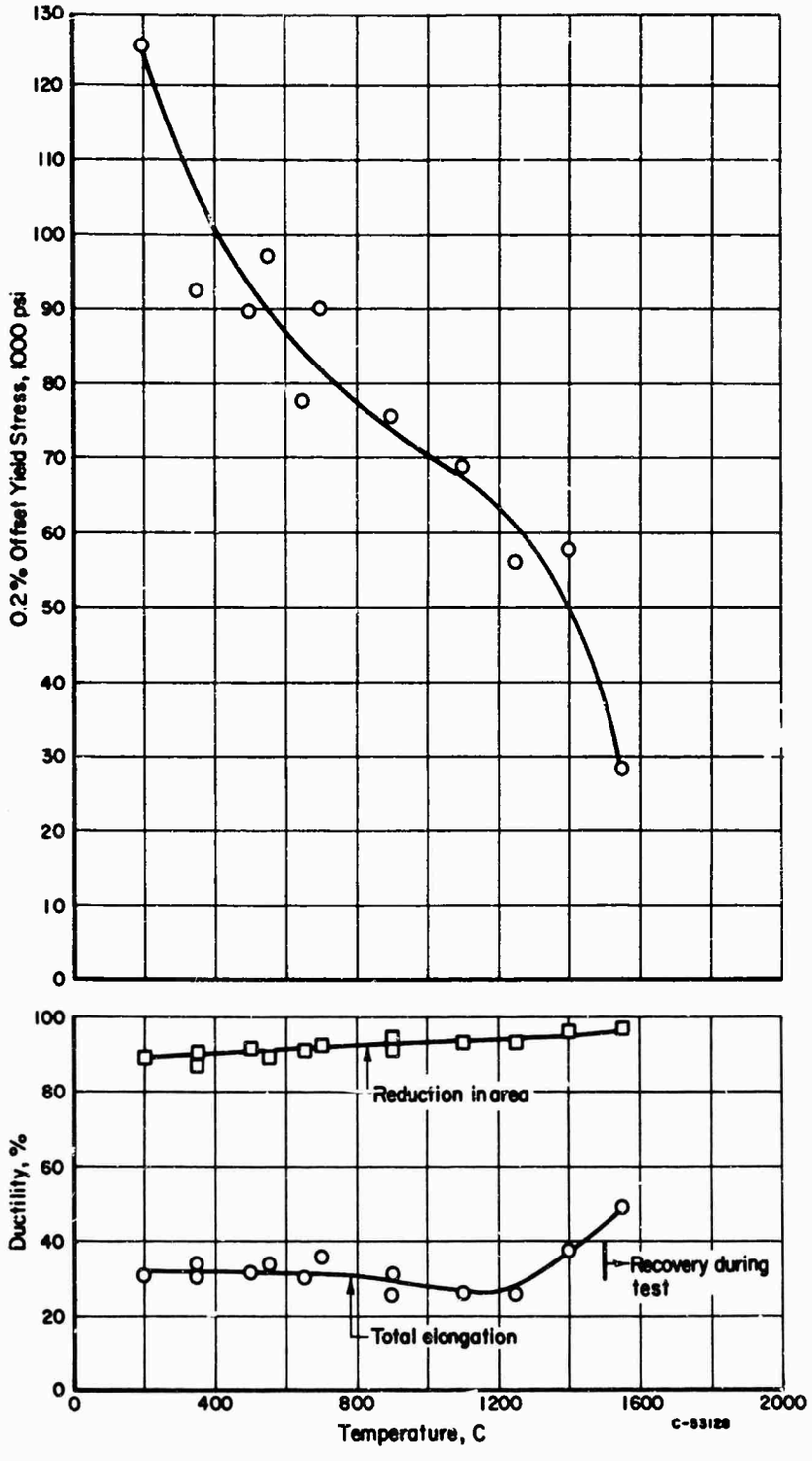

FIGURE 58. MECHANICAL PROPERTIES OF WROUGHT-STRESS-RELIEVED HIGH-CARBON Mo-TZM (190 PPM CARBON), TESTED AT $\dot{\varepsilon} = 600\ \text{MIN}^{-1}$

TABLE XVI. MECHANICAL-PROPERTY DATA FOR WROUGHT-STRESS-RELIEVED HIGH-CARBON Mo-TZM (190 PPM CARBON)

Test Temperature, C	Total Elongation, percent	Reduction in Area, percent	0.2% Offset Yield Strength, ksi	Ultimate Tensile Strength, ksi	True Fracture Stress, ksi	Deformation Characteristics
			$\dot{\epsilon} = 0.01\ Min^{-1}$			
200	38.4	93.2	91.8	95.6	~460	No yield drop, slight work hardening
350	32.8	91.0	83.1	85.3	~350	Ditto
500	26.4	92.7	82.5	82.5	~340	Small yield drop, immediate plastic instability
650	22.8	94.8	70.3	70.3	--	Ditto
800	28.7	93.0	67.8	75.3	--	No yield drop, slight work hardening
950	27.2	96	61.3	66.2	--	Ditto
1100	27.2	97	54.4	57.9	--	"
1250	31.2	97	47.8	49.5	--	"
1400	58.0	~100	29.8	30.9	--	"
1550	86.2	~100	9.4	12.3	--	"
			$\dot{\epsilon} = 2\ Min^{-1}$			
200	37.2	89.8	92.7	94.2	~440	Yield drop, slight work hardening
350	32.4	90.6	90.0	91.8	~440	Ditto
500	30.4	92.5	82.7	83.0	~425	"
650	32.0	95	79.0	79.0	--	Yield drop, immediate plastic instability
800	28.0	97	70.8	72.1	--	No yield drop, slight work hardening
950	31.6	97	60.8	68.0	--	Ditto
1100	37.2	~100	60.4	65.0	--	"
1250	33.6	~100	52.0	54.2	--	"
1400	36.0	~100	46.0	46.0	--	No yield drop, immediate plastic instability
1550	73.6	~100	20.6	22.6	--	No yield drop, slight work hardening
			$\dot{\epsilon} = 600\ Min^{-1}$			
200	30.8	89.2	125.0	125.0	--	Yield drop, immediate plastic instability
350	33.8	90.6	92.4	96.9	--	Yield drop, slight work hardening
350	31.4	86.6	--	102.0	--	--
500	31.9	91.2	89.6	89.4	--	Ditto
550	34.0	89.3	96.8	98.1	--	"
650	30.0	90.7	77.4	82.0	--	"
700	36.0	92.7	90.0	95.4	--	"
900	25.6	94.0	75.5	76.5	--	"
900	30.6	92.5	--	--	--	--
1100	26.4	93.4	69.1	69.1	--	No yield drop, slight work hardening
1250	26.2	93.4	55.8	61.3	--	Ditto
1400	37.8	96.0	57.9	60.4	--	"
1550	49.0	97.0	28.2	40.0	--	"

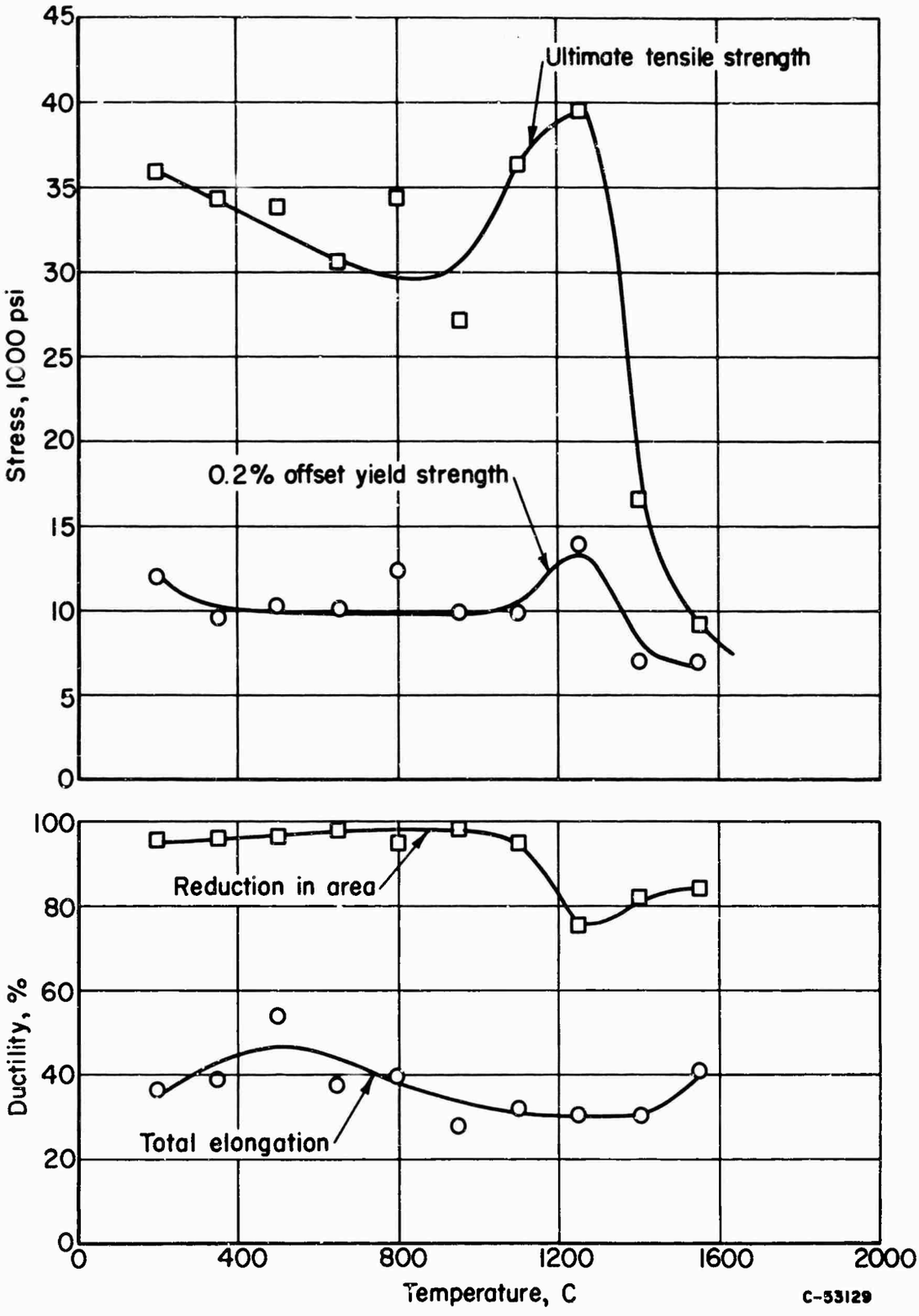

FIGURE 59. MECHANICAL PROPERTIES OF RECRYSTALLIZED HIGH-CARBON Mo-TZM (190 PPM CARBON), TESTED AT $\dot{\epsilon} = 0.01$ MIN^{-1}

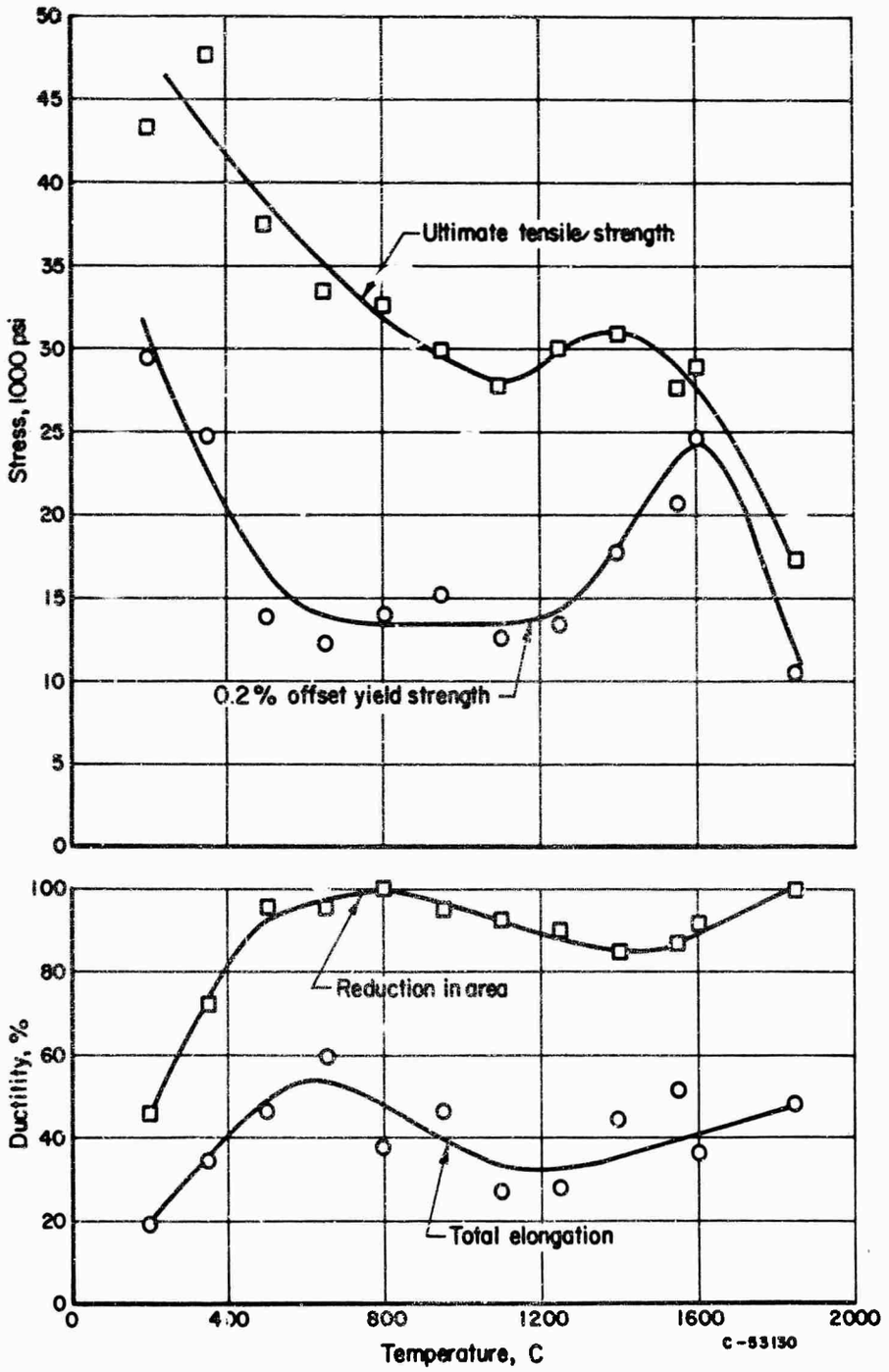

FIGURE 60. MECHANICAL PROPERTIES OF RECRYSTALLIZED HIGH-CARBON Mo-TZM (190 PPM CARBON), TESTED AT $\dot{\epsilon} = 2$ MIN^{-1}

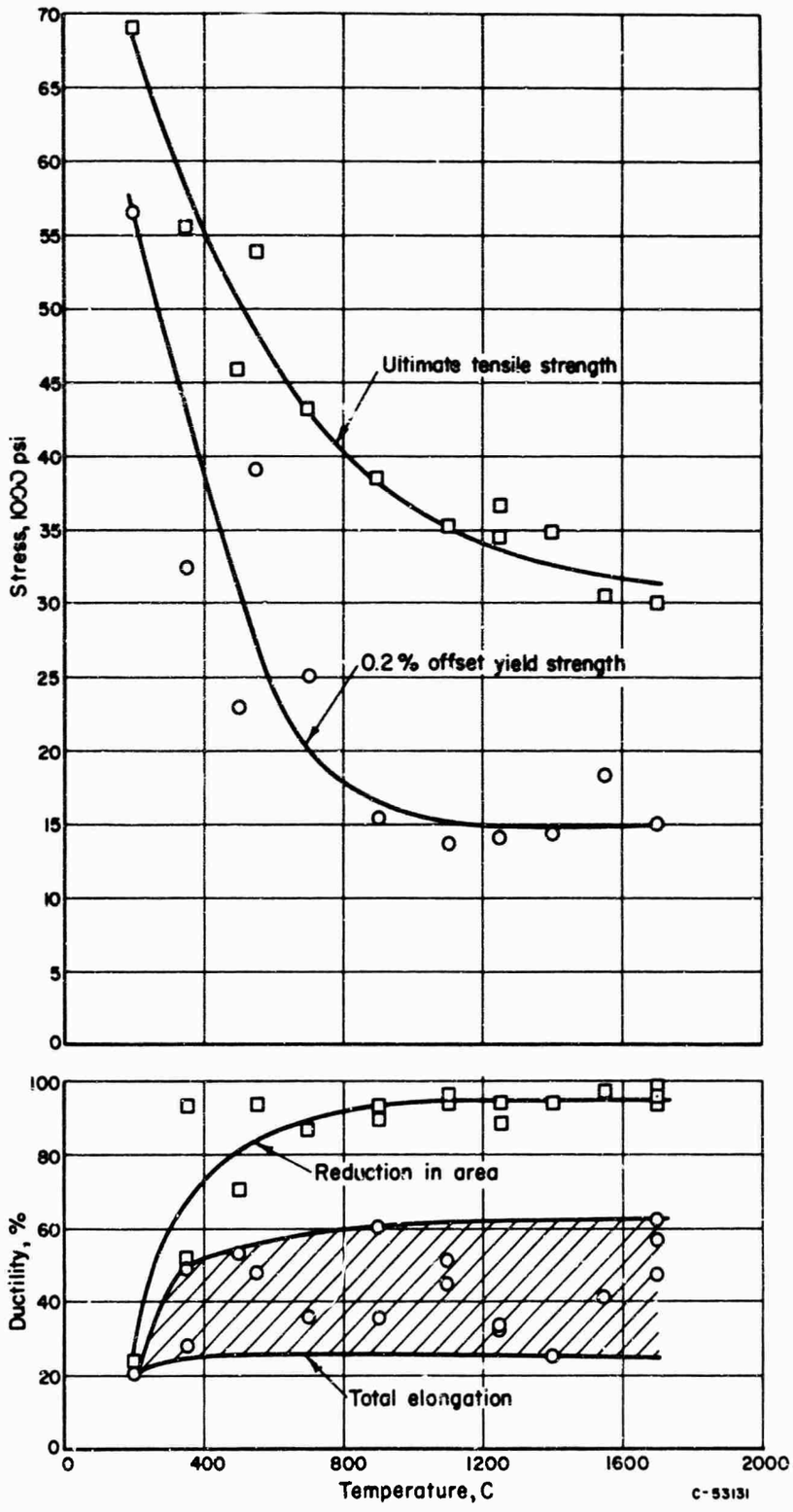

FIGURE 61. MECHANICAL PROPERTIES OF RECRYSTALLIZED HIGH-CARBON Mo-TZM (190 PPM CARBON), TESTED AT $\dot{\epsilon} = 600\ \text{MIN}^{-1}$

TABLE XVII. MECHANICAL-PROPERTY DATA FOR RECRYSTALLIZED (AND FURNACE COOLED) HIGH-CARBON Mo-TZM (190 PPM CARBON)

Test Temperature, C	Total Elongation, percent	Reduction in Area, percent	0.2% Offset Yield Strength, ksi	Ultimate Tensile Strength, ksi	True Fracture Stress, ksi	Deformation Characteristics
			$\dot{\epsilon}$ = 0.01 Min^{-1}			
200	36.2	95.5	12.1	35.9	--	No yield drop, strong work hardening
350	39.3	96.0	9.6	34.4	--	Ditto
500	54.2	97.1	10.3	33.9	--	"
650	37.6	98	10.1	30.6	--	No yield drop, strong work hardening, serrated flow
800	40.0	95.5	12.5	34.3	--	Ditto
950	27.8	98	10.0	27.0	--	"
1100	32.0	95	9.7	36.4	--	No yield drop, strong work hardening, serrated flow, grain-boundary cracks
1250	30.8	75	13.9	39.6	--	Ditto
1400	30.0	82	7.0	16.5	--	"
1550	40.6	84	6.8	9.0	--	"
			$\dot{\epsilon}$ = 2 Min^{-1}			
200	19.8	44.1	29.5	43.3	77	No yield drop, strong work hardening
350	34.0	72.3	24.8	47.7	150	Ditto
500	46.8	95	13.8	32.1	--	"
650	59.6	95	12.3	37.5	--	"
800	37.2	~100	14.0	32.5	--	"
950	46.4	95	15.1	29.7	--	"
1100	26.8	92.1	12.6	27.7	--	No yield drop, strong work hardening, grain-boundary cracks
1250	28.0	90.2	13.4	30.0	--	Ditto
1400	45.2	85.0	17.6	30.9	--	"
1550	52.0	87.1	20.8	27.5	--	"
1600	35.6	92	24.9	28.8	--	No yield drop, strong work hardening
1850	48.0	~100	10.3	17.1	--	Ditto
			$\dot{\epsilon}$ = 600 Min^{-1}			
200	21.2	23.8	56.5	69.2	85	Yield drop, slight work hardening
350	49.0	93.8	32.3	55.4	--	Ditto
350	28.6	51.7	--	--	--	--
500	53.2	70.6	23.0	46.0	81	"
550	48.0	94.0	39.0	54.0	--	"
700	26.2	86.1	25.0	43.1	--	Yield drop, strong work hardening
900	60.2	93.2	15.5	38.5	--	Ditto
900	35.6	88.9	--	--	--	--
1100	51.2	93.8	13.7	35.1	--	No yield drop, strong work hardening
1100	45.0	96.0	--	--	--	--
1250	32.8	88.5	14.2	36.8	--	Ditto
1250	33.2	94.4	--	34.5	--	--
1400	25.2	94.6	14.3	34.9	--	"
1550	41.6	97.4	18.5	30.5	--	"
1700	57.2	95.0	--	--	--	--
1700	63.0	98.3	15.0	30.0	--	"
1700	48.0	95.9	--	--	--	--

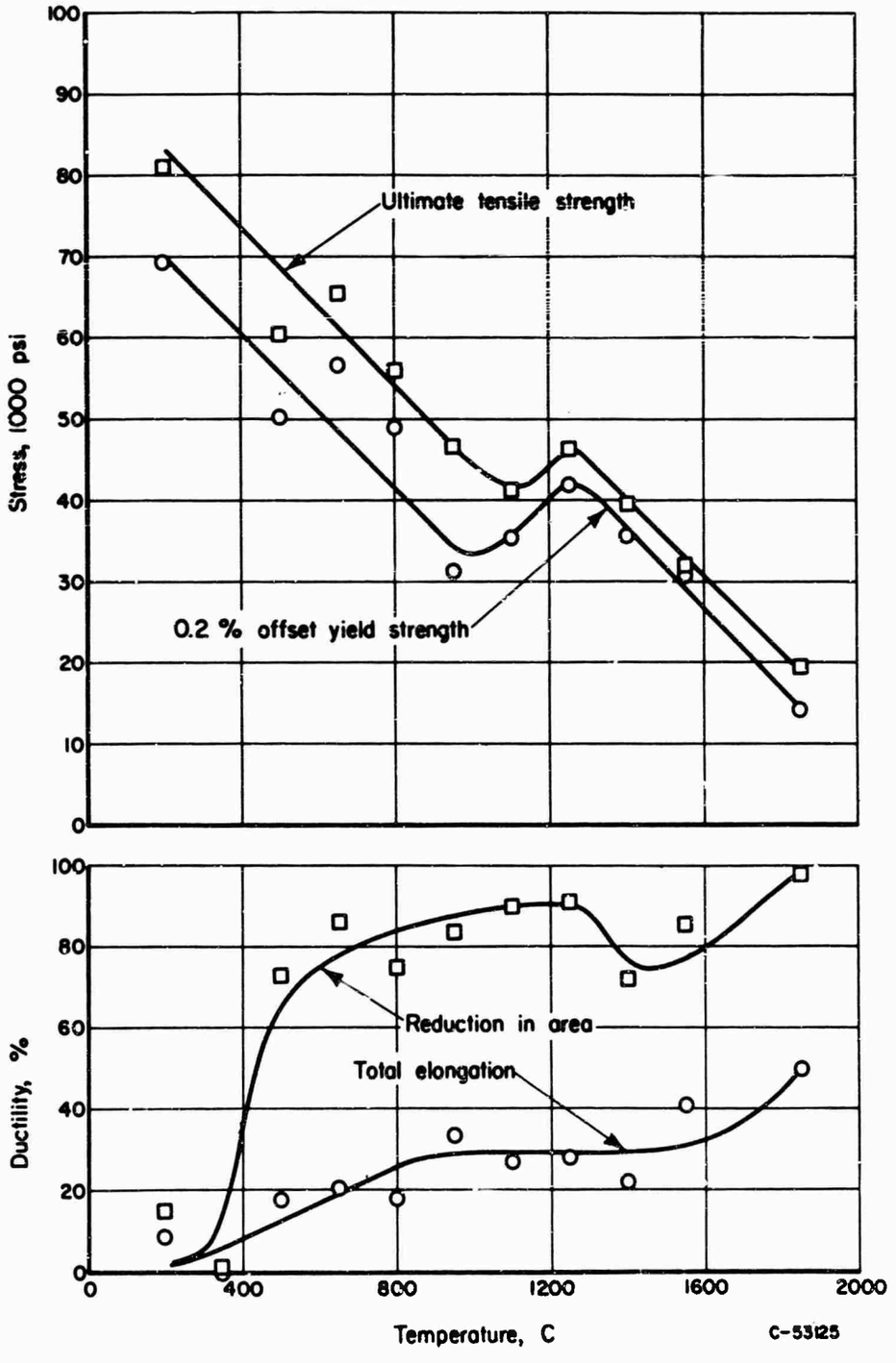

FIGURE 62. MECHANICAL-PROPERTY DATA FOR QUENCHED HIGH-CARBON Mo-TZM (190 PPM CARBON), TESTED AT $\dot{\epsilon}$ = 2 MIN^{-1}

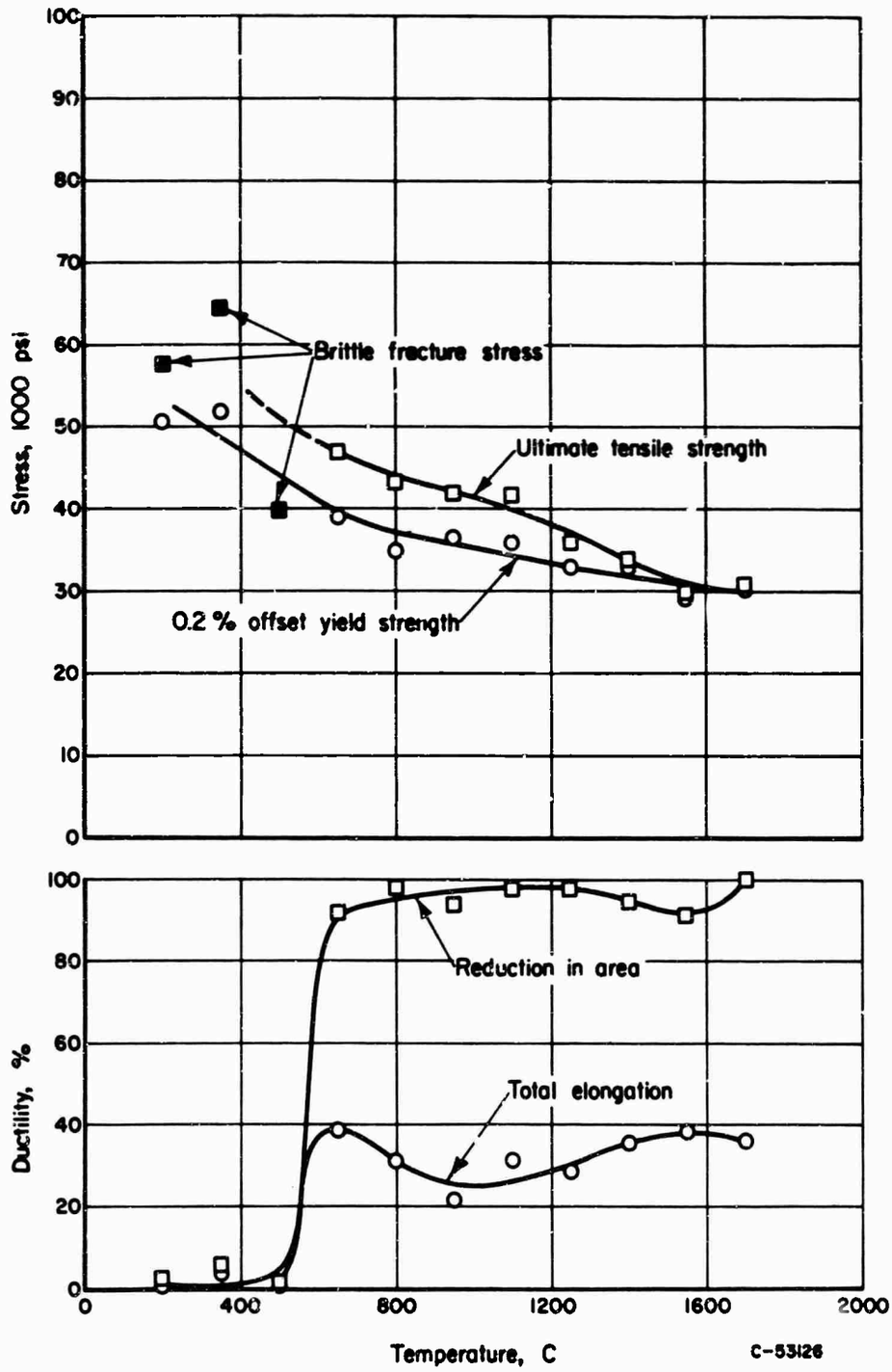

FIGURE 63. MECHANICAL-PROPERTY DATA FOR QUENCHED-PLUS-AGED HIGH-CARBON Mo-TZM (190 PPM CARBON), TESTED AT $\dot{\epsilon} = 2$ MIN^{-1}

TABLE XVIII. MECHANICAL-PROPERTY DATA FOR QUENCHED AND QUENCHED-PLUS-AGED HIGH-CARBON Mo-TZM (190 PPM CARBON) TESTED AT $\dot{\epsilon} = 2$ MIN^{-1}

Test Temperature, C	Total Elongation, percent	Reduction in Area, percent	0.2% Offset Yield Strength, ksi	Ultimate Tensile Strength, ksi	True Fracture Stress, ksi	Deformation Characteristics
			Annealed 1 Hr at 2100 C, Quenched into Molten Tin			
200	8.0	17.5	69.0	81.2	98	No yield drop, strong work hardening, brittle fracture
350	0	0	--	--	56	Brittle fracture
500	18.1	73.3	50.6	60.2	~145	No yield drop, strong work hardening
650	20.4	86.5	56.7	65.2	--	Ditto
800	18.8	75.0	49.0	55.9	--	No yield drop, strong work hardening, serrated flow, grain boundary cracks
950	34.0	84.1	31.1	46.4	--	Ditto
1100	27.2	90.0	35.5	41.3	--	"
1250	28.0	91.6	41.8	46.6	--	No yield drop, slight work hardening, serrated flow, grain-boundary cracks
1400	22.8	71.0	36.5	39.6	--	No yield drop, slight work hardening, grain-boundary cracks
1550	41.6	85.1	31.1	31.7	--	Ditto
1850	50.0	97	14.5	19.7	--	No yield drop, slight work hardening
			Annealed 1 Hr at 2100 C, Quenched into Molten Tin, Aged 100 Hr at 1300 C			
200	2.0	2.1	50.6	56.4	57	No yield drop, strong work hardening, brittle fracture
350	5.6	4.2	51.7	62.8	64	Ditto
500	0	0	--	--	39	Brittle fracture
650	28.4	92.1	39.0	46.7	--	No yield drop, slight work hardening
800	30.1	97	35.0	43.1	--	Ditto
950	21.6	93.2	36.7	42.0	--	"
1100	31.5	97	35.8	41.7	--	Yield drop, slight work hardening
1250	28.4	97	32.5	35.8	--	Yield drop, slight work hardening, few grain-boundary cracks
1400	36.1	94.1	33.3	33.3	--	Yield drop, immediate plastic instability, few grain-boundary cracks
1550	38.8	92.3	29.3	29.3	--	Ditto
1700	36.8	~100	30.0	30.2	--	Yield drop, immediate plastic instability

REFERENCES

(1) Pugh, J. W., Proc. ASTM, 57, 906 (1957).

(2) Staff of Union Carbide Metals Company, "Investigation of the Properties of Tungsten and Its Alloys", WADD TR 60-144, May, 1960.

(3) Bechtold, J. H., and Shewmon, P. G., Trans. ASM, 46, 397 (1954).

(4) Atkinson, R. H., et al., "Physical Metallurgy of Tungsten and Tungsten-Base Alloys", WADD TR 60 37, May, 1960.

(5) Schmidt, F. F., and Ogden, H. R., "The Engineering Properties of Molybdenum and Molybdenum Alloys", DMIC Report 190 (September 20, 1963).

(6) Dotson, C. L., and Adams, P. G., "Mechanical and Physical Properties of TZM Molybdenum Alloy Sheet and of Tungsten Sheet", Southern Res. Inst., 7th Qtr. Prog. Rept. on Contract No. N600(19)59530, Sept. 30, 1964.

(7) Neff, C. W., Frank, R. G., and Luft, L., "Refractory Metals Structural Development Program", McDonnell Aircraft Corp. and Gen. Elec. Co., Refractory Alloy and Coating Development, ASD TR 61-392, Vol II (Oct., 1961).

(8) Jones, O., Bennett, A., and Albom, M. J., "Fabrication Techniques and Mechanical Properties at Elevated Temperatures of TZM Alloy Sheet", The Marquardt Corp., ASD-TDR-62-936 (Sept. 14, 1962).

(9) Sikora, P. F., and Hall, R. W., "High Temperature Tensile Properties of Wrought Sintered Tungsten", NASA TN D-79, Sept., 1959.

(10) Taylor, J. L., and Boone, D. H., Trans. ASM, 56, 643 (1963).

(11) Sikora, P. F., and Hall, R. W., "Effect of Strain Rate on Mechanical Properties of Wrought Sintered Tungsten at Temperatures Above 2500 F", NASA TN D-1094, Oct., 1961.

(12) Chang, W. H., and Perlmutter, I., High Temperature Materials, Vol 18, Met. Soc. Conf. AIME, Interscience Publishers, Inc., New York (1963), pp 347-370.

(13) Ashby, M. Z. Metallk., 55, 5 (1964).

(14) Fullman, R. L., Trans. AIME, 197, 447 (1953).

(15) Krafft, J. M., and Hahn, J. C., U. S. Patent No. (3,194,062), "Tension-Compression Testing Machine", July 13, 1965.

(16) Gilbert, A., and Wilcox, B. A., Rev. Sci. Inst., 36, 863 (1965).

(17) Nabarro, F. R. N., Rept. of a Conf. on Strength of Solids, Univ. of Bristol, The Physical Society, London, 1948, p 38.

(18) Schoeck, G., and Seeger, A., Acta Met., 7, 469 (1959).

REFERENCES
(Continued)

(19) Dotson, C. L., Southern Research Inst., private communication.

(20) Chang, W. H., Trans. ASM, 57, 527 (1964).

(21) Chang, W. H., Trans. ASM, 57, 565 (1964).

(22) Chang, W. H., Trans. ASM, 56, 107 (1963).

(23) Gilbert, A., "Factors Influencing the Ductility of Chromium", paper presented 1965 Annual AIME Meeting, Chicago, Illinois.

(24) Kelly, A., and Nicholson, R. B., Progr. Mater. Sci., 10, 289 (1963).

(25) Hill, W. H., Shimmin, K. D., and Wilcox, B. A., Proc. ASTM, 61, 890 (1961).

(26) Houck, J. A., "Physical and Mechanical Properties of Commercial Molybdenum-Base Alloys", DMIC Rept. 140, Nov. 30, 1960.

(27) Embury, J. D., and Fisher, R. M., Acta Met., 14, 147 (1966).

(28) Brodrick, R. F., "Development of an Electron Beam Heating Facility and Its Use in Mechanical Testing of Tungsten to 6000 F", ASD-TDR-63-484, July 1963.

(29) Doering, H., and Shahinian, P., "Brightness and Two-Color Pyrometry Applied to the Electron Beam Furnace", NRL Rept. No. 6062, December 1963.

(30) Schnitzel, R. H., Trans. AIME, 233, 186 (1965).

Unclassified

Security Classification

DOCUMENT CONTROL DATA - R&D

(Security classification of title, body of abstract and indexing annotation must be entered when the overall report is classified)

1 ORIGINATING ACTIVITY (Corporate author) Battelle Memorial Institute Columbus Laboratories Columbus, Ohio 43201	2a. REPORT SECURITY CLASSIFICATION Unclassified 2b GROUP N/A

3 REPORT TITLE

Intermediate-Temperature Ductility and Strength of Tungsten and Molybdenum TZM

4 DESCRIPTIVE NOTES (Type of report and inclusive dates)

Final Report - 1 July 1964 - 30 August 1965

5. AUTHOR(S) (Last name, first name, initial)

Wilcox, B. A.
Gilbert, A.
Allen, B. C.

6. REPORT DATE	7a. TOTAL NO. OF PAGES	7b. NO. OF REFS
AFML-TR-66-89	100	30

8a. CONTRACT OR GRANT NO. AF33(615)-1727 b. PROJECT NO. 7351 cTask Number 735101 d.	9a. ORIGINATOR'S REPORT NUMBER(S) 9b. OTHER REPORT NO(S) (Any other numbers that may be assigned this report)

10. AVAILABILITY/LIMITATION NOTICES "This document is subject to special export controls and each transmittal to foreign governments or foreign nationals may be made only with prior approval of Metals and Ceramics Division, MAM, Air Force Materials Laboratory, Wright-Patterson AFB, Ohio 45433."

11. SUPPLEMENTARY NOTES	12. SPONSORING MILITARY ACTIVITY AFML(MAMP) Wright-Patterson AFB, Ohio

13. ABSTRACT

The ductility and strength of tungsten and molybdenum-TZM have been studied as a function of temperature with emphasis on investigating the effects of strain rate, structural condition, and carbon content on mechanical properties.

Both wrought-stress-relieved and recrystallized tungsten and Mo-TZM have been tested at strain rates of 0.01, 2, and 600 min^{-1} over the temperature range -200 to 1850 C.

In recrystallized Mo-TZM alloys, an intermediate-temperature region (~1100-1500 C) of reduced ductility at the two lower strain rates was found to be caused by pronounced grain-boundary cracking. This phenomenon is associated with dynamic strengthening of the matrix as a result of precipitation during deformation.

DD FORM 1 JAN 64 1473

Unclassified

Security Classification

Unclassified

Security Classification

14 KEY WORDS	LINK A		LINK B		LINK C	
	ROLE	WT	ROLE	WT	ROLE	WT

INSTRUCTIONS

1. ORIGINATING ACTIVITY: Enter the name and address of the contractor, subcontractor, grantee, Department of Defense activity or other organization *(corporate author)* issuing the report.

2a. REPORT SECURITY CLASSIFICATION: Enter the overall security classification of the report. Indicate whether "Restricted Data" is included. Marking is to be in accordance with appropriate security regulations.

2b. GROUP: Automatic downgrading is specified in DoD Directive 5200.10 and Armed Forces Industrial Manual. Enter the group number. Also, when applicable, show that optional markings have been used for Group 3 and Group 4 as authorized.

3. REPORT TITLE: Enter the complete report title in all capital letters. Titles in all cases should be unclassified. If a meaningful title cannot be selected without classification, show title classification in all capitals in parenthesis immediately following the title.

4. DESCRIPTIVE NOTES: If appropriate, enter the type of report, e.g., interim, progress, summary, annual, or final. Give the inclusive dates when a specific reporting period is covered.

5. AUTHOR(S): Enter the name(s) of author(s) as shown on or in the report. Enter last name, first name, middle initial. If military, show rank and branch of service. The name of the principal author is an absolute minimum requirement.

6. REPORT DATE: Enter the date of the report as day, month, year; or month, year. If more than one date appears on the report, use date of publication.

7a. TOTAL NUMBER OF PAGES: The total page count should follow normal pagination procedures, i.e., enter the number of pages containing information.

7b. NUMBER OF REFERENCES: Enter the total number of references cited in the report.

8a. CONTRACT OR GRANT NUMBER: If appropriate, enter the applicable number of the contract or grant under which the report was written.

8b, 8c, & 8d. PROJECT NUMBER: Enter the appropriate military department identification, such as project number, subproject number, system numbers, task number, etc.

9a. ORIGINATOR'S REPORT NUMBER(S): Enter the official report number by which the document will be identified and controlled by the originating activity. This number must be unique to this report.

9b. OTHER REPORT NUMBER(S): If the report has been assigned any other report numbers *(either by the originator or by the sponsor)*, also enter this number(s).

10. AVAILABILITY/LIMITATION NOTICES: Enter any limitations on further dissemination of the report, other than those imposed by security classification, using standard statements such as:

(1) "Qualified requesters may obtain copies of this report from DDC."

(2) "Foreign announcement and dissemination of this report by DDC is not authorized."

(3) "U. S. Government agencies may obtain copies of this report directly from DDC. Other qualified DDC users shall request through _____."

(4) "U. S. military agencies may obtain copies of this report directly from DDC. Other qualified users shall request through _____."

(5) "All distribution of this report is controlled. Qualified DDC users shall request through _____."

If the report has been furnished to the Office of Technical Services, Department of Commerce, for sale to the public, indicate this fact and enter the price, if known.

11. SUPPLEMENTARY NOTES: Use for additional explanatory notes.

12. SPONSORING MILITARY ACTIVITY: Enter the name of the departmental project office or laboratory sponsoring *(paying for)* the research and development. Include address.

13. ABSTRACT: Enter an abstract giving a brief and factual summary of the document indicative of the report, even though it may also appear elsewhere in the body of the technical report. If additional space is required, a continuation sheet shall be attached.

It is highly desirable that the abstract of classified reports be unclassified. Each paragraph of the abstract shall end with an indication of the military security classification of the information in the paragraph, represented as *(TS), (S), (C), or (U)*.

There is no limitation on the length of the abstract. However, the suggested length is from 150 to 225 words.

14. KEY WORDS: Key words are technically meaningful terms or short phrases that characterize a report and may be used as index entries for cataloging the report. Key words must be selected so that no security classification is required. Identifiers, such as equipment model designation, trade name, military project code name, geographic location, may be used as key words but will be followed by an indication of technical context. The assignment of links, rules, and weights is optional.

Unclassified

Security Classification